THE AUSTRALIAN GEOMECHANICS JOURNAL

PRINCIPAL CONTENTS

Complex Flow through Porous Media—D. H. Trollope, K. P. Stark & R. E. Volker 1

Longitudinal Shear Stress Concentration Produced by a Long Straight Opening in an Elastic Mass—R. G. Friday 11

A Mathematical Method for Determining the Anisotropic Velocity of P-Wave Propagation and for the Seismic Location of Rockbursts—S. Budavari 15

Settlement and Load Distribution Analysis of Pile Groups—H. G. Poulos & N. S. Mattes 18

Displacements in a Soil Mass Due to Pile Groups—H. G. Poulos & N. S. Mattes 29

A Study of the Settlement Characteristics of the Soil Deposits at Kingsford-Smith Airport, Sydney—I. K. Lee, E. H. Davis, B. Rodway & R. Mallam 36

VOL. G 1, NO. 1 **1971**

REGISTERED AT THE G.P.O. SYDNEY FOR TRANSMISSION THROUGH THE POST AS A BOOK.

INCORPORATED BY ROYAL CHARTER 1955

INCORPORATED BY ROYAL CHARTER 1955

The Australian Geomechanics Journal

of

The Institution of Engineers, Australia

and

The Australasian Institute of Mining and Metallurgy

VOL. G1, No. 1 **1971**

EDITED BY THE SECRETARY OF THE INSTITUTION OF ENGINEERS, AUSTRALIA

Published once a year by
THE INSTITUTION OF ENGINEERS, AUSTRALIA
SCIENCE HOUSE, GLOUCESTER & ESSEX STS., SYDNEY, 2000
Telegraphic Address: Enjoaust, Sydney. *Telephones*: 27 8261, (5 lines) and 27 5844 (2 lines)

The Institution of Engineers, Australia, subscribes to the Fair Copying Declaration of the Royal Society, and reprints of any portion of this publication may be made provided that exact reference thereto be quoted.

Subscriptions per annum: members $4.00; non-members $5.00 (post free).

CONTENTS

		Page
Complex Flow through Porous Media	*D. H. Trollope, K. P. Stark & R. E. Volker*	1
Longitudinal Shear Stress Concentration Produced by a Long Straight Opening in an Elastic Mass	*R. G. Friday*	11
A Mathematical Method for Determining the Anisotropic Velocity of P-Wave Propagation and for the Seismic Location of Rockbursts	*S. Budavari*	15
Settlement and Load Distribution Analysis of Pile Groups	*H. G. Poulos & N. S. Mattes*	18
Displacements in a Soil Mass Due to Pile Groups	*H. G. Poulos & N. S. Mattes*	29
A Study of the Settlement Characteristics of the Soil Deposits at Kingsford-Smith Airport, Sydney	*I. K. Lee, E. H. Davis, B. Rodway & R. Mallam*	36

Complex Flow through Porous Media

BY D. H. TROLLOPE, M.SC., PH.D., F.I.E.AUST., K. P. STARK, B.E., B.ECON., M.I.E.AUST. and R. E. VOLKER, B.E., PH.D., GRAD.I.E.AUST.*

1.—INTRODUCTION

1.1 General:

By definition, a porous medium is an assembly of solid particles or grains which encloses a system of interconnected voids through which a fluid may flow under the influence of an appropriate pressure gradient.

Such media are therefore particulate in nature and any attempt to describe their internal geometry in detail is fraught with virtually insurmountable complexity.

As a statement of boundary geometry is essential to all solutions involving theoretical mechanics, the prospect of representing exactly the flow of a fluid through such a medium is remote.

In common with other problems involving the transport of physical phenomena such as heat, force, etc., through real materials a remarkable degree of success has been achieved during the past century or so by completely neglecting the complexity of internal geometry and adopting the concept of the equivalent continuum.

It is presumed that a representative sample of this continuum can be obtained and subjected to testing to ascertain average values of these properties which govern the particular behaviour under consideration.

In the case of flow through porous media Darcy (Ref. 1) is credited with being the first person to adopt this approach in his well known experiments involving seepage flow through a variety of sand samples which led to the identity now generally known as Darcy's law—

$$V = k\,i \qquad \text{.....(1)}$$

in which V = the superficial or average seepage velocity,
k = the coefficient of permeability in the direction of flow,
i = the (negative) total piezometric head gradient.

Slichter (Ref. 2) indicated that Eq. (1) did not hold for relatively high values of V. Slichter was particularly interested in the influence of pore geometry on the onset of turbulence and it became generally accepted that Darcy's law is only applicable when the flow is laminar and breaks down on the onset of turbulent conditions.

Since that time a number of attempts have been made to develop improved relationships to describe flow through porous materials. They fall generally into two categories. First those which are an extension of Slichter's approach in that they seek to use idealised physical models to describe the fluid behaviour in the pore space and second those which are of the continuum type but employ mathematical expressions more sophisticated than Darcy's law to describe the flow through an " element ".

The first group may be further subdivided into the capillary theories and the hydraulic radius theories. Both find their origin in classical pipe and channel flow mechanics. The capillary theories assume that the pore space of a porous medium may be represented by a series of straight capillary tubes and the flow is assumed to be governed by the Hagen-Poiseuille equation. Examples of the use of this approach are given by Adzumi (Ref. 3), Childs and Collis-George (Ref. 4), and Marshall (Ref. 5).

The principal objection to the extrapolation of these methods outside the strict Darcy regime lies in the fact that inertial effects due to curvature of the fluid paths in real media are completely ignored. The hydraulic radius theories represent an advance in that inertial effects may be recognised although, until recently, they have not been taken into account.

Kozeny (Ref. 6) originally developed a hydraulic radius theory by considering the medium as an assemblage of channels of fixed length but of varying section. Carman (Ref. 7), Wyllie and Gregory (Ref. 8) also employ this approach and in 1956 Hubbert (Ref. 9) showed that, using a method analogous to Kozeny's, Darcy's law is valid only for flow velocities such that the inertial forces are negligible compared with those due to viscosity.

It may be noted that both Kozeny and Hubbert used the Navier-Stokes equations ignoring inertia terms to express the overall flow in the assumed channels.

Among the continuum flow equations two stand out.

In 1901, Forchheimer (Ref. 10) suggested a simple polynomial expression to describe the flow conditions—

$$i = a\,V + b\,V^2 \qquad \text{.....(2)}$$

where a and b are constants determined by the properties of the fluid and medium. Although Forchheimer subsequently added a third term in an attempt to obtain improved fit with experimental results, Eq. (2) is generally referred to as Forchheimer's equation.

A number of workers have inferred that Forchheimer's equation has sound physical backing apart from its attraction as a relatively simple non-linear expression.

Aravin and Numerov (Ref. 11) stated that from their investigations the soundest law both from theoretical and experimental viewpoints seemed to be the drag law of seepage which they gave as Eq. (2).

Ward (Ref. 12) derived an equation of the Forchheimer type from dimensional analysis and the results of experiments carried out by Lindquist (Ref. 13) can be expressed in this form.

One of the most important recent developments is due to Irmay (Ref. 14) who derived the Forchheimer relation by inferred argument from the fundamental Navier-Stokes equations for the general case when inertia terms are considered.

The second important flow relationship in this category is attributed to Missbach (Ref. 15) who suggested the use of an equation of the general form

$$i = c\,V^m \qquad \text{.....(3)}$$

where c = constant determined by the properties of the medium and the fluid,
m = an exponent with values lying between 1 and 2.

Eq. (3) has been used extensively by White (Ref. 16), Escande (Ref. 17), Wilkins (Ref. 18), Parkin et al (Ref. 19), and Anandakrishnan and Varadarajulu (Ref. 20).

Dudgeon (Ref. 21) carried out tests on coarse materials including a number of gravels, sands and packings of uniform spheres and confirmed that while the results followed closely expressions of the form of Eq. (3) the values of c and m were not constant for the one material for all flow conditions.

1.2 Watson's Model:

A significant advance in the use of particulate models was introduced by Watson (Ref. 22). Extending an approach described by Philip (Ref. 23) he suggested the use of the regular " square " model shown in Fig. 1. Such an arrangement is essentially a clastic model as defined by Trollope (Ref. 24) and, following extensive analyses of its properties, which are to be described in this paper, it has been found to be of very great value in aiding the understanding of complex flow in porous media.

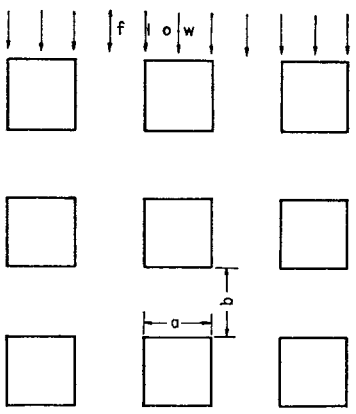

Fig. 1.—An Idealised Porous Medium Model.

One of the most encouraging results of recent work is the demonstration that analysis of Watson's model using the Navier-Stokes equations, including the inertia terms, leads directly to Forchheimer's equation, thus linking the particulate and continuum approaches. It has also been shown that the terms a and b are subject to small variations depending on the Reynolds number of the flow regime which is in accord with Dudgeon's experimental observations. In general however, when included in the Forchheimer expressions these variations are not likely to be of major practical significance.

*Paper No. 2937, submitted by the authors on 18th June, 1970.

Professor Trollope is Professor of Civil Engineering, James Cook University of North Queensland, Townsville.
Associate Professor Stark is with the Department of Engineering (Civil), James Cook University of North Queensland.
Dr. Volker is a Design Engineer, Queensland Government Railways, and was formerly a Water Research Foundation of Aust. Ltd. Research Scholar, James Cook University of North Queensland.

2.—THE FUNDAMENTAL CHARACTERISTICS OF FLOW THROUGH POROUS MEDIA

2.1 Flow Regimes:

It is convenient to classify flow regimes in terms of the behaviour of the fluid in the pore space, these are

(i) The pre-laminar regime,
(ii) The laminar regime,
(iii) The turbulent regime.

The *pre-laminar regime* is associated with very low velocities so that in these circumstances even water ceases to act as a Newtonian fluid. Such flows are frequently associated with extremely small pore sizes, e.g., in clay soils, and the physico-chemical interaction of particles and fluid then has a profound influence on the overall regime. Flows of this type are outside the scope of this paper.

The *laminar regime* is one where, under steady flow conditions an element of the fluid follows a smooth path. At first it was thought that Darcy's law was valid for all laminar conditions. It is now understood however that the laminar regime is always non-linear in character and that the use of the linear Darcy equation is a justifiable approximation only when the effect of the inertia terms in the Navier-Stokes equations is negligible compared with that of the viscosity terms. These conditions occur when the flow velocity is small and this is sometimes called " creeping flow ".

For practical purposes the linear approximation is useful for Reynolds numbers up to the order of unity and fortunately this covers a wide range of natural situations involving materials of particle size less than 1 mm.

It is clear however that the non-linear behaviour of laminar flows through porous media is a topic of considerable practical interest and importance and this paper is primarily concerned with theoretical and experimental evaluation of this phenomenon.

Not the least of the items of theoretical and practical significance is the fact that non-linear flow observations in these circumstances cannot necessarily be attributed to the onset of turbulence.

A *turbulent regime* develops at high Reynolds numbers when the fluid velocities are sufficient to cause instantaneous fluctuations or eddies in the flow path. Under these circumstances changes in flow characteristics with time must be considered and the solution of the fundamental Navier-Stokes equations is extremely difficult even for the simplest geometrical configurations.

Nevertheless the available evidence suggests that the continuum Eqs. (2) and (3) are sufficiently flexible to permit their use in turbulent conditions within porous media.

2.2 Theoretical Investigations of the Laminar Regime:

Fluid flow within the interstices of any porous material will be governed by the basic fluid mechanics relations—the Navier-Stokes equations. As the boundary conditions imposed by the irregularity of the pore spaces are, in general, highly complex and variable the governing equations, which in themselves are fourth order and nonlinear defy analytical solution. As previously noted however it is possible to

(i) consider numerical solutions within a porous medium with simplified or idealised boundary conditions (the particulate approach),
(ii) derive the generalised flow equation in terms of the characteristics of the flow (such as those obtained from a solution of the Navier-Stokes equations) and the properties of the fluid and porous medium (the continuum approach).

Both approaches as developed in this paper start with the assumption that for compressible viscous flow the Navier-Stokes equations may be written as

$$\rho \frac{dU}{dt} = -\operatorname{grad}(\gamma h) + \mu \nabla^2 U \qquad \text{.....(4)}$$

and continuity gives

$$\operatorname{div} U = 0 \qquad \text{.....(5)}$$

where the velocity $U = u\hat{i} + v\hat{j} + w\hat{k}$, t represents time, piezometric head is h and the fluid has density ρ, specific weight γ, dynamic viscosity μ, and kinematic viscosity ν.

If the velocity values are known throughout the flow field the pressure and piezometric head may be deduced at every point from these values and, further, the head gradient between any two points can then be evaluated.

For simplicity the relations will be deduced here for two-dimensional flows—the corresponding three-dimensional arguments are given as the Appendix.

For two-dimensional flow the velocity is given by

$$U = u\hat{i} + v\hat{j} \qquad \text{.....(6)}$$

a stream function ψ may be defined by

$$u = -\frac{\partial \psi}{\partial y}, \quad v = \frac{\partial \psi}{\partial x} \qquad \text{.....(7)}$$

and the vorticity ε is given by

$$\varepsilon = \frac{\partial v}{\partial x} - \frac{\partial u}{\partial y} = \nabla^2 \psi \qquad \text{.....(8)}$$

Using Eq. (8) the piezometric head gradients in the x- and y-directions are obtained from Eq. (4) as

$$-\frac{1}{\rho}\frac{\partial(\gamma h)}{\partial x} = \frac{\partial u}{\partial t} + \frac{1}{2}\frac{\partial U^2}{\partial x} - v\varepsilon + \nu \frac{\partial \varepsilon}{\partial y} \qquad \text{.....(9a)}$$

and

$$-\frac{1}{\rho}\frac{\partial(\gamma h)}{\partial y} = \frac{\partial v}{\partial t} + \frac{1}{2}\frac{\partial U^2}{\partial y} + u\varepsilon - \nu \frac{\partial \varepsilon}{\partial x} \qquad \text{.....(9b)}$$

It is useful to convert these equations into dimensionless form by introducing representative parameters V (velocity) and L (distance) such that

$$\bar{u} = \frac{u}{V}, \ \bar{v} = \frac{v}{V}, \ \bar{x} = \frac{x}{L}, \ \bar{y} = \frac{y}{L}, \qquad \text{.....(10)}$$
$$\bar{\psi} = \frac{\psi}{VL}, \ \bar{\varepsilon} = \frac{\varepsilon L}{V}, \ \bar{h} = \frac{h}{L}, \ \bar{t} = \frac{tV}{L}, \text{ etc.}$$

where the bar indicates a dimensionless quantity.

Reynolds number (RN) may then be defined in conventional fashion by

$$RN = \frac{VL}{\nu} \qquad \text{.....(11)}$$

and the differential equations for the piezometric head gradient may be written in dimensionless form. Thus Eq. (9b) becomes

$$-\frac{\partial \bar{h}}{\partial \bar{y}} \cdot \frac{\gamma L^2}{\mu V} = RN\left(\frac{\partial \bar{v}}{\partial \bar{t}} + \frac{1}{2}\frac{\partial \bar{U}^2}{\partial \bar{y}} + \bar{u} \cdot \bar{\varepsilon}\right) - \frac{\partial \bar{\varepsilon}}{\partial \bar{x}} \qquad \text{.....(12)}$$

and a similar equation is obtained for the gradient in any pertinent direction.

It should be noted that the piezometric head gradient depends upon

(1) field variations of velocity (including vorticity),
(2) RN, V and L which are related, and
(3) γ and μ which are properties of the fluid.

Therefore to assist with the further analysis of this relation it is useful to write it in the form

$$-\frac{\partial \bar{h}}{\partial \bar{y}} = \frac{\mu V}{\gamma L^2}[\alpha_1 + \beta_1 \cdot RN] \qquad \text{.....(13)}$$

where α_1 and β_1 are expressions (not usually constants) derivable from the characteristics of the flow patterns under study and dependent only on Reynolds numbers and the pore geometry.

The *particulate* approach is now followed by assuming a simplified void geometry and solving Eq. (13) for these boundary conditions. If steady flow is considered, numerical solutions of the vorticity-transport equations (Ref. 25) will give the flow characteristics required to evaluate α_1 and β_1 throughout the flow. Such solutions were obtained by Stark (Ref. 26) for a variety of idealised particle arrangements and Figs. 2, 3, 4 and 5 show some typical stream-function solutions.

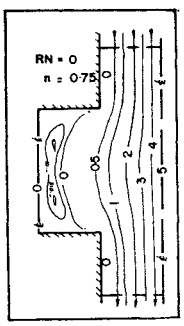

Fig. 2.—Streamlines.

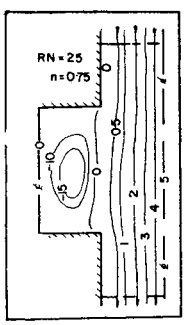

Fig. 3.—Streamlines.

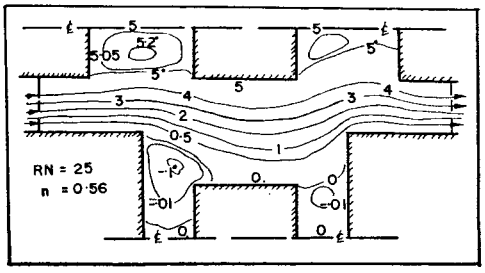

Fig. 4.—Streamlines.

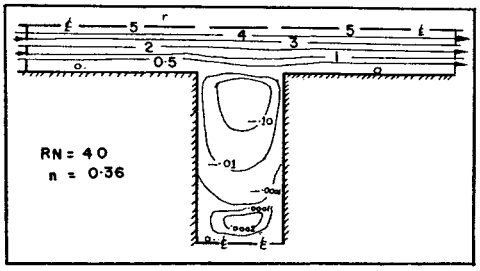

Fig. 5.—Streamlines.

The *continuum* approach is one whereby the average properties within a pore space are assumed to pertain over the adjacent space and each pore is considered as an infinitely small element within the whole porous medium. Consider a typical pore space as shown in Fig. 6 in which the relavant properties of the continuum element shown dotted are given as V and i where V is the seepage velocity and i is the piezometric head drop gradient across the element.

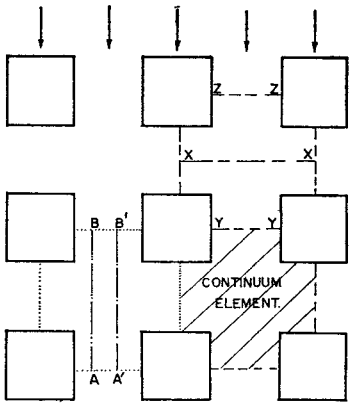

Fig. 6.

Now if the representative velocity (V) used in the flow derivations is chosen as the seepage velocity it follows from Eq. (13) that if the distance AB is given by S

$$i = -\int_A^B \frac{dh}{dy}\frac{dy}{S} = -\frac{\mu V}{S\,\gamma\,L^2}\int_A^B (\alpha_1 + \beta_1 \,.\, RN)\,dy$$

$$= +\frac{\mu V}{\gamma\,L^2}(\alpha + \beta \,.\, RN) \qquad \text{.....(14)}$$

where again α and β may be calculated for an idealised medium from the numerical solutions of the Navier-Stokes equation.

If a particular porous medium is considered (i.e., L is fixed), and the fluid properties (μ and γ) are known then this relation reduces to

$$i = aV + bV^2 \qquad \text{.....(15)}$$

where $a = \dfrac{\mu\alpha}{\gamma L^2}$ and $b = \dfrac{\beta}{gL}$.

It is important to note here that whereas α and β are functions of RN and the pore geometry only, b is also a function of the pore (or particle) size while a is a function of RN, pore geometry, pore (or particle) size and the fluid.

It is still necessary to consider a further two points,

(*a*) whether i is in fact the appropriate representative head gradient across the pore space to be used in the continuum flow relations, and

(*b*) under what circumstances a and b may be assumed constants for a given fluid in a given porous medium.

(*a*) If the element illustrated in Fig. 6 is representative of the surrounding flow (and this is usually the case where the same macroscopic flow relations are used over extensive regions of the flow) then although, by virtue of the nonlinearity of the Navier-Stokes equations, xx, yy and zz will not be lines of symmetry (except when $RN = 0$) the flow patterns crossing zz and yy will show periodic similarity and, as the piezometric head gradients at a point are dependent only upon the surrounding velocity characteristics, it follows that the pressure drops between A-A' and B-B' are identical and therefore that the head gradients along AB, $A'B'$ and any other line parallel to these and crossing the pore space will all be identical. Further, if the medium is isotropic and homogeneous, the same values for a and b will apply for any direction of flow.

(*b*) An examination of the streamline profiles obtained in the numerical solutions shows that over quite extensive ranges of RN there is little change in the dimensionless velocity characteristics—particularly in the main body of flow. Although the position of the separation streamline (separating the main flow from the wake flow) and the vortex patterns alter significantly with changes in RN they do not appear to have an important effect on the head gradient *versus* velocity relation unless the change in RN involves at least one order of magnitude. This observation is supported by a study of the numerically calculated gradients (Refs. 26 and 27) and is illustrated by considering the results (Table I) in which values of $(\alpha + \beta \,.\, RN)$ (Eq. (14)) are tabulated for flow through the idealised model of Fig. 1 at three different pore geometries.

TABLE I

$a/b = 1$, $n = 0.75$		$a/b = 4$, $n = 0.36$		$a/b = 1/3$, $n = 0.937$	
RN	H_G	RN	H_G	RN	H_G
0.0	18.78	0.0	876.2	0.0	1.16
0.05	18.79	8.0	879.6	2.5	1.20
0.5	18.81	40.0	898.3	12.5	1.32
2.5	18.86	50.0	901.8	25.0	1.42
5.0	19.02	80.0	911.9	50.0	1.50
10.0	19.42	$RN = V\,.\,(a/v)$			
15.0	19.80	V = seepage velocity			
25.0	20.22	$H_G = (\alpha + \beta \,.\, RN)$			
50.0	20.82	n = porosity			
100.0	21.44	a = particle size (see Fig. 1)			
150.0	21.62	b = void size (see Fig. 1).			
200.0	21.66				

Darcy Flow: In the limiting case when $RN = 0$ the particulate flow relation (13) and the continuum relation (15) reduce to their respective forms of Darcy's equation which may be written in the form

$$V = k\,i \qquad \text{.....(16)}$$

k in Darcy flow is assumed as a constant but the analyses above show that this is only an approximation. For creeping flows, however, where RN is approximately zero this assumption is well within experimental accuracy and has formed the basis of many studies of seepage flow. The numerical studies suggest that the limit of validity of Darcy's law depends upon the properties of the medium involved, however, generally it may be assumed to hold within $\pm$ 1% if RN (based on seepage velocity and mean particle size) is less than 1. The solutions in Table I support this assumption.

If the continuum is considered then within this continuum the differential form of Darcy's Law may be written

$$V = k\frac{dh}{ds} \qquad \text{.....(17)}$$

and this relation satisfies the potential definition for irrotational flow within the boundary conditions, and therefore h satisfies Laplace equation

$$\nabla^2 h = 0 \qquad \text{.....(18)}$$

Thus all the solutions and methods of solution available for Laplace's equation become available for finding the value of h (and therefore V) at any point in the continuum.

It should be noted that the corresponding particulate equations do not satisfy potential flow requirements because the boundary conditions within the pore spaces must then satisfy " no slip " conditions.

Alternatively (in terms of stream-function) for creeping flow in the continuum $\nabla^2 \psi = 0$ and the boundary conditions of irrotational flow apply whereas for creeping flow within the pore spaces $\nabla^4 \psi = 0$ and " no slip " conditions apply on the particle boundaries.

2.3 The Forchheimer Relation:

The more general relation for laminar flow given by Eq. (15) is sometimes referred to as the non-linear laminar relation and the regime of flow for which this equation applies is the non-linear laminar or non-Darcy laminar regime. When a and b are considered as constants this equation becomes the Forchheimer relation. It should be noted then that just as Darcy's equation applies over a limited range of RN with reasonable accuracy so too as explained above the Forchheimer relation will hold over limited ranges of RN within the laminar flow range. The actual flow range and accuracy with which a given set of values of a and b will apply will depend on the geometry of the pore space involved. As a guide, Darcy's Law will generally hold for RN = 0-1 with an accuracy of $\pm$ 1% whereas a Forchheimer relation can approximate with about the same accuracy for RN = 0-5, 5-25, 25-100. Naturally, if the accuracy stipulated is reduced the applicable range of RN can be increased.

It follows therefore that whenever permeameter tests are performed on a given porous medium and a smooth curve is fitted to the results to obtain an appropriate value of a and b these values will have an accuracy dependent on the range of flows used in the tests. Further, such values should only be used in calculations involving Reynolds numbers appropriate to this range of flows. It is always inadvisable to extrapolate coefficients from a given series of permeameter tests.

2.4 Other Relations

Eq. (14) can be rewritten in the form

$$i = \frac{\mu V}{\gamma L^2} \alpha_0 \left(1 + \frac{\beta}{\alpha_0} . RN\right) \quad \text{.....(19)}$$

by assuming α has a constant value α_0 where α_0 is the value obtained for α when $RN = 0$. If the permeability k at any RN is defined by

$$V = k_{RN}\, i \quad \text{.....(20)}$$

then

$$\frac{k_{RN}}{k_0} = 1 + \frac{\beta}{\alpha_0} . RN \quad \text{.....(21)}$$

This relation which Tek (Ref. 28) deduced empirically is essentially a Forchheimer relation which will be adequate for low Reynolds numbers, e.g., RN = 0-5 but will have decreasing accuracy for higher flows. Tek's experimental results show this and illustrate that the velocity distributions for RN = 5-10 differ sufficiently from those in the range RN = 0-5 to invalidate the implicit assumption in Tek's original expression that α_0 equals α at any other Reynolds number.

The Carman-Kozeny relation for creeping flows is deduced directly from Eq. (14) also by noting

(i) $RN = 0$ for creeping flows,
(ii) L = Hydraulic Radius,
(iii) $\alpha = F(n)$ .....(22)

where n is porosity.

Carman-Kozeny, in effect, assumed that $\alpha = K_1/n$ where K_1 is known as the Carman-Kozeny constant and supposedly has a universal value of 5.

Introducing also the concept of specific surface S_0, defined by the ratio of surface area of particles to particle volume. Eq. (14) results in the Carman-Kozeny relation—

$$i = \frac{\mu}{\gamma} . V K_1 S_0^2 \frac{(1-n)^2}{n^3} \quad \text{.....(23)}$$

Many experimental results have illustrated that K_1 is not a constant even for creeping flow and Stark (Ref. 26) has suggested a relation between α and porosity which appears to be more appropriate than Eq. (22).

3.—LABORATORY EXPERIMENTAL RESULTS

3.1 General:

The rationale of the Forchheimer relation has not generally been heeded by experimentalists and, as a result, the literature abounds in different empirical relations that have been deduced to fit particular experimental evidence.

A close examination of the more reliable reported results (e.g., Refs. 19, 21 and 29) show that very often a Forchheimer relation can be obtained which fits the experimental results more accurately than the empirical relations nominated. Generally, results plotted on log-log paper illustrate a tendency to form a straight line (or a series of straight lines depending on the range of values) and this has resulted in the widespread adoption of a logarithmic relation of the Missbach type. It may not generally be realised that a Forchheimer relation plots on logarithmic paper approximately as a series of straight lines and therefore a Forchheimer relation may be fitted to such results just as accurately as a Missbach type relation.

Although three-dimensional permeameter tests, many of which extend into the turbulent flow range, vindicate the adoption of a Forchheimer relation, they are not usually suited to a general evaluation, of the effect of the different variables, e.g., porosity, particle shape and size and RN on the head-flow relation. A study of the flow variables is simplified by using idealised media. Slichter (Ref. 2) recognised this in his analysis of a mass of uniform spheres while Lindquist (Ref. 13), Ward (Ref. 12), Parkin (Ref. 19), Dudgeon (Ref. 21), Gunn and Malik (Ref. 30) and How Lum (Ref. 31) have all used spheres in at least part of their experimental programme.

3.2 Permeameter Tests—Uniform Spheres:

How Lum's experiments involved a variety of glass balls of diameters 2, 5, 6, 12.5, 15 and 17 mm. which were tested in randomly packed arrangements in large permeameters chosen to avoid " side and end boundary effects ". Each set of tests involved balls of only one diameter and the porosity of the packings were all similar ranging from 39.7% to 40.9%. A correction based on the Carman-Kozeny relation can be used to convert the results to a standard porosity with reasonable accuracy for this range of porosities (Ref. 26).

This conversion is given by

$$\left[\frac{iD^2}{V}\right]_{\text{modified}} = \left[\frac{iD^2}{V}\right]_{\text{experimental}} \frac{n^3}{(1-n)^2} \cdot \frac{(1-n_s)^2}{n_s^3} \quad \text{...(24)}$$

where D = particle diameter,
V = velocity,
n = porosity of experimental material,
n_s = standard porosity.

Now from Eq. (14) it follows that if $\frac{iL^2}{V\nu}$ is calculated for flow through porous materials which are geometrically similar a unique value should be obtained for each RN. This is so for How Lum's tests where L equals D within the accuracy of the experimental results (Ref. 32).

Thus, although the flow paths for each arrangement are not strictly geometrically similar, provided similarly shaped particles are packed in a similar fashion to give the same porosity the condition of hydrodynamic similarity may be satisfactorily assumed.

3.3 The Parallel Plate Model:

Volker (Ref. 33) has used idealised media in an interesting adaptation of the well known Hele-Shaw apparatus. In this series of experiments the apparatus involved two parallel plates $\frac{1}{16}$ in. apart which was sufficient to ensure that non-linear inertial effects (and even turbulence at high flows) were present in the water flowing around the flat " porous media " particles of regular shape(s) and size(s) and arranged in arrays between the plates.

A view of the model is illustrated in Fig. 7. It consists of an inlet box, the flow channel between the parallel plates and an outlet tank. The inlet

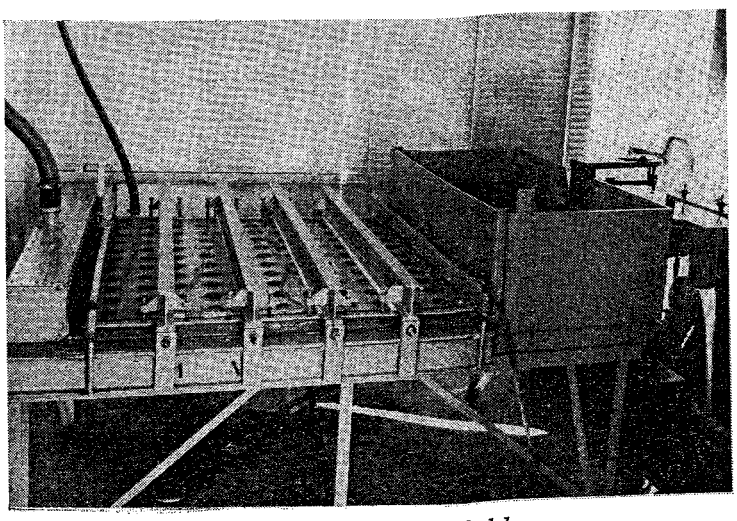

Fig. 7.—Parallel Plate Model.

box and bottom parallel plate were supported on a flat steel $\frac{3}{16}$-in. sheet mounted on a steel frame of rigidly interconnected rolled steel joists which maintained the model in a level position.

Water was conducted into the space between the plates by an inlet pressure box fed by a 2-in. pipe from an overhead supply tank. The inlet box was half-filled with gravel and separated from the actual inlet to the parallel plates by a gauze sheet. The gravel dispersed the flow from the pipe and presented a reasonably uniform distribution of flow at the inlet to the channel between the plates.

The parallel plates themselves were two perspex sheets each $\frac{1}{4}$ in. thick and 4 ft. square which were held at constant spacing by the particles forming the idealised porous medium. The top sheet was held by superimposing a pressure tank on it by cementing strips of perspex $\frac{3}{4}$ in. high to the upper parallel plate around its edges, then another perspex sheet was cemented to these strips to form the top of a closed perspex box.

An inlet (one in. dia., and incorporated in the top of the box) was attached to a static pressure line which extended 4 ft. above the water level in the overhead suppy tank. The pressure in this box thus exerted a downward force on the upper parallel plate and counteracted the upward force from the flow while the presence of the particles prevented the plate from bowing downwards. The downwards pressure also helped to maintain the particles in position and prevented their movement under the action of the drag forces produced by the flow. The perspex box was itself anchored by four rolled steel beams bolted to the steel framework.

At the outlet of the model, the outlet tank formed the approach channel for a half-vee notch weir which could be discharged through a gravimetric flow system when required.

Five pressure tappings spaced 9 in. apart were attached at each end of the perspex sheets to allow measurement of head loss across the model and a hypodermic syringe connected to three needles mounted at the centre of the inlet to the flow channel between the parallel plates was used for dye injection. These needles which were $\frac{3}{4}$ in. apart produced three dye-lines down the central portion of the flow area. Finally a network of lines at 1-in. spacing drawn on the steel base under the bottom perspex sheet facilitated arrangement of the " particles " according to the predetermined patterns. The particles, circles and hexagons of 2-in. dia. and squares (and diamonds) of 1-in. and 2-in. sides were punched from $\frac{1}{16}$-in. sheets of rubber insertion.

The head difference between the inlet and outlet was measured by manometers and averaged over the width of flow. The manometer fluids were petrol ether for low flows, air-water for intermediate flows and water-mercury for high flows.

The pressure head-velocity relations deduced from this parallel plate apparatus not only support the conclusions reached from the numerical solutions but illustrate that the Forchheimer relation can be extended well into the turbulent flow regime.

Laminar Flow Range :

The appropriate equations governing the flow between the particles are given by

$$\mu \frac{\partial^2 u}{\partial z^2} - \frac{\partial(\gamma h)}{\partial x} = \rho\left(\frac{\partial u}{\partial t} + u\frac{\partial u}{\partial x} + v\frac{\partial u}{\partial y}\right) \quad \text{.....(25)}$$

$$\mu \frac{\partial^2 v}{\partial z^2} - \frac{\partial(\gamma h)}{\partial y} = \rho\left(\frac{\partial v}{\partial t} + u\frac{\partial v}{\partial x} + v\frac{\partial v}{\partial y}\right) \quad \text{.....(26)}$$

$$\frac{\partial(\gamma h)}{\partial z} = 0 \quad \text{.....(27)}$$

where the flow occurs in the x, y plane and it is assumed that

(i) w and its derivatives are all zero, and

(ii) second derivatives of u and v with respect to x and y are negligible compared with those in the z-direction.

Comparing these equations with those (Eqs. (4) and (5)) used in the two-dimensional numerical analysis it is evident that the viscous terms are quite different whereas the inertial terms are similar but, these too, will be affected by the boundaries imposed by the parallel plate.

In the conventional Hele-Shaw model the inertial terms are negligible so these equations illustrate the important difference between the parallel plate apparatus and the Hele-Shaw model.

The flows used in the tests corresponded to Reynolds numbers based on the seepage velocity and the particle size from $RN = 50$ to 50,000 (and based on the plate separation from $RN = 1.5$ to 1,500) and dye tests were used to indicate the onset of turbulence in the higher ranges.

As discussed previously a single Forchheimer relation cannot be expected to hold accurately over a wide range of velocities and heads such as that encompassed. On the other hand realising that the velocity distributions change relatively slowly with RN and separating the results into several (2 or 3) ranges Forchheimer expressions were obtained which fitted the results in each range with an accuracy of better than the experimental error of about 5%.

The results for some of these tests with the appropriate Forchheimer " constants " are given in Table II.

TABLE II

Forchheimer Coefficients in Parallel Plate Tests

Particle Arrangement*	Size	Seepage Velocity (ft./sec.)	a	b
Circles	2-in. dia.	0.0357- 1.06	0.0723	0.0159
		1.13 - 2.43	0.0715	0.0185
		2.52 -10.88	0.0745	0.0234
Squares	2-in. side	0.0324- 1.06	0.0756	0.0085
		1.12 - 2.30	0.0631	0.0182
		2.44 -10.62	0.0623	0.0255
Hexagons 1	2-in. inscribed dia.	0.0814- 1.23	0.0669	0.0249
		1.28 - 2.19	0.0500	0.0363
		2.37 - 6.50	0.0505	0.0379
Hexagons 2	2-in. inscribed dia.	0.0079- 5.67	0.831	0.1173
Diamonds	2-in. side	0.0233- 1.065	0.0900	0.0704
		1.115 - 2.10	0.0665	0.0866
		2.32 - 6.16	0.0586	0.0929
Squares	2-in. side and 1-in. side	0.0202- 6.52	0.0718	0.0812

*Particle arrangements are in a square grid excepting Hexagons 2 which is on a diamond grid. In the two-squares arrangement the smaller squares were placed centrally in each continuum element.

Turbulent Flow Range :

The onset of turbulence in porous materials is not readily pinpointed because it appears to be associated with the development of instability in the wake regions behind the particle—and with the passage of these and any other disturbances throughout the medium. In the parallel plate model tests turbulence appeared to have permeated the flow at $RN =$ 2,000 (based on the particle dimension) or 60 (based on plate spacing) although at even lower flows turbulence appeared to be present at least in some parts of the flow.

An examination of the turbulent flow equations (see the Appendix) shows that the " Reynolds stress " terms are similar in form to the inertial terms so that the continuum equation expressing the macroscopic flow through porous materials will have an additional term in the turbulent flow regime which is of the same form as the inertial term—$b\,V^2$.

Thus the Forchheimer relation (15) still expresses the flow relation but the value of b incorporates two terms one characterised by the laminar flow, the other related to the changes which turbulence introduces to the velocity distributions.

4.—THE TWO-DIMENSIONAL FIELD EQUATION FOR FORCHHEIMER FLOW

4.1 General :

Having established the applicability of the Forchheimer relationship both theoretically and with respect to flow through a typical element it is now necessary to derive equations which will describe satisfactorily the conditions obtaining in a " field " throughout which the constitutive law applies.

Previous derivations of field equations for non-linear flow have been carried out by Kristianovich (Ref. 34) and Engelund (Ref. 35) who introduced auxiliary independent variables in place of the cartesian co-ordinates in an attempt to simplify the analysis.

Irmay (Ref. 14) has given a brief discussion of the general problem by deducing a differential field equation using the Forchheimer equation, but the nonlinear characteristics present formidable difficulties with regard to formal analytical solution.

Recognising that practically important solutions can only be obtained at the present time by recourse to numerical analysis Volker (Ref. 36) has derived the field equation in a form suitable for this purpose.

4.2 The Field Equation :

The Forchheimer head loss relation (Eq. (15)) may be written in the form

$$-\text{grad}\, h = a\,V + b\,V^2 \quad \text{.....(28)}$$

where a and b are constants (under the assumptions outlined above) determined by the properties of the fluid and medium. Assuming that

grad h and $\underline{V}$ are oppositely directed vectors, Eq. (28) in vector form becomes:

$$-\text{grad}\, h = (a + b\,|V|)\,\underline{V} \quad \ldots\ldots(29)$$

where $|V|$ is the magnitude of vector $\underline{V}$. If $\underline{i}$ and $\underline{j}$ are unit vectors in the x- and y-directions respectively, and $\underline{s}$ is a unit vector normal to the surface of constant h in the scalar field and adopting the notion $h_s = \partial h/\partial s$, $h_x = \partial h/\partial x$ and $h_y = \partial h/\partial y$, then from vector theory it can be shown that:

$$-h_s\,\underline{s} = -h_x\,\underline{i} - h_y\,\underline{j} \quad \ldots\ldots(30)$$

also from Eq. (29)

$$h_s\,\underline{s} = (a + |b|\,V)\,(u\,\underline{i} + v\,\underline{j}) \quad \ldots\ldots(31)$$

Equating corresponding components of vectors in Eqs. (30) and (31)

$$\left.\begin{aligned} -h_x &= (a + b\,|V|)\,u \\ -h_y &= (a + b\,|V|)\,v \end{aligned}\right\} \quad \ldots\ldots(32)$$

Again from Eq. (29) it can be shown that

$$|V| = -\frac{a}{2b} + \sqrt{\left(\frac{a}{2b}\right)^2 + \frac{|h_s|}{b}} \quad \ldots\ldots(33)$$

Substituting for V in Eq. (32) and rearranging

$$\left.\begin{aligned} u &= \frac{-h_x}{\frac{a}{2} + \sqrt{\frac{a^2}{4} + b\,|h_s|}} \\ v &= \frac{-h_y}{\frac{a}{2} + \sqrt{\frac{a^2}{4} + b\,|h_s|}} \end{aligned}\right\} \quad \ldots\ldots(34)$$

The continuity relation for two-dimensional flow (Eq. (5)) may be written

$$\frac{\partial u}{\partial x} + \frac{\partial v}{\partial y} = 0 \quad \ldots\ldots(35)$$

Substitution for u and v from Eq. (34) in Eq. (35) yields the required field equation for the Forchheimer head loss relation as

$$\frac{\partial}{\partial x}\left[\frac{h_x}{\frac{a}{2} + \sqrt{\frac{a^2}{4} + b\,|h_s|}}\right] + \frac{\partial}{\partial y}\left[\frac{h_y}{\frac{a}{2} + \sqrt{\frac{a^2}{4} + b\,|h_s|}}\right] = 0 \quad \ldots(36)$$

4.3 Finite Difference Technique of Solution:

Eq. (36) is simplified by introducing the term f which is written:

$$f = f(|h_s|) = \left\{\frac{a}{2} + \sqrt{\frac{a^2}{4} + b\,|h_s|}\right\}^{-1} \quad \ldots\ldots(37)$$

Eq. (36) may then be written as

$$\frac{\partial}{\partial x}(h_x f) + \frac{\partial}{\partial y}(h_y f) = 0 \quad \ldots\ldots(38)$$

or

$$h_x f_x + f\,h_{xx} + h_y f_y + f\,h_{yy} = 0 \quad \ldots\ldots(39)$$

It has been shown (Ref. 37) that differentiation of Eq. (37) and substitution in Eq. (39) leads to the field equation in a form suitable for direct application of finite differences

$$h_{xx} - \frac{h_x}{|h_s|}\frac{f}{2}\,b\left(\frac{a^2}{4} + b\,|h_s|\right)^{-\frac{1}{2}}(h_x\,h_{xx} + h_y\,h_{yx}) + \\ + h_{yy} - \frac{h_y}{|h_s|}\frac{f}{2}\,b\left(\frac{a^2}{4} + b\,|h_s|\right)^{-\frac{1}{2}}(h_y\,h_{yy} + h_y\,h_{xy}) = 0 \quad \ldots\ldots(40)$$

The finite difference formulation of Eq. (40) is best carried out in a number of steps. The flow field is divided into a discrete number of points by a regular grid in the usual way and values of piezometric head are assumed for all points whose values are not fixed. The gradients h_x and h_y at any particular point are evaluated in terms of the piezometric head at that point and at adjacent nodes. This enables the term $|h_s|$ to be calculated, and substitution in Eq. (37) yields f. Finite difference formulae also give the value of the second derivatives h_{xx} and h_{yy}. Thus Eq. (40) when applied at each node in the field yields a set of simultaneous equations in terms of the unknown piezometric heads and the solution of these equations, usually by iterative techniques, then represents a solution to the problem.

For axisymmetric flow, the field Eq. (36) must be modified to allow for the radial convergence of the flow. For axisymmetric flow the continuity equation is

$$\frac{\partial V_r}{\partial r} + \frac{V_r}{r} + \frac{\partial V_z}{\partial z} = 0 \quad \ldots\ldots(41)$$

where V_r and V_z are the velocities in the r- and z-directions respectively. Substituting for V_r and V_z, Eq. (41) becomes

$$\frac{\partial}{\partial r}\left[\frac{h_r}{\frac{a}{2} + \sqrt{\frac{a^2}{4} + b\,|h_s|}}\right] + \frac{h_r}{h_s}\frac{V}{r} + \frac{\partial}{\partial z}\left[\frac{h_z}{\frac{a}{2} + \sqrt{\frac{a^2}{4} + b\,|h_s|}}\right] = 0 \quad (42)$$

where V is the velocity in the s-direction and is given by Eq. (33). The finite difference approximation to Eq. (42) is obtained by an analogous procedure to that used for Eq. (36).

At the boundaries of the flow field the boundary values are either fixed or adjusted by finite difference forms of the boundary conditions. The imposition of Dirichlet type boundary conditions, on boundaries where the piezometric head is known, is relatively simple since the field value of each node on such boundaries is set equal to the appropriate piezometric head. A Neumann type boundary condition is imposed by first calculating the normal derivative at the boundary, in terms of h values at nodes on, and adjacent to, the boundary; and when this normal derivative is set equal to zero, new values of piezometric head h on the boundary can be obtained. In regions with a free surface of flow, including a boundary condition of mixed type, some difficulty is introduced because the position of this free surface is not known a priori. The treatment of this top flow line may be undertaken in a manner similar to that described in Ref. 38. An assumed position is first employed and is adjusted as the solution proceeds to give the final correct location of the free surface.

4.4 Finite Element Technique of Solution:

Many problems involving elliptic partial differential equations can be related to the minimization or maximization of an integral. This property which is discussed more fully by Courant and Hilbert (Ref. 39) leads to an alternative variational formulation of the problem. Instead of attempting to solve the partial differential equation in its original form, the problem is converted to one of maximizing or minimizing an integral throughout the field.

Although originally developed as a direct application of the principles of structural analysis, the method of finite elements has since been shown to have wider applications. Zienkiewicz and Cheung (Ref. 40) demonstrated the logical extension of the method of finite elements to solve the alternative variational formulation of field problems involving elliptic partial differential equations. It has also been shown (Ref. 36) that the method can be applied to the solution of the Forchheimer field equation for non-linear flow through porous media and has certain advantages when dealing with flow fields of irregular shape.

For the general variational problem

$$E(h) = \iint_R G(h, h_x, h_y, x, y)\,dx\,dy \quad \ldots\ldots(43)$$

the Euler equation, from the calculus of variations (Ref. 41) for the minimization of E in the region R is

$$\frac{\partial G}{\partial h} - \frac{\partial}{\partial x}\left(\frac{\partial G}{\partial h_x}\right) - \frac{\partial}{\partial y}\left(\frac{\partial G}{\partial h_y}\right) = 0 \quad \ldots\ldots(44)$$

and if the boundary condition is of the form

$$-\frac{\partial G}{\partial h_x}\cdot\frac{dy}{ds} + \frac{\partial G}{\partial h_y}\cdot\frac{dx}{ds} = 0 \quad \ldots\ldots(45)$$

it is called the natural boundary condition because it is automatically satisfied by the function h minimising $E(h)$, without being imposed.

For application of the finite element method of analysis the field Eq. (36) is more suitably restated as

$$\frac{\partial}{\partial x}\left[\left\{\frac{-a}{2b} + \sqrt{\left(\frac{a}{2b}\right)^2 + \frac{|h_s|}{b}}\right\} - \frac{h_x}{|h_s|}\right] + \\ + \frac{\partial}{\partial y}\left[\left\{\frac{-a}{2b} + \sqrt{\left(\frac{a}{2b}\right)^2 + \frac{|h_s|}{b}}\right\} - \frac{h_y}{|h_s|}\right] = 0 \quad \ldots\ldots(46)$$

In order to express Eq. (46) as equivalent to the minimization of an integral, a function G must be obtained which satisfied Eqs. (44)-(45).

These requirements are fulfilled by the function

$$G = -\frac{a}{2b}|h_s| + \frac{2}{3}b\left\{\left(\frac{a}{2b}\right)^2 + \frac{|h_s|}{b}\right\}^{3/2} \quad \text{.....(47)}$$

and the integral to be minimized is

$$E(h) = \int\int\left[\frac{-a}{2b}|h_s| + \frac{2}{3}b\left\{\left(\frac{a}{2b}\right)^2 + \frac{|h_s|}{b}\right\}^{3/2}\right]dx\,dy \quad \text{.....(48)}$$

Substitution in Eq. (45) shows that the natural boundary condition coincides with a zero gradient normal to the boundary and therefore with no flow across the boundary. Thus this boundary condition on any particular boundary does not have to be imposed on the solution but is automatically accounted for.

To obtain a solution for flow in any region, the field is first discretized into a finite number of nodes at which values of piezometric head are required. Minimisation of the integral E in Eq. (48) with respect to the piezometric head h at each node leads to a set of simultaneous equations in terms of unknown h values. The equations are usually arranged into matrix form and the solution is carried out systematically to yield the required piezometric head distribution over the region of flow. Other quantities as required can then be calculated from the piezometric heads.

5.—FIELD SOLUTIONS USING MISSBACH'S RELATION

If the Missbach relation (Eq. (3) is used instead of the Forchheimer relation then following the above procedure the appropriate field relation for two dimensional flow is given by

$$\frac{\partial}{\partial x}\left[\frac{|h_s|^{1/m}}{c}\frac{(-h_x)}{|h_s|}\right] + \frac{\partial}{\partial y}\left[\frac{|h_s|^{1/m}}{c}\frac{(-h_y)}{|h_s|}\right] = 0 \quad \text{.....(49)}$$

and the appropriate integral to be minimised using the finite element technique is given by

$$E(h) = \int\int C^{-(1/m)}\frac{m}{m+1}|h_s|^{(m+1)/m}\,dx\,dy \quad \text{.....(50)}$$

when c and m are constants this relation reduces to

$$E(h) = \int\int h_s^{(m+1)/m}\,dz\,dy \quad \text{.....(51)}$$

These relations were deduced independently by Fenton (Ref. 42) and Volker (Refs. 36 and 37) whereas Parkin (Ref. 43) had earlier derived the field equation using a slightly different approach. Fenton has analysed a number of seepage problems based on the exponential (Missbach) head loss equation, including free surface conditions, and using both finite difference and finite element techniques.

6.—SOME SOLUTIONS AND COMPARISONS WITH EXPERIMENTAL RESULTS

6.1 General :

In order to test the predictions of the non-linear theory in some significant practical situations it was necessary to carry out some relatively large scale laboratory experiments.

The situations which are of most immediate significance are

(*a*) the confined aquifer of known geometry,
(*b*) the unconfined aquifer,
(*c*) the vertical sided permeable wall,
(*d*) the triangular section enbankment.

Experiments covering (*a*) and (*b*) were carried out in a 20-ft. dia. × 6 ft. deep steel tank. Water could be introduced around the wall of the tank, passed through the medium in the tank to a central well from which it was pumped through a discharge measuring device back into a reservoir.

Experiments on the vertical wall and model embankments were carried out in an open flume 2 ft. wide × 2 ft. deep with one clear perspex side for viewing purposes.

Full details of the testing procedures are given in Ref. 37.

6.2 Confined Axisymmetric Flow Experiments :

The arrangement for these tests is shown diagrammatically in Fig. 8 and the material used was a nominal $\frac{3}{16}$ in. size crushed granite aggregate. A series of permeameter tests was carried out over a range of velocities comparable with those in the tank experiments. With such tests however the difficulty remains of ensuring that the material in the permeameter is in the same physical condition as that in the tank. As a check on the procedure the model aquifer flow at the lowest discharge (flow No. 1) was selected as a situation wherein the maximum fluid velocity (at the well) was entirely within the range of the permeameter experiments. The measured discharge in this situation was compared with that predicted from the use of the Forchheimer equation (Eq. (2)) with values of the constants a and b derived from the independent permeameter tests with the following results.—

Measured discharge	0.177 cusec.
Calculated discharge	0.179 cusec.

The agreement is therefore acceptable.

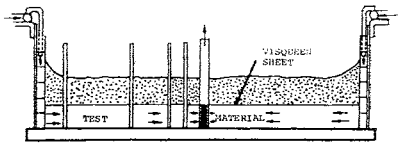

Fig. 8.—Section showing Path of Water Through Model.

Thereafter the value of the Darcy permeability coefficient (k) calculated from this model flow (No. 1) and the values of Forchheimer constants (a and b) were used to predict flows at higher velocities.

The results are shown in Fig. 9. It will be seen that up to flow No. 3 there is excellent agreement between the calculated values based on the predictions of the Forchheimer equation and the measured discharges, whereas the extrapolated values using the Darcy constant are increasingly in error up to a value of 20%.

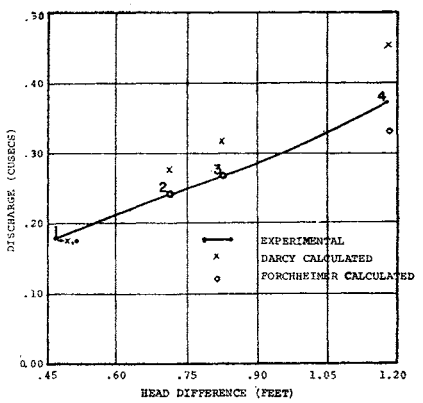

Fig. 9.—Discharge Results for Confined Flow Experiments.

The velocities developed in flow No. 3 have been estimated (Ref. 37) to have maximum values at the well interface of 0.15 ft./sec. compared with a velocity of 0.06 ft./sec. which was the maximum developed in the permeameter tests.

This velocity of 0.06 ft./sec. was also exceeded within a cylindrical column of radius 6 in. around the well.

When the flow was increased (flow No. 4) to the condition where the velocity at the well interfacd was approximately 0.25 ft./sec. (i.e., four times the maximum permeameter velocity) and the excess region around the well was 8.5 in. radius then both the non-linear (Forchheimer) and the linear (Darcy) values were considerably in error, although the non-linear prediction was closer to the measured value.

This emphasises that whichever constitutive law is used predictive extrapolation beyond the range of actual test values is not generally warranted.

Other things being equal however the non-linear (Forchheimer) relationship is measurably superior to the Darcy equation.

Workers familiar with the problems of using the Darcy equation in practical situations frequently express the view that it is difficult enough to relate observed values of flow to a single variable—the Darcy coefficient of permeability, so that even greater difficulty is to be expected when dealing with a non-linear relationship such as the Forchheimer equation.

These experiments indicate the fundamental error encompassed in this opinion. In fact, it is much easier to relate the Forchheimer equation to actual flows now that the analytical difficulties inherent in handling non-linear equations have been overcome by the development of computer based numerical methods.

6.3 The Unconfined Aquifer :

Again, an axially symmetric situation was used with material similar to that described in section 6.2, i.e., $\frac{3}{16}$ in. nominal single size crushed granite aggregate. In this case both the Forchheimer and Missbach equations were used to predict the non-linear flow in a bed 5 ft. thick in the 20-ft. dia. tank.

Again, a reference flow (No. 2) was used and the results are shown in Fig. 10. The superiority of both the non-linear expressions in this case

is striking, the Darcy Law based predictions overestimating the maximum flow by 48%.

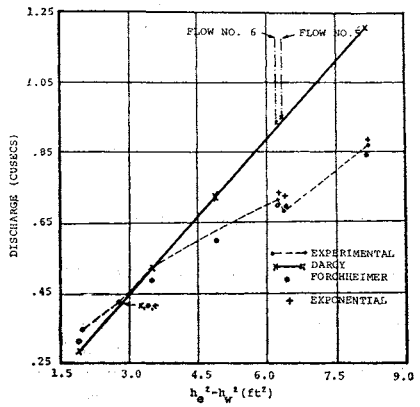

Fig. 10.

Figs. 11, 12 and 13 show a set of typical predicted flow nets at flow No. 5. Again, although there is a significant difference between predicted and measured head differences with the non-linear equations, both are markedly superior to the Darcy Law based net.

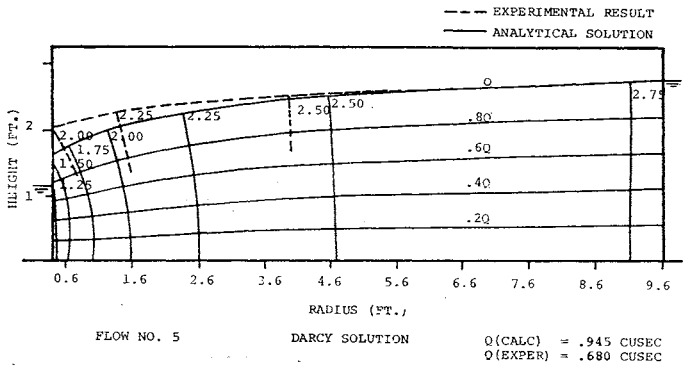

FLOW NO. 5 DARCY SOLUTION Q(CALC) = .945 CUSEC
Q(EXPER) = .680 CUSEC

Fig. 11.

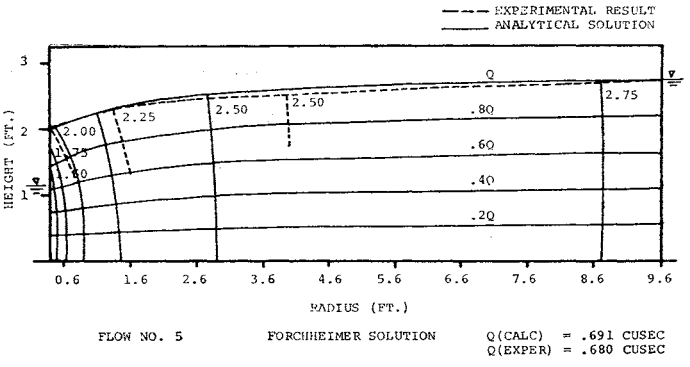

FLOW NO. 5 FORCHHEIMER SOLUTION Q(CALC) = .691 CUSEC
Q(EXPER) = .680 CUSEC

Fig. 12.

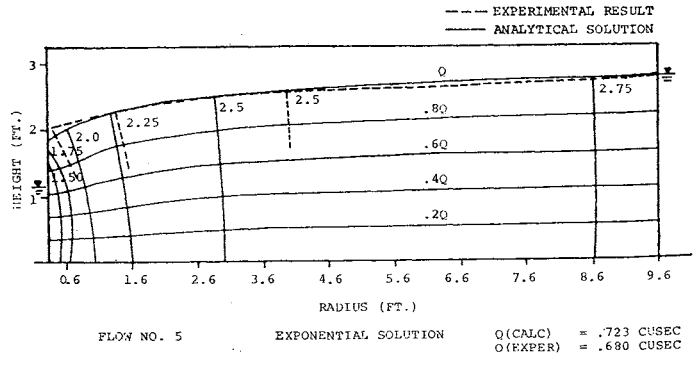

FLOW NO. 5 EXPONENTIAL SOLUTION Q(CALC) = .723 CUSEC
Q(EXPER) = .680 CUSEC

Fig. 13.

6.4 Unconfined Flow Through a Permeable Wall:

In this case the aggregate was retained between two vertical sheets of metal gauze placed perpendicular to the direction of flow and approximately 3 ft. apart, thus simulating a simple two-dimensional cofferdam situation.

The results are shown in Fig. 14 and in this case the error involved in using Darcy's Law is 46% whereas both non-linear predictions are within 1%.

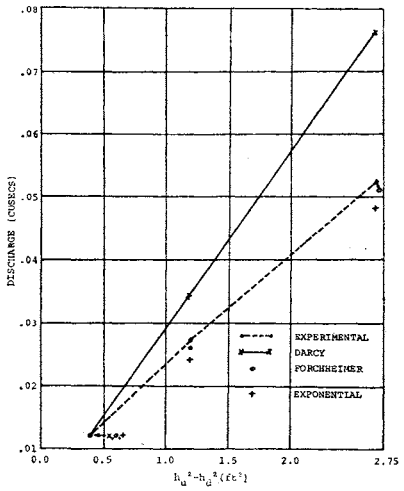

Fig. 14.—*Discharge Comparisons for Permeable Wall Flows.*

6.5 Flow Through Model Dams:

Details of these experiments have been reported elsewhere (Ref. 36) but the resulting flow nets together with the relevant discharges are reproduced below for convenience (Fig. 15).

FLOW THROUGH DAM WITH NO CUT-OFF WALL

EXPERIMENTAL DISCHARGE = .114 CUSEC/FT
THEORETICAL DISCHARGE (DARCY) = .890 CUSEC/FT
THEORETICAL DISCHARGE (FORCHHEIMER) = .110 CUSEC/FT
THEORETICAL DISCHARGE (EXPONENTIAL) = .107 CUSEC/FT

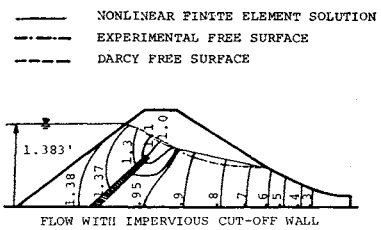

FLOW WITH IMPERVIOUS CUT-OFF WALL

EXPERIMENTAL DISCHARGE = .076 CUSEC/FT
THEORETICAL DISCHARGE (FORCHHEIMER) = .073 CUSEC/FT
THEORETICAL DISCHARGE (EXPONENTIAL) = .071 CUSEC/FT

Fig. 15.

Again it will be evident that the non-linear equations give much better predictions than the Darcy equation with respect to discharge.

It is interesting to note however that there is little to choose between the methods as far as the prediction of the flow net is concerned. This is of considerable significance in relation to stability calculations.

CONCLUSIONS

Traditionally, analyses of flows in porous materials have been largely restricted to flows for which Darcy's Law holds. There have been two reasons for this:

(i) flows through fine grained materials (less than 1 mm. average dimension) generally obey Darcy's Law and

(ii) analytical techniques for solving Laplace's equation, which is the field equation for Darcy flow, are well developed and, indeed, analogous field relations hold in a number of other disciplines.

More recently it has become possible to investigate complex solutions of the Laplace equation using numerical techniques. Extension of these numerical procedures to solve more complex field equations has been a

logical development so that it is now possible with very little additional effort (and possibly some additional computer time) to solve seepage problems which extend the basic head loss-flow relation well beyond the limits of validity of Darcy's relation.

A natural step in this development has been to seek the most suitable and appropriate head loss-flow relation and although the literature abounds in empirical formulae it is interesting to note that a closer look at the fluid dynamics of porous media flow in terms of advanced numerical techniques has yielded a rational method of attack.

Flow through porous material can be viewed: (i) as a clastic problem and (ii) as a continuum problem. By considering the clastic problem it has been possible by integration to extend the basic flow relation within the power to a continuum relation which is representative of a given porous material and a given fluid.

It has been shown that under certain circumstances this relation reduces exactly to a Forchheimer relation whereas more generally the constants in the Forchheimer relation must be treated as variable. For certain idealised flows these variables can be accurately determined by numerical methods.

The rationale of the Forchheimer relation has been supported by a variety of experimental studies including a comprehensive series of tests using a parallel plate model—an extension of the Hele-Shaw apparatus.

Development of finite difference and finite element methods for solving the field equations resulting from a Forchheimer relation has been undertaken to illustrate that such problems present no serious difficulties to the present day engineer.

Finally the construction of a large scale experimental porous media tank has allowed the accuracy of these techniques to be checked against field conditions simulated in the laboratory. These tests have shown that serious errors in discharge estimation may be made if the Forchheimer relation is not used to replace Darcy's equation and that the Forchheimer relation appears to give satisfactory results providing the appropriate coefficients are carefully determined.

ACKNOWLEDGMENTS

The work described in this paper has been carried out in the Engineering laboratories at the James Cook University of North Queensland (formerly the University College of Townsville) and has been assisted financially from university funds.

The major financial support was provided by a series of grants from the Water Research Foundation of Australia Ltd. to whom the authors would express their appreciation.

Thanks are also due to Mrs. S. E. Hobson for assistance in typing and preparing the manuscript.

APPENDIX

(a) Three-Dimensional Derivation of Forchheimer Relation :

The three-dimensional Navier-Stokes equation in the x-direction for steady, incompressible flow is

$$u\frac{\partial u}{\partial x}+v\frac{\partial u}{\partial y}+w\frac{\partial u}{\partial z}=-\frac{1}{\rho}\frac{\partial(\gamma h)}{\partial x}+\nu\nabla^2 u \qquad \text{.....(A1)}$$

and therefore

$$-\frac{1}{\rho}\frac{\partial(\gamma h)}{\partial x}=u\frac{\partial u}{\partial x}+v\frac{\partial v}{\partial x}+w\frac{\partial w}{\partial x}+v\frac{\partial u}{\partial y}-v\frac{\partial v}{\partial x}+ +w\frac{\partial u}{\partial z}-w\frac{\partial w}{\partial x}-\nu\nabla^2 u$$

$$=\frac{1}{2}\frac{\partial U^2}{\partial x}-v\,\varepsilon_z-w\,\varepsilon_y-\nu\nabla^2 w \qquad \text{.....(A2)}$$

where $U=u\hat{i}+v\hat{j}+w\hat{k}$, and ε_x, ε_y, ε_z are vorticity components defined in the usual way.

Converting Eq. (A2) into dimensionless form as in Section 2.2 where $RN=VL/\nu$ gives

$$\frac{\partial h}{\partial x}=\frac{\mu V}{\gamma L^2}\left[\nabla^2\bar{u}-RN\left(\frac{1}{2}\frac{\partial\bar{U}^2}{\partial x}-\bar{v}\,\bar{\varepsilon}_z-\bar{w}\,\bar{\varepsilon}_y\right)\right] \qquad \text{.....(A3)}$$

$$=\frac{\mu V}{\gamma L^2}(\alpha_3+\beta_3\,.\,RN) \qquad \text{.....(A4)}$$

which can be compared with Eq. (13).

(b) Turbulent Flow—Two-Dimensional Derivation :

Note.—In this derivation bars over symbols are used to denote mean values with respect to time. Dimensionless quantities are distinguished by using the subscript d as in $\bar{u}_d$.

If instantaneous velocities, e.g., u are defined by $u=\bar{u}+\bar{u}^1$ where u^1 is the instantaneous variation from the mean then the two-dimensional equations for steady flow (Ref. 44) are given by

$$\rho\left(\bar{u}_j\frac{\partial\bar{u}_i}{\partial x_j}+\overline{u^1{}_j\frac{\partial u^1{}_i}{\partial x_j}}\right)=-\frac{\partial(\gamma\bar{h})}{\partial x_i}+\mu\nabla^2\bar{u} \qquad \text{.....(A5)}$$

which can be rewritten as

$$-\frac{1}{\rho}\frac{\partial(\gamma\bar{h})}{\partial x}=\bar{u}\frac{\partial\bar{u}}{\partial x}+\bar{v}\frac{\partial\bar{u}}{\partial y}+\overline{u^1\frac{\partial u^1}{\partial x}}+\overline{v^1\frac{\partial u^1}{\partial y}}-\nu\nabla^2\bar{u} \qquad \text{(A6)}$$

$$=\frac{1}{2}\frac{\partial\bar{U}^2}{\partial x}-\bar{v}\,\bar{\varepsilon}+\overline{u^1\frac{\partial u^1}{\partial x}}+\overline{v^1\frac{\partial u^1}{\partial y}}-\nu\nabla^2\bar{u} \qquad \text{(A7)}$$

where

$$\bar{U}^2=\bar{u}^2+\bar{v}^2 \qquad \text{.....(A8)}$$

and in dimensionless terms

$$i=\frac{\mu}{\gamma}\frac{V}{L^2}\left[\nabla^2\bar{u}_d-RN\left(\frac{1}{2}\frac{\partial\bar{U}^2{}_d}{\partial x_d}-\bar{v}_d\,\bar{\varepsilon}_d+\overline{u^1{}_d\frac{\partial u^1{}_d}{\partial x_d}}+\overline{v^1{}_d\frac{\partial u^1{}_d}{\partial y_d}}\right)\right] \qquad \text{.....(A9)}$$

which can be written in a Forchheimer format as for Eq. (A4) with modified coefficients.

References

1. DARCY, H.—*Les Fontaines Publiques de la Ville de Dijon.* Paris, Victor Dalmont, 1856.
2. SLICHTER, C. S.—Theoretical Investigation of the Motion of Groundwaters. *U.S. Geol. Survey, 19th Annual Report,* Part 2, 1897, p. 329.
3. ADZUMI, H.—The Flow of Gases through Metallic Capillaries at Low Pressures. *Bulletin Chem. Soc. Japan,* 1939, pp. 343-7.
4. CHILDS, E. C. and COLLIS-GEORGE, N.—The Permeability of Porous Materials. *Proc. Roy. Soc., Series A,* Vol. 201, No. 1066, May 23, 1950, pp. 392-405.
5. MARSHALL, T. J.—Permeability Equations and Their Models. *Proc. Symposium on Interaction between Fluids and Particles.* London, Adlard, 1962, pp. 299-303.
6. KOZENY, J.—Soil Permeability. *Wassers in Boden Setz-Ber. Wiener Akad.,* Vol. 136, 1927, pp. 271-306.
7. CARMAN, P. C.—Fluid Flow through Granular Beds. *Trans. I. Chem. E.,* Vol. 15, 1937, pp. 150-66.
8. WYLLIE, M. R. J. and GREGORY, A. R.—*Gulf Research and Development Co., Pittsburgh, Geol. Div., Report No.* 41, 1954.
9. HUBBERT, M. K.—Darcy's Law and the Field Equations of Flow of Underground Fluids. *Jour. Petrol. Technology,* Vol. 8, 1956, pp. 222-39.
10. FORCHHEIMER, P. H.—*Hydraulik.* Berlin, Teubner, 1930.
11. ARAVIN, B. I. and NUMEROV, S. N.—*Theory of Fluid Flow in Undeformable Porous Media.* Jerusalem, Israel Program for Scientific Translations, 1965.
12. WARD, J. C.—Turbulent Flow in Porous Media. *Proc. A.S.C.E., Jour. Hydraulic Div.,* Vol. 90, No. HY5, Sept., 1964, pp. 1-12.
13. LINDQUIST, E.—On the Flow of Water through Porous Soil. *Trans. First Congress on Large Dams, Stockholm,* 1933, Vol. 5, pp. 81-101.
14. IRMAY, S.—On the Theoretical Derivation of Darcy and Forchheimer Formulas. *Trans. Amer. Geophys. Union,* Vol. 39, 1958, pp. 702-7.
15. MISSBACH, A.—*Listy Cukrova,* Vol. 55, 1937, p. 293.
16. WHITE, A. M.—Pressure Drop and Loading Velocities in Packed Towers. *Chem. Engg. Progress,* Vol. 31, 1935, pp. 390-408.
17. ESCANDE, L.—Experiments Concerning the Infiltration of Water through a Rock Mass. *Proc. Minnesota Int. Hydraulics Convention, Minneapolis,* 1953, pp. 547-53.
18. WILKINS, J. K.—The Flow of Water through Rockfill and its Application to the Design of Dams. *Proc. Second Aust.-New Zealand Conf. Soil Mechanics and Foundation Engg., Christchurch,* 1956, pp. 141-7.
19. PARKIN, A. K., TROLLOPE, D. H. and LAWSON, J. D.—Rockfill Structures Subject to Water Flow. *Proc. A.S.C.E., Jour. Soil Mechanics and Foundations Div.,* Vol. 92, No. SM6, Nov., 1966, pp. 135-51.

20. ANANDAKRISHNAN, M. and VARADARAJULU, G. H.—Laminar and Turbulent Flow of Water through sand. *Proc. A.S.C.E., Jour. Soil Mechanics and Foundations Div.*, Vol. 89, No. SM5, Sept., 1963, pp. 1-15.

21. DUDGEON, C. R.—*Flow of Water through Coarse Granular Materials.* Thesis (M.E.), University of New South Wales, 1964.

22. WATSON, K. K.—The Permeability of an Idealised Two-Dimensional Porous Medium using the Navier-Stokes Equations. *Proc. Fourth Aust.-New Zealand Conf. Soil Mechanics and Foundation Engg., Adelaide,* 1963, pp. 37-40.

23 PHILIP, J. R.—Fluid Flow in Porous Media from the Viewpoint of Classical Hydrodynamics. *Proc. Second Aust. Conf. Soil Science,* 1957, Vol. 1, pp. 1-9.

24. TROLLOPE, D. H.—The Mechanics of Discontinua or Clastic Mechanics in Rock Problems. Chapter 9 of *Rock Mechanics in Engineering Practice.* Edited by Stagg, K. G. and Zienkiewicz, O. C. London, Wiley, 1968.

25. SCHLICHTING, H.—*Boundary Layer Theory.* New York, McGraw-Hill, 1960.

26. STARK, K. P.—*Some Aspects of the Non-linear Laminar Regime of Flow in Porous Media.* Thesis (Ph.D.), University of Queensland, 1968.

27. STARK, K. P.—A Numerical Study of the Non-linear Laminar Regime of Flow in an Idealized Porous Medium. *Proc. I.A.H.R. Symposium, on "The Phenomena in Porous Media", Haifa, Feb.,* 1969.

28. TEK, M. R.—Development of a Generalised Darcy Equation. *Trans. A.I.M.M.E.*, Vol. 210, 1957, pp. 376-8.

29. ROSE, H. E.—Fluid Flow through Beds of Granular Material. *Some Aspects of Fluid Flow.* London, Edward Arnold, 1951, pp. 136-62.

30. GUNN, D. J. and MALIK, A. A.—Flow through Expanded Beds of Solids. *Trans. I. Chem. E.*, Vol. 44, 1966, pp. T371-87.

31. HOW LUM, C.—*An Investigation into Porous Media Flow.* Thesis (B.E.), University College, Townsville, 1966.

32. STARK, K. P. and VOLKER, R. E.—Non-linear Flow through Porous Materials—Some Theoretical Aspects. *University College, Townsville, Dept. of Engg., Research Bulletin No.* 1, 1967.

33. VOLKER, R. E.—*Flow through Idealized Particle Arrays.* Thesis (M.Eng.Sc.), University College, Townsville, 1966.

34. KRISTIANOVICH, S. A.—Movement of Groundwaters Violating Darcy's Law. *Jour. Applied Math. and Mechanics,* Vol. 4, 1940, pp. 33-52.

35. ENGELUND, F.—On the Laminar and Turbulent Flows of Groundwater through Homogeneous Sand. *Tech. University of Denmark, Hydraulic Labs., Bulletin No.* 4, 1953.

36. VOLKER, R. E.—Non-linear Flow in Porous Media by Finite Elements. *Proc. A.S.C.E., Jour. Hydraulic Div.*, Vol. 95, No. HY6, Nov., 1969, pp. 2093-114.

37. VOLKER, R. E.—*Numerical Solutions to Problems of Non-linear Flow through Porous Materials.* Thesis (Ph.D.), James Cook University of North Queensland, 1969.

38. BOULTON, N. S.—The Flow Pattern near a Gravity Well in a Uniform Water Bearing Medium. *Proc. I. C. E.*. Vol. 36, 1950-51, pp. 534-50.

39. COURANT, R. and HILBERT, D.—*Methods of Mathematical Physics.* Vol. 1. New York, Interscience Publications, 1953.

40. ZIENKIEWICZ, O. C. and CHEUNG, Y. K.—Finite Elements in the Solution of Field Problems. *The Engineer,* Vol. 220, No. 5722, Sept. 24th, 1965, pp. 507-10.

41. PARS, L. A.—*An Introduction to the Calculus of Variations.* London, Heinemann, 1962.

42. FENTON, J. D.—Hydraulic and Stability Analyses of Rockfill Dams. *University of Melbourne, Dept. of Civil Engg., Report No.* DR15, 1968.

43. PARKIN, A. K.—Rockfill Dams with Inbuilt Spillways, Part 1—Hydraulic Characteristics. *Water Research Foundation of Aust., Bulletin No.* 6, 1963.

44. HINZE, J. O.—*Turbulence.* New York, McGraw-Hill, 1959.

Longitudinal Shear Stress Concentration Produced by a Long Straight Opening in an Elastic Mass

BY R. G. FRIDAY, B.E., M.ENG.SC., M.I.E.AUST.*

Summary.—The stress concentration factors relating three dimensional field stress to stresses at the boundary of a long straight opening of uniform cross-section, may be readily determined except for those relating longitudinal shear stresses. A theory developed in this paper leads to the principle that longitudinal shear stress at any point is given by modulus of rigidity times the gradient of longitudinal displacement (w), where w satisfies Laplace's equation in the region outside the opening and the necessary boundary conditions. A method of solution by conformal mapping is outlined and results for certain openings are tabulated.

LIST OF SYMBOLS

x, y, z	Reference axes (see Fig. 1 (a)).
n	Normal
t	Tangential } axes at a point on opening boundary.
l	Longitudinal
σ	Direct stress } Subscript F applies to stresses remote
τ	Shear stress } from opening.
ν	Poisson's ratio.
G	Modulus of rigidity.
a_x, a_{xy}, etc.	Stress Concentration factors.
u, v, w	Displacements in x, y, z directions.
ϵ	Direct strain.
γ	Shear strain.
r, θ	Polar co-ordinates (see Fig. 2).
a	Radius of a circular opening.
$Z = x + iy$	Complex variable.
$\zeta = \alpha \text{ cis } \beta$	Complex variable.
A, B, C - - -	Transformation coefficients.
m, N	Integers.

1.—INTRODUCTION

In designing an underground opening it is generally required to estimate the stresses in the rock close to the excavation boundary. This paper is concerned with the relation between the three-dimensional field stress and the stresses around a long straight opening of uniform cross-section. This relation must also be known to calculate virgin stresses from stress measurements taken at a tunnel boundary.

It is assumed that the opening occurs in a homogeneous, isotropic elastic mass of material which, away from the disturbing influence of the opening, is uniformly stressed. The stress distribution around the opening is the same whether the opening is cut before stress application, as in many engineering structures, or after stress application as for excavations in rock.

Fig. 1 (a) shows the six components of the virgin stress field and the opening with its axis in the z-direction. The x-axis has been directed vertically for convenience in analysis later. Fig. 1 (b) shows the three stress components at a point P on the opening boundary. These three components may be expressed in terms of the field stress components thus:

$$\sigma_t = a_x \sigma_{xF} + a_y \sigma_{yF} + a_{xy} \tau_{xyF} \quad \text{.....(1)}$$

$$\sigma_l = \sigma_{zF} + \nu(a_x - 1)\sigma_{xF} + \nu(a_y - 1)\sigma_{yF} + \nu a_{xy} \tau_{xyF} \quad \text{.....(2)}$$

$$\tau_{tl} = a_{yz} \tau_{yzF} + a_{zx} \tau_{zxF} \quad \text{.....(3)}$$

in which the a's are stress concentration factors applying at the point P considered. These three equations were given by Hiramatsu and Oka (Ref. 1). The stresses σ_{xF}, σ_{yF} and τ_{xyF} appear in Eq. (2) to satisfy the condition that excavation of the opening produces no change in longitudinal strain.

The stress concentration factors a_x, a_y and a_{xy} may be determined readily by two-dimensional photoelastic models (Ref. 2) or by mathematical methods (Ref. 3).

The author could find no reference giving a general solution for determining the longitudinal shear stress concentration factors a_{yz} and a_{zx}. Ref. 6, Ref. 1 and others provide theoretical results for the region around a circular opening. Hiramatsu and Oka (Ref. 1) determined values of a_{yz} and a_{zx} for certain openings by three-dimensional photo-elastic experiments. However, the technique is rather specialized and the results obtained for a circular opening did not agree well with the theoretical ones.

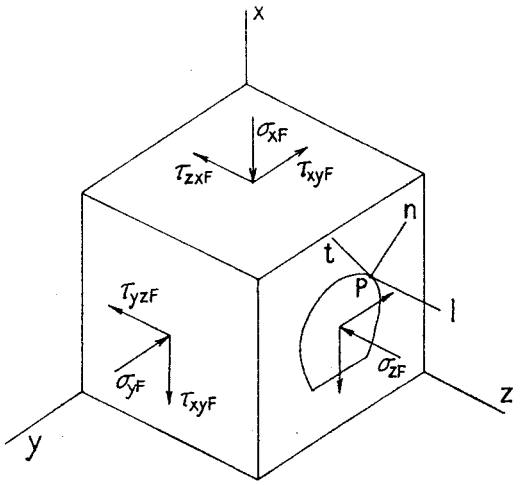

Fig. 1 (a).—*Opening in Three-Dimensional Stress Field.*

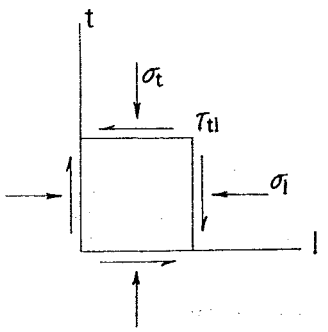

Fig. 1 (b).—*Stresses at a Point on the Opening Boundary.*

2.—THEORY FOR LONGITUDINAL SHEAR

2.1 General Solution:

The approach followed is similar to that in the Saint-Venant solution for torsion of prismatic bars (Ref. 4, p. 259).

The application of a field longitudinal shear stress such as τ_{yzF} or τ_{zxF} will produce warping of planes perpendicular to the opening axis (z-axis).

$$w = w(x, y)$$

Since the cross-section is uniform there will be no change with respect to z. Therefore

$$\frac{\partial w}{\partial z} = 0 \quad \text{.....(4)}$$

No displacement perpendicular to the z-axis can occur. For example, if the application of τ_{zxF} were to produce a displacement $u = k\,\tau_{zxF}$ at a point, then the application of $-\tau_{zxF}$ would have to produce a displacement $u = -k\,\tau_{zxF}$ at the same point. Such behaviour is inconceivable in the model considered. Therefore

$$u = v = 0 \quad \text{.....(5)}$$

Because of Eqs. (4) and (5),

$$\epsilon_x = \epsilon_y = \epsilon_z = \gamma_{xy} = 0$$

$$\therefore \quad \sigma_x = \sigma_y = \sigma_z = \tau_{xy} = 0 \quad \text{.....(6)}$$

But

$$\tau_{yz} = G\,\gamma_{yz} = G\left(\frac{\partial v}{\partial z} + \frac{\partial w}{\partial y}\right)$$

*Paper No. 2978, submitted by the author on 21st September, 1970.

The author is Senior Mining Engineer, Research and Development Section, North Broken Hill Ltd.

and since $v = 0$

$$\tau_{yz} = G\frac{\partial w}{\partial y} \quad \text{.....(7)}$$

Similarly

$$\tau_{zx} = G\frac{\partial w}{\partial x} \quad \text{.....(8)}$$

For equilibrium, since σ_z does not vary with z

$$\frac{\partial \tau_{yz}}{\partial y} + \frac{\partial \tau_{zx}}{\partial x} = 0 \quad \text{(Ref. 4, p. 229) .....(9)}$$

Substituting Eqs. (7) and (8) gives

$$\frac{\partial^2 w}{\partial y^2} + \frac{\partial^2 w}{\partial x^2} = 0 \quad \text{.....(10)}$$

That is, the displacement parallel to the opening axis satisfies Laplace's equation.

2.2 Boundary Conditions:

At the boundary of the opening

$$\tau_{nt} = 0$$

and

$$\tau_{nl} = 0$$

The first is already satisfied by Eq. (6). The second will be satisfied by putting

$$\gamma_{nl} = \frac{\partial w}{\partial n} = 0 \quad \text{.....(11)}$$

at the opening boundary.

The conditions away from the influence of the opening are

$$\tau_{yz} = \tau_{yzF}$$
$$\tau_{zx} = \tau_{zxF}$$

Substituting Eqs. (7) and (8) gives the conditions remote from the opening:

$$\frac{\partial w}{\partial y} = \frac{1}{G}\tau_{yzF}$$
$$\frac{\partial w}{\partial x} = \frac{1}{G}\tau_{zxF} \quad \text{.....(12)}$$

2.3 Principle:

The magnitude of the longitudinal shear stress at any point is given by G times the gradient of w (longitudinal displacement) where w satisfies Laplace's equation (10) and the boundary conditions (11) and (12). The direction of the shear stress on the x-y plane is given by the direction of the gradient.

3.—METHODS OF SOLUTION

3.1 General:

The shear stress distribution around an opening of given cross-section could be determined by mathematical analysis, finite difference method or analogue methods.

An attempt was made to obtain solutions by measuring relative voltage gradients on a sheet of conducting paper with a hole cut at the centre to represent the opening shape. Consistent results were not obtained. The results below were obtained by mathematical analysis.

3.2 Circular Hole:

The solution for shear stress in the region around a circular hole in a mass under longitudinal shear stress is mathematically identical to that for ideal fluid flow past a circular cylinder (Ref. 5, p. 547) (see Fig. 2).

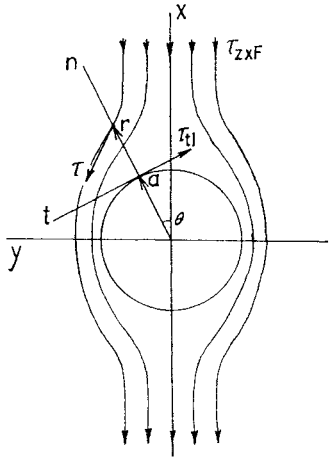

Fig. 2.—Longitudinal Shear Stress Distribution Around a Circular Opening.

For field stress τ_{zxF}

$$\tau = \tau_{zxF}\sqrt{1 - 2\left(\frac{a}{r}\right)^2 \cos 2\theta + \left(\frac{a}{r}\right)^4}$$

At the boundary $r = a$

$$\tau_{tl} = -2\,\tau_{zxF}\sin\theta \quad \text{.....(13)}$$

This agrees with previous theoretical solutions (Ref. 1 and Ref. 6).

3.3 Openings of Other Shapes:

A single opening of any cross-section may, in principle, be dealt with by conformal mapping using transformations $Z = f(\zeta)$ of the form

$$Z = A\,\zeta + \frac{B}{\zeta} + \frac{C}{\zeta^2} + \frac{D}{\zeta^3} + - - - + P \quad \text{.....(14)}$$

This produces a 1-to-1 transformation of points outside the unit circle on the ζ-plane to points outside a corresponding boundary on the Z-plane.

If the transformation coefficients A to P are restricted to real values then only openings symmetrical about the x-axis may be dealt with. This restriction is applied to simplify the work from here on.

An opening boundary on the ζ plane defined by the unit circle $\zeta = \cos\beta + \iota\sin\beta$ is transformed on the Z-plane to an opening boundary defined by

$$x = (A + B)\cos\beta + C\cos 2\beta + D\cos 3\beta + - - - + P$$
$$y = (A - B)\sin\beta - C\sin 2\beta - D\sin 3\beta - - - - \quad \text{.....(15)}$$

where $Z = x + \iota y$.

By choosing suitable values for the coefficients A to P the boundary on the Z-plane may be made to approximate any shape having symmetry about the x-axis.

Laplace's equation is still satisfied after the transformation and by analogy with solutions for fluid flow (Ref. 5, p. 543) it is found that the magnitude of the shear stress at a point Z_0 on the Z plane is obtained by dividing the magnitude of the shear stress at the corresponding point ζ_0 on the ζ-plane by $|f'(\zeta_0)|$.

$$\tau_{tlZ_0} = \tau_{tl\zeta_0}/|f'(\zeta_0)| \quad \text{.....(16)}$$

Now for the transformation (14)

$$f'(\zeta) = A - \frac{B}{\zeta^2} - \frac{2C}{\zeta^3} - \frac{3D}{\zeta^4} - \frac{4E}{\zeta^5} - - -$$

For points on the opening boundary $\zeta = \cos\beta + \iota\sin\beta$, the first five terms of (14) give

$$\begin{aligned}|f'(\zeta_0)| = \sqrt{[}&A^2 + B^2 + 4C^2 + 9D^2 + 16E^2 \\ &+ 2\cos\beta\,(2BC + 6CD + 12DE) \\ &+ 2\cos 2\beta\,(-AB + 3BD + 8CE) \\ &+ 2\cos 3\beta\,(-2AC + 4BE) \\ &+ 2\cos 4\beta\,(-3AD) + 2\cos 5\beta\,(-4AE)] \quad \text{...(17)}\end{aligned}$$

For points remote from the opening $|f'(\zeta)|$ approaches A. To obtain equality between the shear stresses remote from the opening on the Z- and ζ-planes the factor A is introduced to Eq. (16). Eq. (13) is re-written to refer to the ζ-plane:

$$\tau_{tl\zeta_0} = -2\,\tau_{zxF}\sin\beta$$

and substituted in Eq. (16). Then

$$\tau_{tlZ_0} = -2\,\tau_{zxF}\sin\beta\frac{A}{|f'(\zeta_0)|}$$

The shear stress concentration factor is then

$$a_{zx} = \frac{\tau_{tlZ}}{\tau_{zxF}} = -\frac{2\sin\beta\,A}{|f'(\zeta_0)|} \quad \text{.....(18)}$$

where $|f'(\zeta_0)|$ may be calculated from Eq. (17).

For field stress τ_{yzF} Eq. (13) becomes (see Fig. 2)

$$\tau_{tl} = -2\,\tau_{yzF}\sin\left(\theta - \frac{\pi}{2}\right)$$
$$= 2\,\tau_{yzF}\cos\theta.$$

The shear stress concentration factor is then

$$a_{yz} = \frac{\tau_{tlZ}}{\tau_{yzF}} = \frac{2\cos\beta\,A}{|f'(\zeta_0)|} \quad \text{.....(19)}$$

TABLE I

Transformation Coefficients and Longitudinal Shear Stress Concentration Factors for Various Openings

Opening (Height 'h' = 1) / Coefficients in Eqs. (15)	Circle		2:1 Ellipse		Square		2:1 Rectangle		Horseshoe		Particular Tunnel	
	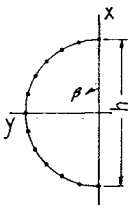		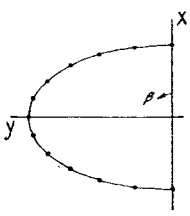		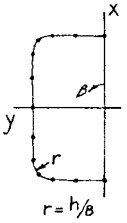		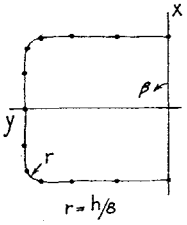		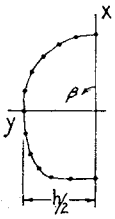		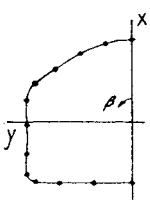	
A	0.5		0.75		0.5763		0.8639		0.5215		0.6586	
B	0		−0.25		0.0000		−0.2652		0.0047		−0.1272	
C	0		0		0.0000		0.0000		0.0170		0.0585	
D	0		0		−0.0777		−0.1161		−0.0218		−0.0438	
E	0		0		0.0000		0.0000		0.0137		0.0257	
F	0		0		0.0000		0.0146		−0.0044		0.0159	
G	0		0		0.0000		0.0000		0.0005		−0.0081	
H	0		0		0.0013		0.0022		−0.0001		−0.0035	
β	a_{xx}	a_{yz}	a_{xx}	a_{yz}	a_{xx}	a_{yz}	a_{xx}	a_{yz}	a_{xx}	a_{yz}	a_{xx}	a_{yz}
0	0.00	2.00	0.00	1.50	0.00	1.44	0.00	1.24	0.00	2.03	0.00	1.91
15	−0.52	1.93	−0.40	1.49	−0.41	1.54	−0.34	1.26	−0.53	1.97	−0.49	1.82
30	−1.00	1.73	−0.83	1.44	−1.13	1.96	−0.82	1.42	−1.01	1.76	−0.85	1.48
45	−1.41	1.41	−1.34	1.34	−2.44	2.44	−2.02	2.02	−1.42	1.42	−1.23	1.23
60	−1.73	1.00	−1.96	1.13	−1.96	1.13	−3.00	1.73	−1.74	1.01	−2.08	1.20
75	−1.93	0.52	−2.64	0.71	−1.54	0.41	−1.97	0.53	−1.89	0.51	−2.34	0.63
90	−2.00	0.00	−3.00	0.00	−1.44	0.00	−1.72	0.00	−1.83	0.00	−1.72	0.00
105	−1.93	−0.52	−2.64	−0.71	−1.54	−0.41	−1.97	−0.53	−1.72	−0.46	−1.82	−0.49
120	−1.73	−1.00	−1.96	−1.13	−1.96	−1.13	−3.00	−1.73	−1.74	−1.01	−3.12	−1.80
135	−1.41	−1.41	−1.34	−1.34	−2.44	−2.44	−2.02	−2.02	−1.85	−1.85	−2.12	−2.12
150	−1.00	−1.73	−0.83	−1.44	−1.13	−1.96	−0.82	−1.42	−1.21	−2.10	−0.84	−1.46
165	−0.52	−1.93	−0.40	−1.49	−0.41	−1.54	−0.34	−1.26	−0.44	−1.66	−0.35	−1.30
180	0.00	−2.00	0.00	−1.50	0.00	−1.44	0.00	−1.24	0.00	−1.50	0.00	−1.27

4.—COMPUTER PROGRAM

A computer program was developed to

(*a*) determine the transformation coefficients for an opening boundary defined by x and y co-ordinates of up to 10 points above the x-axis and 2 points on the x-axis,

(*b*) plot the resulting mathematical outline according to Eq. (15),

(*c*) calculate shear stress concentration factors according to Eqs. (18) and (19) for a succession of points around the boundary.

Part (*a*) was based on the method followed in Ref. 3 and is outlined in the Appendix. The program was run on the CDC.6400 computer at the University of Adelaide.

5.—RESULTS

Table I shows transformation coefficients and longitudinal shear stress concentration factors for several opening shapes. All the openings are symmetrical about the x-axis.

It was found that 8 terms in the transformation Eq. (14) were sufficient to give a good approximation to the opening shapes considered. In the diagrams of Table I the y-axis has been positioned to make the term P zero.

6.—CONCLUSIONS

A theory and procedure for determining the distribution of longitudinal shear stress around a long straight opening of uniform cross section in an elastic mass, has been developed.

The procedure used in Ref. 3 to mathematically represent openings having two axes of symmetry has been extended to openings with one axis of symmetry and could be extended to unsymmetrical openings if required.

ACKNOWLEDGMENTS

The author would like to thank the management of North Broken Hill Ltd. for permission to publish this paper.

References

1. HIRAMATSU, Y. and OKA, Y.—Stress Around a Shaft or Level Excavated in Ground with a Three-Dimensional Stress State. *Mem. Fac. Engg. Kyoto*, Vol. 24, Part 1, Jan., 1962, pp. 56-76.
2. HIRAMATSU, Y. and OKA, Y.—Stress on the Wall of Levels with Cross Sections of Various Shapes. *Int. Jour. Rock Mechanics and Min. Sciences*, Vol. 1, No. 2, March, 1964, p. 199.
3. HELLER, S. R., BROCK, J. S. and BART, R.—The Stresses Around a Rectangular Opening with Rounded Corners in a Uniformly Loaded Plate. *Proc. Third U.S. Congress on Applied Mechanics, Providence, Rhode Island*, 1958, pp. 357-68. New York, A.S.M.E., 1958.
4. TIMOSHENKO, S. and GOODIER, J. N.—*Theory of Elasticity*. 2nd ed. New York, McGraw-Hill, 1951.
5. HILDEBRAND, F. B.—*Advanced Calculus for Engineers*. New York, Prentice Hall, 1949.
6. FAIRHURST, C.—Methods of Determining In-Situ Rock Stresses at Great Depths. *U.S. Army, Corps of Engineers, Missouri River Division, Tech. Report No.* 1-68, Feb., 1968, Appendix 3, p. 13.

APPENDIX

The shape of the opening boundary to be mathematically approximated may be defined by listing pairs of x and y co-ordinates through which the boundary must pass. Because of symmetry about the x-axis points with $y \geqslant 0$ only, need be considered. The corresponding range of β on the ζ plane is $0 \leqslant \beta \leqslant \pi$.

Consider N points above the x-axis and two points on the x-axis. Substituting in Eqs. (15) gives:

For $\beta = 0$,

$$x_0 = A + B + C + D + - - - + P$$
$$y_0 = 0$$

For $\beta = \pi$,

$$x_\pi = -A - B + C - D + E - - - - + P$$
$$y_\pi = 0$$

$$\therefore \quad P = \frac{(x_0 + x_\pi)}{2} - C - E - - - -$$

and

$$A + B = \frac{(x_0 - x_\pi)}{2} - D - F - - - -$$

For $0 < \beta < \pi$,

$$x_m = (A + B)\cos\beta_m + C\cos 2\beta_m + D\cos 3\beta_m + - - - + P$$
$$y_m = (A - B)\sin\beta_m - C\sin 2\beta_m - D\sin 3\beta_m - - - -$$

where $m = 1$ to N and β_m is unknown.

Substituting for P and $(A + B)$ gives

$$\left.\begin{aligned} &C(1 - \cos 2\beta_m) + D(\cos \beta_m - \cos 3\beta_m) + \\ &+ E(1 - \cos 4\beta_m) + F(\cos \beta_m - \cos 5\beta_m) + \\ &+ - \\ &- \frac{(x_0 + x_\pi)}{2} - \frac{(x_0 - x_\pi)}{2} \cos \beta_m + x_m = 0 \end{aligned}\right\} \quad \ldots(20)$$

and

$$Q \sin \beta_m + C \sin 2\beta_m + D \sin 3\beta_m + - - - + y_m = 0$$

where $Q = B - A$.

There are thus $2N$ non-linear equations to determine values for N β's and N coefficients Q, C, D, E, $- - -$.

The equations were solved as in Ref. 3 using Newton's method. Let the left-hand side of one of the Eqs. (20) be g. Choose approximate values for the coefficients and β_m. g should be equal to zero. If it is not, then the changes required in the values are related by

$$\frac{\partial g}{\partial Q} \Delta Q + \frac{\partial g}{\partial C} \Delta C + \frac{\partial g}{\partial D} \Delta D + \frac{\partial g}{\partial E} \Delta E + - - - + \frac{\partial g}{\partial \beta_m} \Delta \beta_m + g = 0 \quad \ldots\ldots\ldots\ldots(21)$$

The changes required are determined by solving the $2N$ linear equations of the form of Eq. (21). Successive iterations usually give convergent values for the β's and coefficients. If not, a fresh start should be made with altered initial estimates.

The data required to run the program is:

x-co-ordinate for top of opening (x_0).

x-co-ordinate for bottom of opening (x_π).

Number of intermediate co-ordinated points (N).

Tolerance on fitting to co-ordinated points.

Maximum number of iterations.

β-interval between points for plotting and determination of shear stress concentration factors.

Plotting scale.

N pairs of x, y co-ordinates through which the boundary must pass with stated tolerances.

One or more sets of estimated β values for each of the co-ordinated points.

A Mathematical Method for Determining the Anisotropic Velocity of P-Wave Propagation and for the Seismic Location of Rockbursts

By S. Budavari, Ph.D., M.Aus.I.M.M.*

Summary.—A mathematical method is presented for determining the velocities of P-wave propagation when the anisotropy of the rock mass is characterised by an ellipsoidal type velocity law. The analysis is developed using measured seismic data obtained by firing charges of explosives at known locations in the rock and registered by a network of seismometers distributed around the mine workings. In the second part of the paper the already determined in-situ seismic velocities of P-wave propagation are utilised in the derivation of a set of simultaneous linear equations necessary for the location of the focus of an actual rockburst.

INTRODUCTION

One of the major hazards generally associated with deep level mining is the phenomenon of rockburst which is a sudden and violent failure of the rock in the vicinity of mine openings. For several years, intensive research has been carried out into the causes and the nature of rockbursts. The statistical analysis of empirical data, the study of rock properties and the seismic location of the foci of rockbursts have been used to enhance the basic understanding of the mechanism of rockbursts (Ref. 1).

In this search, the application of seismic techniques to locate the foci of rockbursts with respect to the underground workings is particularly important. Although several research centres and large mining companies (Refs. 1, 2, 3 and 4) built recording equipment and carried out field observations, most of the publications on this subject is due to Cook. Calibration measurements conducted underground in homogeneous massive quartzites by Cook (Ref. 1) showed that 90% of the seismic paths had velocities between 18.1 and 18.9 ft./millisec. Under these circumstances the assumption of isotropic propagation of P-wave velocity was justified. However, preliminary analysis of the field observations recorded by Bhattacharyya (Ref. 5) at Kolar Gold Field in India indicates that the velocity of P-wave propagation is directionally dependent. Anisotropic behaviour with an ellipsoidal distribution of moduli was also found by Douglass and Voight (Ref. 6) and Peres Rodrigues (Ref. 7) to be a characteristic of several granites. When such anisotropy is significant, it may be necessary to apply a method of analysis to the location of the origin of a rockburst which takes into account the anisotropic velocity of a seismic wave propagation. It is the purpose of this paper to describe a mathematical method which can be used to determine this inherent rock property and to locate the focus of a rockburst in an idealised anisotropic rock.

In the context of this paper the network of seismometers distributed in that region of a rock mass where a rockburst is to be expected to occur can serve a dual purpose. First they can be used to register the times of arrival of a seismic event initiated by firing a charge of explosive at a point of known location. If the initiation time of the blast is also obtained from the recording of a seismometer placed very near the blast location, then the in-situ velocity of the P-wave propagation can be determined by the general analysis to be described. The second purpose of the seismometers is to register the times of arrival of the P-waves in case of an actual rockburst. From the recorded data, using the already determined seismic velocities, the co-ordinates of the rockburst focus can be easily calculated. It is assumed in what follows that the variation of the velocities of P-wave propagation around a point are governed by an ellipsoidal type of law and that these velocities are uniform in their respective directions. Because of the law accuracy of recording the time of arrival of the S-wave on short distances involved, the time of arrival of the P-wave is used only in the analysis presented here.

DETERMINATION OF THE ELLIPSOID OF ANISOTROPIC VELOCITY

In order to obtain the necessary information from an experimental investigation it is required to record the initiation time of a blast and the corresponding times of arrival of the P-wave at the individual seismometers in the network. From these data the time interval for the transmission of the seismic event through the rock to each of the seismometers are determined. Then, knowing the co-ordinates of the blast point and those of the seismometers, the P-wave velocities along respective lines from the centre of the explosion to the individual seismometers are directly calculated. If the network contains a sufficient number of seismometers both the magnitudes and orientations of the principal axes of the ellipsoid of anisotropic velocity of P-wave propagation can be determined.

Using the mine co-ordinate system as a basic frame of reference, let the co-ordinates of the blast point be denoted by

$$(x_0 , y_0 , z_0)$$

and those of the seismometers by

$$(x_1 , y_1 , z_1); (x_2 , y_2 , z_2); \ldots (x_i , y_i , z_i); \ldots (x_n , y_n , z_n).$$

The distance d_i between the blast point and the i-th seismometer is given by

$$d_i = \sqrt{(x_i - x_0)^2 + (y_i - y_0)^2 + (z_i - z_0)^2} \quad \ldots\ldots\ldots\ldots(1)$$

Denoting the time of arrival of the wave by t_i and the initiation time by t_0 the velocity v_i to the i-th seismometer along the assumed straight seismic path is

$$v_i = \frac{d_i}{t_i - t_0} \quad \ldots\ldots\ldots\ldots(2)$$

If $\alpha_i , \beta_i , \gamma_i$ are the angles between a directed line and the x, y, z axes of the co-ordinate system, the direction cosines of the line from the blast point to the corresponding seismometer are expressed by:

$$\cos \alpha_i = \frac{x_i - x_0}{d_i}, \quad \cos \beta_i = \frac{y_i - y_0}{d_i}, \quad \cos \gamma_i = \frac{z_i - z_0}{d_i} \quad \ldots\ldots(3)$$

From Eqs. (2) and (3) the equations for the velocity components of v_i along the x, y, z axes respectively can be deduced:

$$v_{xi} = v_i \cos \alpha_i , \; v_{yi} = v_i \cos \beta_i , \; v_{zi} = v_i \cos \gamma_i \quad \ldots\ldots\ldots(4)$$

If a new co-ordinate system, with its axes v_x , v_y , v_z directed parallel to the x, y, z co-ordinate axes respectively, is introduced so that its origin coincides with the blast location, then the general equation of the central velocity ellipsoid in this co-ordinate system may be written as:

$$a v_x^2 + b v_y^2 + c v_z^2 + 2f v_y v_z + 2g v_z v_x + 2h v_x v_y - 1 = 0 \quad \ldots(5)$$

The unknown constants a, b, c, f, g and h can be determined by substituting the velocity components, calculated from the actual measurements as shown above, into Eq. (5). The observations at each seismometer yields one such equation and for n seismometers the following set of equations is obtained:

$$\begin{aligned}
&a v_{x1}^2 + b v_{y1}^2 + c v_{z1}^2 + 2f v_{y1} v_{z1} + 2g v_{z1} v_{x1} + \\
&\qquad + 2h v_{x1} v_{y1} - 1 = 0 \\
&a v_{x2}^2 + b v_{y2}^2 + c v_{z2}^2 + 2f v_{y2} v_{z2} + 2g v_{z2} v_{x2} + \\
&\qquad + 2h v_{x2} v_{y2} - 1 = 0 \\
&\cdots\cdots\cdots

If more than six seismometers yield equally weighted observations, it can be shown that using the principle of least squares, the most probable values of the constants can be calculated from the normal equations:

$$
\begin{aligned}
&(\Sigma v_{xi}^4)a + (\Sigma v_{xi}^2 v_{yi}^2)b + (\Sigma v_{xi}^2 v_{zi}^2)c + \\
&\quad + 2(\Sigma v_{xi}^2 v_{yi} v_{zi})f + 2(\Sigma v_{xi}^3 v_{zi})g + \\
&\quad + 2(\Sigma v_{xi}^3 v_{yi})h - \Sigma v_{xi}^2 = 0 \\
&(\Sigma v_{xi}^2 v_{yi}^2)a + (\Sigma v_{yi}^4)b + (\Sigma v_{yi}^2 v_{zi}^2)c + \\
&\quad + 2(\Sigma v_{yi}^3 v_{zi})f + 2(\Sigma v_{xi} v_{yi}^2 v_{zi})g + \\
&\quad + 2(\Sigma v_{xi} v_{yi}^3)h - \Sigma v_{yi}^2 = 0 \\
&(\Sigma v_{xi}^2 v_{zi}^2)a + (\Sigma v_{yi}^2 v_{zi}^2)b + (\Sigma v_{zi}^4)c + \\
&\quad + 2(\Sigma v_{yi} v_{zi}^3)f + 2(\Sigma v_{xi} v_{zi}^3)g + \\
&\quad + 2(\Sigma v_{xi} v_{yi} v_{zi}^2)h - \Sigma v_{zi}^2 = 0 \\
&(\Sigma v_{xi}^2 v_{yi} v_{zi})a + (\Sigma v_{yi}^3 v_{zi})b + (\Sigma v_{yi} v_{zi}^3)c + \\
&\quad + 2(\Sigma v_{yi}^2 v_{zi}^2)f + 2(\Sigma v_{xi} v_{yi} v_{zi}^2)g + \\
&\quad + 2(\Sigma v_{xi} v_{yi} v_{zi})h - \Sigma v_{yi} v_{zi} = 0 \\
&(\Sigma v_{xi}^3 v_{zi})a + (\Sigma v_{xi} v_{yi}^2 v_{zi})b + (\Sigma v_{xi} v_{zi}^3)c + \\
&\quad + 2(\Sigma v_{xi} v_{yi} v_{zi}^2)f + 2(\Sigma v_{xi}^2 v_{zi}^2)g + \\
&\quad + 2(\Sigma v_{xi}^2 v_{yi} v_{zi})h - \Sigma v_{xi} v_{zi} = 0 \\
&(\Sigma v_{xi}^3 v_{yi})a + (\Sigma v_{xi} v_{yi}^3)b + (\Sigma v_{xi} v_{yi} v_{zi}^2)c + \\
&\quad + 2(\Sigma v_{xi} v_{yi}^2 v_{zi})f + 2(\Sigma v_{xi}^2 v_{yi} v_{zi})g + \\
&\quad + 2(\Sigma v_{xi}^2 v_{yi}^2)h - \Sigma v_{xi} v_{yi} = 0
\end{aligned}
\qquad \ldots(7)
$$

In Eqs. (7) the summations are carried out over the range from 1 to k, where k is the number of observations. As stated above, it is necessary that k should be greater than 6.

When it is possible to assign weights to the individual readings (w_i), the normal equations become

$$
\begin{aligned}
&(\Sigma w_i v_{xi}^4)a + (\Sigma w_i v_{xi}^2 v_{yi}^2)b + (\Sigma w_i v_{xi}^2 v_{zi}^2)c + \\
&\quad + 2(\Sigma w_i v_{xi}^2 v_{yi} v_{zi})f + 2(\Sigma w_i v_{xi}^3 v_{zi})g + \\
&\quad + 2(\Sigma w_i v_{xi}^3 v_{yi})h - \Sigma w_i v_{xi}^2 = 0 \\
&(\Sigma w_i v_{xi}^2 v_{yi}^2)a + (\Sigma w_i v_{yi}^4)b + (\Sigma w_i v_{yi}^2 v_{zi}^2)c + \\
&\quad + 2(\Sigma w_i v_{yi}^3 v_{zi})f + 2(\Sigma w_i v_{xi} v_{yi}^2 v_{zi})g + \\
&\quad + 2(\Sigma w_i v_{xi} v_{yi}^3)h - \Sigma w_i v_{yi}^2 = 0 \\
&(\Sigma w_i v_{xi}^2 v_{zi}^2)a + (\Sigma w_i v_{yi}^2 v_{zi}^2)b + (\Sigma w_i v_{zi}^4)c + \\
&\quad + 2(\Sigma w_i v_{yi} v_{zi}^3)f + 2(\Sigma w_i v_{xi} v_{zi}^3)g + \\
&\quad + 2(\Sigma w_i v_{xi} v_{yi} v_{zi}^2)h - \Sigma w_i v_{zi}^2 = 0 \\
&(\Sigma w_i v_{xi}^2 v_{yi} v_{zi})a + (\Sigma w_i v_{yi}^3 v_{zi})b + (\Sigma w_i v_{yi} v_{zi}^3)c + \\
&\quad + 2(\Sigma w_i v_{yi}^2 v_{zi}^2)f + 2(\Sigma w_i v_{xi} v_{yi} v_{zi}^2)g + \\
&\quad + 2(\Sigma w_i v_{xi} v_{yi}^2 v_{zi})h - \Sigma w_i v_{yi} v_{zi} = 0 \\
&(\Sigma w_i v_{xi}^3 v_{zi})a + (\Sigma w_i v_{xi} v_{yi}^2 v_{zi})b + (\Sigma w_i v_{xi} v_{zi}^3)c + \\
&\quad + 2(\Sigma w_i v_{xi} v_{yi} v_{zi}^2)f + 2(\Sigma w_i v_{xi}^2 v_{zi}^2)g + \\
&\quad + 2(\Sigma w_i v_{xi}^2 v_{yi} v_{zi})h - \Sigma w_i v_{xi} v_{zi} = 0 \\
&(\Sigma w_i v_{xi}^3 v_{yi})a + (\Sigma w_i v_{xi} v_{yi}^3)b + (\Sigma w_i v_{xi} v_{yi} v_{zi}^2)c + \\
&\quad + 2(\Sigma w_i v_{xi} v_{yi}^2 v_{zi})f + 2(\Sigma w_i v_{xi}^2 v_{yi} v_{zi})g + \\
&\quad + 2(\Sigma w_i v_{xi}^2 v_{yi}^2)h - \Sigma w_i v_{xi} v_{yi} = 0
\end{aligned}
\qquad \ldots(8)
$$

Having obtained the values of constants a, b, c, f, g and h the general equation of the ellipsoid of anisotropic velocity of P-wave propagation is given by Eq. (5).

ORIENTATION OF THE ELLIPSOID OF ANISOTROPIC VELOCITY

It is known from co-ordinate geometry (Ref. 8), that in order to calculate the magnitudes of the principal axes of the velocity ellipsoid, it is necessary to determine the roots of the discriminating cubic:

$$\lambda^3 - \lambda^2(a + b + c) + \lambda(bc + ca + ab - f^2 - g^2 - h^2) - e = 0, \quad \ldots(9)$$

where $e = a(bc - f^2) - h(hc - fg) + g(hf - bg)$. It is shown in Ref. 8, that all the roots of this discriminating cubic are real.

It can also be shown, that when the principal axes are taken as co-ordinate axes Eq. (5) transforms into

$$\lambda_{\mathrm{I}}\,\xi^2 + \lambda_{\mathrm{II}}\,\eta^2 + \lambda_{\mathrm{III}}\,\zeta^2 = 1 \quad \ldots\ldots(10)$$

In Eq. (10) λ_{I}, λ_{II} and λ_{III} denote the roots of the cubic equation and ξ, η and ζ are the co-ordinates measured along the principal axes of the velocity ellipsoid. The index notation I, II and III is introduced here to distinguish between the reference number of seismometers and the principal axes.

The comparison of Eq. (10) with the normal equation of an ellipsoid yields the following relations for the magnitudes of the principal semi-axes of the velocity ellipsoid:

$$v_{\mathrm{I}} = \sqrt{1/\lambda_{\mathrm{I}}}\,, \quad v_{\mathrm{II}} = \sqrt{1/\lambda_{\mathrm{II}}}\,, \quad v_{\mathrm{III}} = \sqrt{1/\lambda_{\mathrm{III}}} \quad \ldots\ldots(11)$$

The direction cosines of the principal axes, relative to the mine co-ordinate system, can be determined by solving the following three sets of simultaneous linear equations for the corresponding values of l_j, m_j and n_j the direction cosines:

$$
\begin{aligned}
l_j(a - \lambda_j) + m_j h + n_j g &= 0 \\
l_j h + m_j(b - \lambda_j) + n_j f &= 0 \\
l_j g + m_j f + n_j(c - \lambda_j) &= 0
\end{aligned}
\quad \ldots\ldots(12)
$$

where j represents indices I, II and III in turn.

LOCATION OF THE FOCUS OF A ROCKBURST

From the recording of the seismic signals initiated by an actual rockburst, the times of arrival of the P-waves and consequently the time intervals can be determined. In this part of the paper the time intervals Δt_i denote the time lag between the seismometer which first registers the seismic event and each of the other seismometers in the network. The Δt_i's are measured quantities and include Δt_1 which is introduced for mathematical convenience, but its value will be taken to be zero. Using this notation the relative arrival time of the seismic event at the i-th seismometer can be written as

$$t_i = (t_1 + \Delta t_i) \quad \ldots\ldots(13)$$

where t_1 is an undetermined quantity and denotes the transmission time of the P-wave from the focus to the first seismometer. It should be noted that in what follows the reference numbers of the seismometers must coincide with the order in which they register the seismic signals. Therefore, the seismometer being the first, second, third and i-th in registering the arrival of the P-wave are referred to by the suffixes 1, 2, 3 and i respectively. Although the analysis includes the determination of the numerical value of t_1, it is the ultimate aim to derive expressions from which x_c, y_c and z_c, the co-ordinates of the focus of a rockburst can be calculated.

The equation of an ellipsoid referred to the principal axes of the velocity ellipsoid is given by Eq. (10). Replacing λ_{I}, λ_{II} and λ_{III} by $1/v_{\mathrm{I}}^2$, $1/v_{\mathrm{II}}^2$ and $1/v_{\mathrm{III}}^2$ respectively, Eq. (10) takes the form:

$$\frac{\xi^2}{v_{\mathrm{I}}^2} + \frac{\eta^2}{v_{\mathrm{II}}^2} + \frac{\zeta^2}{v_{\mathrm{III}}^2} = 1 \quad \ldots\ldots(14)$$

If it is required to represent the ellipsoidal travelling wave surface, Eq. (14) must be made to be a function of time. This is achieved by multiplying the semi-axes of the ellipsoid by t, the time variable. Eq. (14) then becomes:

$$\frac{\xi^2}{v_{\mathrm{I}}^2} + \frac{\eta^2}{v_{\mathrm{II}}^2} + \frac{\zeta^2}{v_{\mathrm{III}}^2} = t^2 \quad \ldots\ldots(15)$$

Since the initial data are referred to the mine co-ordinate system, it is convenient to carry out the calculations using this co-ordinate system as the basic frame of reference. Consequently Eq. (15) has to be expressed with respect to the mine co-ordinate axes. This transformation is effected by the following equations:

$$
\begin{aligned}
\xi &= l_{\mathrm{I}}\,(x_i - x_c) + m_{\mathrm{I}}\,(y_i - y_c) + n_{\mathrm{I}}\,(z_i - z_c) \\
\eta &= l_{\mathrm{II}}\,(x_i - x_c) + m_{\mathrm{II}}\,(y_i - y_c) + n_{\mathrm{II}}\,(z_i - z_c) \\
\zeta &= l_{\mathrm{III}}\,(x_i - x_c) + m_{\mathrm{III}}\,(y_i - y_c) + n_{\mathrm{III}}\,(z_i - z_c)
\end{aligned}
\quad \ldots\ldots(16)
$$

Insertion of Eqs. (13) and (16) into Eq. (15) and using the relations given by Eqs. (11) yields

$$
\begin{aligned}
&\lambda_{\mathrm{I}}\{l_{\mathrm{I}}(x_i - x_c) + m_{\mathrm{I}}(y_i - y_c) + n_{\mathrm{I}}(z_i - z_c)\}^2 + \\
&\quad + \lambda_{\mathrm{II}}\{l_{\mathrm{II}}(x_i - x_c) + m_{\mathrm{II}}(y_i - y_c) + n_{\mathrm{II}}(z_i - z_c)\}^2 + \\
&\quad + \lambda_{\mathrm{III}}\{l_{\mathrm{III}}(x_i - x_c) + m_{\mathrm{III}}(y_i - y_c) + \\
&\qquad + n_{\mathrm{III}}(z_i - z_c)\}^2 = (t_1 + \Delta t_i)^2
\end{aligned}
\quad \ldots\ldots(17)
$$

When $i = 1$, $\Delta t_1 = 0$ and

$$\lambda_I \{l_I (x_1 - x_c) + m_I (y_1 - y_c) + n_I (z_1 - z_c)\}^2 + + \lambda_{II} \{l_{II} (x_1 - x_c) + m_{II} (y_1 - y_c) + n_{II} (z_1 - z_c)\}^2 + + \lambda_{III} \{l_{III} (x_1 - x_c) + m_{III} (y_1 - y_c) + + n_{III} (z_1 - z_c)\}^2 = t_1^2 \quad \text{.....(18)}$$

Eq. (17) retains its original form when $i = 2, 3, \ldots, n$. Taking the difference of Eqs. (17) and (18) yields

$$\lambda_I \{-2l_I A_i x_c - 2m_I A_i y_c - 2n_I A_i z_c + D_i + 2G_i\} + + \lambda_{II} \{-2l_{II} B_i x_c - 2m_{II} B_i y_c - 2n_{II} B_i z_c + E_i + 2H_i\} + + \lambda_{III} \{-2l_{III} C_i x_c - 2m_{III} C_i y_c - 2n_{III} C_i z_c + + F_i + 2I_i\} = (t_1 + \Delta t_i)^2 - t_1^2 \quad \text{...(19)}$$

where
$$\begin{aligned}
A_i &= l_I (x_i - x_1) + m_I (y_i - y_1) + n_I (z_i - z_1)\\
B_i &= l_{II} (x_i - x_1) + m_{II} (y_i - y_1) + n_{II} (z_i - z_1)\\
C_i &= l_{III} (x_i - x_1) + m_{III} (y_i - y_1) + n_{III} (z_i - z_1)\\
D_i &= l_I^2 (x_i^2 - x_1^2) + m_I^2 (y_i^2 - y_1^2) + n_I^2 (z_i^2 - z_1^2)\\
E_i &= l_{II}^2 (x_i^2 - x_1^2) + m_{II}^2 (y_i^2 - y_1^2) + n_{II}^2 (z_i^2 - z_1^2)\\
F_i &= l_{III}^2 (x_i^2 - x_1^2) + m_{III}^2 (y_i^2 - y_1^2) + n_{III}^2 (z_i^2 - z_1^2)\\
G_i &= l_I m_I (x_i y_i - x_1 y_1) + l_I n_I (x_i z_i - x_1 z_1) + + m_I n_I (y_i z_i - y_1 z_1)\\
H_i &= l_{II} m_{II} (x_i y_i - x_1 y_1) + l_{II} n_{II} (x_i z_i - x_1 z_1) + + m_{II} n_{II} (y_i z_i - y_1 z_1)\\
I_i &= l_{III} m_{III} (x_i y_i - x_1 y_1) + l_{III} n_{III} (x_i z_i - x_1 z_1) + + m_{III} n_{III} (y_i z_i - y_1 z_1)
\end{aligned}$$

After further simplification and rearrangement Eq. (19) takes the form:

$$2L_i x_c + 2M_i y_c + 2N_i z_c + 2\Delta t_i t_1 = K_i - (\Delta t_i)^2 \quad \text{.....(20)}$$

where
$$\begin{aligned}
L_i &= \lambda_I l_I A_i + \lambda_{II} l_{II} B_i + \lambda_{III} l_{III} C_i\\
M_i &= \lambda_I m_I A_i + \lambda_{II} m_{II} B_i + \lambda_{III} m_{III} C_i\\
N_i &= \lambda_I n_I A_i + \lambda_{II} n_{II} B_i + \lambda_{III} n_{III} C_i\\
K_i &= \lambda_I (D_i + 2G_i) + \lambda_{II} (E_i + 2H_i) + \lambda_{III} (F_i + 2I_i)
\end{aligned}$$

When $i = 2$, 3, 4 and 5 Eq. (20) yields four linear equations with four unknowns

$$\begin{aligned}
2L_2 x_c + 2M_2 y_c + 2N_2 z_c + 2\Delta t_2 t_1 &= K_2 - (\Delta t_2)^2\\
2L_3 x_c + 2M_3 y_c + 2N_3 z_c + 2\Delta t_3 t_1 &= K_3 - (\Delta t_3)^2\\
2L_4 x_c + 2M_4 y_c + 2N_4 z_c + 2\Delta t_4 t_1 &= K_4 - (\Delta t_4)^2\\
2L_5 x_c + 2M_5 y_c + 2N_5 z_c + 2\Delta t_5 t_1 &= K_5 - (\Delta t_5)^2
\end{aligned} \quad \text{.....(21)}$$

Since the three-dimensional network has been assumed to contain at least six seismometers, it is possible to obtain a least squares solution for the location of the focus of a rockburst. In the case of equally weighted observations the normal equations replacing Eqs. (21) are

$$\begin{aligned}
(\Sigma L_i^2)x_c + (\Sigma M_i L_i)y_c + (\Sigma N_i L_i)z_c + + (\Sigma \Delta t_i L_i)t_1 - \tfrac{1}{2}\Sigma L_i\{K_i - (\Delta t_i)^2\} &= 0\\
(\Sigma L_i M_i)x_c + (\Sigma M_i^2)y_c + (\Sigma N_i M_i)z_c + + (\Sigma \Delta t_i M_i)t_1 - \tfrac{1}{2}\Sigma M_i\{K_i - (\Delta t_i)^2\} &= 0\\
(\Sigma L_i N_i)x_c + (\Sigma M_i N_i)y_c + (\Sigma N_i^2)z_c + + (\Sigma \Delta t_i N_i)t_1 - \tfrac{1}{2}\Sigma N_i\{K_i - (\Delta t_i)^2\} &= 0\\
(\Sigma L_i \Delta t_i)x_c + (\Sigma M_i \Delta t_i)y_c + (\Sigma N_i \Delta t_i)z_c + + \{\Sigma(\Delta t_i)^2\}t_1 - \tfrac{1}{2}\Sigma \Delta t_i\{K_i - (\Delta t_i)^2\} &= 0
\end{aligned} \quad \text{...(22)}$$

For unequally weighted observations, the appropriate normal equations can easily be written down by following the procedure used for deriving Eqs. (8) from Eqs. (7).

CONCLUDING REMARKS

As was stated earlier, the foregoing analysis is based on the assumption that the homogeneous rock mass is characterised by an anisotropic P-wave propagation with an ellipsoidal velocity distribution. It is obvious that a reliable location of a rockburst focus can only be obtained if this anisotropic behaviour is constant throughout the regions of the rock in which the velocity ellipsoid is determined and the rockburst phenomenon is observed. If the stipulated condition is satisfied then the application of the above analytical approach, due to the acceptance of the ellipsoidal velocity distribution, gives a flexible and a useful description of this anisotropic properties of rocks. In order to investigate the accuracy of the location of a rockburst a further application of the analysis presented is under consideration to the study of a number of important factors regarding the spatial distribution of seismometers and the effects of fractured rock around mine excavations on the velocity of P-wave propagation.

References

1. COOK, N. G. W., HOEK, E., PRETORIUS, J. P. G., ORTLEPP, W. D. and SALAMON, M. D. G.—Rock Mechanics applied to the Study of Rockbursts. *Jour. South African Inst. Min. Met.*, Vol. 66, 1966, pp. 435-528.
2. BHATTACHARYYA, A. K.—*The Application of Seismic Techniques to Problems in Rock Mechanics.* Thesis (Ph.D.), University of Newcastle-upon-Tyne, 1967.
3. BLACK, R. A. L. and HOEK, E.—Status of Rock Mechanics as applied to Mining. Status of Practical Rock Mechanics. *Proc. Ninth Symposium on Rock Mechanics, Golden, Colorado, April*, 1967, pp. 5-26.
4. JOUGHIN, N. C.—An Analysis of the Growth and Extent of the Fracture Zone around a Deep-Level Tabular Mine Excavation. *Proc. First Congress Int. Soc. Rock Mechanics, Lisbon*, 1966, Vol. 2, pp. 261-5.
5. *A Final Report on the Application of Seismic Techniques to the Problem of Rockbursts in the Mines of the Kolar Gold Mining Undertakings.* Issued by Dept. of Mining Engg., University of Newcastle-upon-Tyne, 1970.
6. DOUGLASS, P. M. and VOIGHT, B.—Anisotropy of Granites: a Reflection of Microscopic Fabric. *Geotechnique*, Vol. 19, No. 3, 1969, pp. 376-98.
7. PERES RODRIGUES, F. M.—Anisotropy of Granites. *Proc. First Congress Int. Soc. Rock Mechanics, Lisbon*, 1966, Vol. 1, pp. 721-31.
8. BELL, R. J. T.—*An Elementary Treatise on Co-ordinate Geometry of Three Dimensions.* London, Macmillan, 1928.

Settlement and Load Distribution Analysis of Pile Groups

By H. G. Poulos, B.E., Ph.D., M.I.E.Aust. and N. S. Mattes, B.E., Stud.I.E.Aust.*

Summary.—Analyses are made of the settlement interaction between two compressible floating piles in a semi-infinite mass, and between two compressible piles resting on a rigid bearing stratum. The results of these analyses are expressed in terms of interaction factors relating the increase in settlement due to the second pile to the settlement of a single pile. It is shown that, as previously found with incompressible floating pile groups, the interaction factors for two piles may be superposed to analyse the settlement and load distribution within any compressible pile group.

The influence on group behaviour of the compressibility of the piles relative to the soil is examined for square groups of piles. It is found that, for a floating pile group, the settlement interaction decreases as the piles become relatively less compressible, and for a group with a rigid pile cap, the load distribution within the group becomes more uniform. In contrast, for a group of end-bearing piles, the settlement interaction increases as the piles become relatively less compressible while the load distribution within a group having a rigid cap becomes less uniform.

Comparisons between theoretical group behaviour and that observed from model and field tests generally show good agreement.

LIST OF SYMBOLS

A_p	Cross-sectional area of pile.
D_{ij}	Pile displacement influence factor (end-bearing pile).
$[D]$	Matrix of factors of type D_{ij}.
E_p	Young's modulus of pile.
E_s	Modulus of elasticity of soil.
E'_s	Modulus of elasticity of soil skeleton.
${}_sI_{ij}$	Displacement influence factor for soil displacement at element i due to uniform stress on element j on pile i.
$[I]$	Unit matrix or order $(n + 1)$ by $(n + 1)$.
I	Pile displacement factor.
$[{}_sI]$	Matrix of soil displacement influence factors of type $({}_1I_{ij} + {}_2I_{ij})$.
K	Pile stiffness factor $= (E_p/E_s) \cdot R_A$.
L	Length of pile.
P	Load on pile.
P_{av}	Average pile load in group.
P_G	Total load on pile group.
P_i	Load on pile i in group.
R_A	Area ratio of pile $= A_p/(\pi d^2/4)$.
R_G	Group reduction factor.
R_s	Settlement ratio.
S_d	Maximum differential settlement between centre and corner piles of a group with equally-loaded piles.
S_{max}	Maximum settlement within a group with equally loaded piles.
S_R	Settlement of a group of piles with a rigid pile cap.
S_{TF}	Total final settlement.
S_u	Immediate settlement.
$[Y]$	Matrix of constants.
d	Diameter of pile.
f	Constant $= (L/d)/(n \cdot R_A)$.
h_i	Distance between centre of element i and base of pile.
$[h]$	Vector of values of h_i.
i, j, i', j'	Integers.
m	Number of piles in group.
n	Number of pile elements.
p_b	Uniform normal stress on base of pile.
p_j	Uniform shear stress around periphery of pile element j.
$[p]$	Vector of stresses p_j and p_b.
s	Centre-to-centre spacing of adjacent piles in group.
α	Pile interaction factor.
α_{kj}	Pile interaction factor between piles k and j.
δ	Length of pile element $= L/n$.
ρ	Group displacement.
ρ_1	Displacement of a single pile under unit load.
$[{}_p\rho]$	Vector of pile displacements.
$[{}_s\rho]$	Vector of soil displacements.
ν_s	Poisson's ratio of soil.
ν'_s	Poisson's ratio of soil skeleton.

*Paper No. 2925, submitted by the authors on 6th May, 1970.

The authors are, respectively, Senior Lecturer and Research Student, School of Civil Engineering, The University of Sydney.

1.—INTRODUCTION

Theoretical analyses of the behaviour of pile groups have recently been reported by Pichumani and D'Appolonia (Ref. 8) and Poulos (Ref. 9). In the former paper, solutions have been presented for the distribution of load and the displacement of square pile groups, both floating and end-bearing, in a soil which exhibits perfectly elastic-plastic behaviour. In the latter paper, the behaviour of groups of incompressible floating piles at working loads has been analysed and it has been shown that the principle of superposition may be applied to analyse the settlement and load distribution in any general pile group. Solutions have been presented for square pile groups for a wide range of cases, and the effects of group size, pile spacing and length-to-diameter ratio on the behaviour of the groups have been considered. In both papers, use is made of elastic theory, and comparisons between theoretical and observed group behaviour show reasonable agreement.

Neither of the above papers however examines the influence of the pile compressibility on group behaviour, although the method of analysis of Pichumani and D'Appolonia (Ref. 8) is capable of taking this into account. In this paper, a method for analysing the behaviour of groups of compressible piles, both floating and end-bearing, is presented. The method of analysis presented here for general pile groups has some advantage over the general computer method presented by Pichumani and D'Appolonia in that it is amenable to hand calculation. Also, in the present analysis, the shear stresses acting on the pile surface are approximated by a series of uniformly distributed loads acting around the surface of the pile whereas the analysis of Pichumani and D'Appolonia assumes a series of point loads acting along the pile axis. The former approximation has been shown to be more accurate by Poulos and Davis (Ref. 10).

Theoretical solutions for the settlement and load distribution in compressible pile groups are presented, with emphasis placed on examining the influence on group behaviour of the relative compressibility of the piles. Comparisons are then made between theoretical and observed settlement characteristics to determine the applicability of the theoretical approach to real problems. The use of the theory in practical problems is subsequently discussed.

The work in this paper is an extension of the work described by Poulos (Ref. 9) for incompressible floating groups, Mattes and Poulos (Ref. 7) for a single compressible floating pile, and by Poulos and Mattes (Ref. 11) for a single end-bearing pile. Attention is confined to the case of floating piles in a semi-infinite elastic mass and end-bearing piles resting on a rigid bearing stratum. All groups are assumed to be free-standing, i.e., there is assumed to be no contact between the soil and the pile cap. No account is taken of the effects of yield within the soil, although the analysis could be modified to take this aspect of soil behaviour into account (see for example, Pichumani and D'Appolonia, Ref. 8). However, from the analysis of a single compressible pile by Mattes and Poulos (Ref. 7), it would appear likely that the effects of local yield within the soil at normal working loads are unlikely to be significant unless the piles are very compressible.

2.—ANALYSIS OF A GROUP OF TWO PILES

2.1 Floating Piles:

Two equally-loaded, identical, cylindrical piles in an ideal semi-infinite mass having constant elastic parameters E_s and ν_s are considered, as shown in Fig. 1. The piles are of length L, diameter d and cross-sectional area A_p, and are spaced at a centre-to-centre distance s. The elastic modulus of the pile material is E_p, and each pile is divided into n equal cylindrical elements, any element j being loaded by a uniform vertical

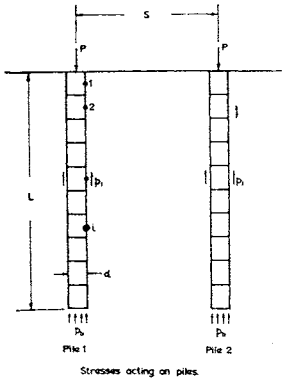

Fig. 1.—Group of Two Floating Piles.

shear stress p_j acting around the periphery of the element, and a circular base acted upon by a uniform vertical stress p_b. Since elastic conditions are assumed at the pile-soil interface, the displacements of the pile and the soil at each element are equated in order to solve for the n unknown stresses p_j, the base stress p_b, and the corresponding displacement distribution along the pile.

It has been shown by Poulos (Ref. 9) that the soil displacements at the element centres along the pile may be written as

$$[{}_s\rho] = \frac{d}{E_s}[{}_sI] \cdot [p] \quad \text{.....(1)}$$

where $[{}_sI]$ is the $n + 1$ by $n + 1$ matrix of soil displacement influence factors, any element ${}_sI_{ij}$ representing the displacement influence at point i of stress on element j of pile 1 and pile 2, and $[p]$ and $[{}_s\rho]$ are $(n + 1)$ stress and soil displacement vectors. All elements of $[{}_sI]$ are obtained by double integration of the Mindlin equation as described by Poulos and Davis (Ref. 10).

Because the condition of no slip between pile and soil has been imposed, Eq. (1) can be combined with the equation obtained by Mattes and Poulos (Ref. 7) relating pile deformations to the stresses acting over the surface of the pile to give the equation

$$[p] = \left[[I] - \frac{n^2}{4(L/d)^2} \cdot K \cdot [{}_pI] \cdot [{}_sI]\right]^{-1} \cdot [Y] \quad \text{.....(2)}$$

where $[I]$ is the unit matrix of order $n + 1$ by $n + 1$,

$K = (E_p/E_s) \cdot R_A$, the pile stiffness factor, which is a measure of the compressibility of the pile relative to the soil (the smaller the value of K, the more compressible is the pile),

$R_A = A_p/(\pi d^2/4)$ = ratio area (for solid piles, $R_A = 1$),

$[{}_pI]$ is an $(n + 1)$ by $(n + 1)$ matrix of coefficients of pile action,

$[Y]$ is an $(n + 1)$ column vector.

Eq. (2) can be solved with the equilibrium equation,

$$P = \frac{\pi dL}{n}\sum_{j=1}^{n} p_j + \frac{\pi d^2}{4} \cdot p_b \quad \text{.....(3)}$$

to obtain the unknown stresses acting on the pile, whence the displacement distribution may be determined from Eq. (1). The range of values of the pile stiffness factor K likely to occur in practical problems is discussed in Section 7 of this paper.

2.2 End-Bearing Piles:

As shown in Fig. 2, two equally-loaded identical cylindrical piles of diameter d, length L, cross-sectional area A_p and material elastic modulus E_p, resting on a perfectly rigid base, are considered. Each pile is divided into n equal cylindrical elements while the soil layer is again assumed to be an ideal elastic material with constant elastic parameters E_s and ν_s.

The soil displacement at each element may be calculated as for the floating piles, except that an allowance must be made for the influence of the rigid base on the soil displacements. An approximate method whereby this may conveniently be done has been suggested by D'Appolonia and Romualdi (Ref. 2) in which a mirror-image element j' of element j, loaded by an equal and opposite shear stress, is introduced. This method has been used by Poulos and Mattes (Ref. 11) in dealing with the behaviour of single end-bearing piles. Taking downwards displacements as positive,

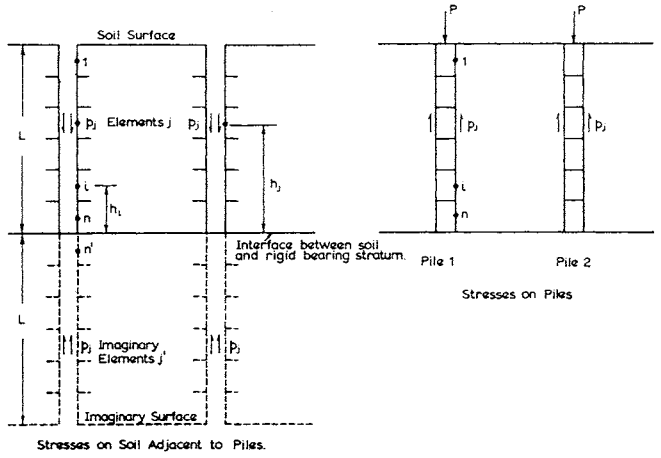

Fig. 2.—Group of Two End-Bearing Piles.

and referring to Fig. 2, the soil displacements along either pile may again be expressed by Eq. (1), where $[{}_sI]$ is now the n by n matrix of soil displacement influence factors, any element ${}_sI_{ij}$ being the influence factor for displacement at i due to the uniform shear stress on elements j of pile 1 and pile 2, and on elements j' of the imaginary mirror-image piles 1 and 2. The elements of $[{}_sI]$ are again obtained by double integration of the Mindlin equation.

Since no slip is allowed between piles and soil, the soil displacement equation may be combined with the pile action equation obtained by Poulos and Mattes (Ref. 11) to give the following equation:

$$\left[[{}_sI] + \frac{1}{Kd} \cdot [D]\right] \cdot [p] = \frac{4P}{\pi d^3 K}[h] \quad \text{.....(4)}$$

where K is the pile stiffness factor, defined in Section 2.1,

$[D]$ is an n by n matrix of coefficients related to the pile geometry,

$[h]$ is the vector of distances from the rigid base to the centre of pile elements.

Eq. (4) may be solved for the unknown stresses p on each pile whereby the displacements can be calculated. The load transferred to the pile tip is calculated as the difference between the applied load P and the sum of the shear forces acting along the pile surface.

3.—SOLUTIONS FOR TWO-PILE GROUPS

It is convenient to define the additional displacement at the top of a pile due to an equally loaded identical adjacent pile in terms of an interaction factor α (Ref. 9) where

$$\alpha = \frac{\text{additional displacement due to adjacent pile}}{\text{displacement of pile under its own load}} \quad \text{.....(5)}$$

TABLE I
Interaction Factors α for 2-Pile Groups

L/d		10				25				100			
	K	10	100	1000	∞	10	100	1000	∞	10	100	1000	∞
	s/d												
Floating Group	0	0.667	0.794	0.968	1.000	0.722	0.618	0.880	1.000	0.903	0.669	0.590	1.000
	2	0.313	0.454	0.548	0.572	0.368	0.407	0.579	0.638	0.557	0.471	0.450	0.739
	5	0.152	0.263	0.323	0.333	0.177	0.264	0.396	0.439	0.324	0.320	0.350	0.568
	10	0.078	0.144	0.180	0.188	0.092	0.164	0.265	0.293	0.176	0.204	0.268	0.440
	25	0.030	0.055	0.069	0.071	0.036	0.071	0.123	0.134	0.069	0.093	0.162	0.283
End-Bearing Group	0	0.554	0.158	0.020	0	0.702	0.388	0.079	0	0.901	0.656	0.397	0
	2	0.212	0.084	0.011	0	0.336	0.245	0.056	0	0.548	0.454	0.304	0
	5	0.062	0.030	0.004	0	0.140	0.134	0.035	0	0.312	0.299	0.230	0
	10	0.009	0.004	0.001	0	0.054	0.060	0.017	0	0.161	0.181	0.165	0
	25	0	0	0	0	0.006	0.006	0.002	0	0.052	0.068	0.080	0

Interaction curves showing the relationship between α and the dimensionless centre-to-centre spacing s/d between the piles may be obtained by solving Eqs. (2) and (3) and Eq. (5) for various values of L/d and K. Typical interaction curves are presented in Appendix A: in all cases the Poisson's ratio of the soil, ν_s, has been taken as 0.5, and the equations have been solved using $n = 10$ elements, this number having been found to give results of sufficient accuracy for practical purposes.

The interaction curves are summarised in Table I, and an inspection of this table reveals several trends in group behaviour. For both floating and end-bearing groups interaction decreases as spacing increases, but for relatively compressible floating piles interaction is still quite significant at relatively large spacings.

For floating piles, the general trend is for interaction to increase as pile stiffness increases; only for slender, very compressible piles (e.g., $K = 10$) at close spacings is the trend reversed.

For end-bearing piles, interaction decreases as L/d decreases since more load is then transmitted to the bearing stratum. In contrast to the floating piles, interaction generally decreases as stiffness increases. In most cases, the interaction between end-bearing piles is much less than for the corresponding floating piles.

In comparison with the effects of K and L/d the effect of ν_s on interaction is found to be relatively slight, and thus attention is confined to the case $\nu_s = 0.5$.

Although the solutions for floating piles are only for the case of piles in a semi-infinite mass, the solutions obtained for a single pile in a finite layer by Mattes and Poulos (Ref. 7) suggest that the finite layer will only significantly influence group behaviour for relatively incompressible piles; in such cases, use may be made of the interaction factors obtained by Poulos (Ref. 9) for incompressible piles in a finite layer.

For end-bearing piles, the influence of a bearing stratum of finite compressibility may be inferred from the solutions for a single end-bearing pile obtained by Poulos and Mattes (Ref. 11). For ratios of modulus of bearing stratum E_b to soil modulus E_s greater than 100, the bearing stratum may be considered as rigid. For smaller values of E_b/E_s, only relatively incompressible short piles are markedly influenced by the base compressibility; in such cases, an approximate, but conservative, estimate of the interaction factor may be obtained by considering the value of α for the corresponding floating pile. In all other cases involving relatively slender or relatively compressible piles, the values of α for an end-bearing pile on a rigid base may be used with sufficient accuracy.

4.—ANALYSIS OF GENERAL PILE GROUPS

As described by Poulos (Ref. 9) the analysis for two piles may be extended to any number of piles, provided that all piles in the group behave identically, i.e., that the piles are symmetrically spaced around the circumference of a circle. It has also been found that for incompressible pile groups, the displacement of the group from such an analysis is almost identical with that obtained by applying the principle of superposition, i.e., by calculating the displacement increase of a pile in the group as the sum of the displacement increases due to all the adjacent piles considered in turn. For example, for a square group of four piles at a spacing of s diameters, the displacement is given, by superposition, as

$$\rho = P_1 \rho_1 (1 + 2\alpha_1 + \alpha_2) \quad \text{.....(6)}$$

where P_1 is the load in each pile,

ρ_1 is the displacement of a single pile under unit load,

α_1 is the value of the interaction factor α for two piles at a spacing of s diameters,

α_2 is the value of α for two piles at a spacing of $s\sqrt{2}$ diameters.

Calculations have shown that the principle of superposition also applies closely to the top displacement of compressible floating and end-bearing piles. For example, the correct and approximate displacements for a three pile floating group generally agree to within 2%, while for the corresponding end-bearing group, the correct and approximate displacements agree to within 10%, the larger errors being associated with high values of K and small spacings. In view of the generally small amount of interaction between piles in the latter case, the accuracy of the method of superposition appears to be quite satisfactory for practical purposes.

As with the incompressible groups considered previously by Poulos (Ref. 9), the applicability of the principle of superposition to symmetrically-spaced groups suggests that it may be employed to analyse general pile groups. Thus, for a group of m piles, the displacement of any pile k in the group is

$$\rho_k = \rho_1 \sum_{j \neq k}^{m} P_j \cdot \alpha_{kj} + \rho_1 P_k \quad \text{.....(7)}$$

where α_{kj} is the value of α for two piles corresponding to the spacing between pile k and pile j,

P_j is the load in pile j,

ρ_1 is the displacement of a single pile under unit load.

TABLE II

Floating Pile Groups, Rigid Cap. Group Reduction Factor, R_G

$\nu_s = 0.5$

Group Size		2^2				3^2				4^2				5^2			
L/d	K / s/d	10	100	1000	∞	10	100	1000	∞	10	100	1000	∞	10	100	1000	∞
10	2	0.457	0.562	0.636	0.654	0.309	0.422	0.491	0.498	0.235	0.343	0.400	0.408	0.190	0.288	0.339	0.347
	5	0.351	0.432	0.471	0.476	0.203	0.277	0.313	0.317	0.141	0.203	0.234	0.239	0.107	0.159	0.188	0.190
	10	0.302	0.347	0.370	0.374	0.158	0.196	0.219	0.221	0.102	0.134	0.154	0.154	0.074	0.101	0.118	0.118
	20	0.276	0.295	0.310	0.310	0.135	0.152	0.166	0.166	0.083	0.097	0.109	0.109	0.056	0.069	0.079	0.079
	∞	0.250	0.250	0.250	0.250	0.111	0.111	0.111	0.111	0.062	0.062	0.062	0.062	0.040	0.040	0.040	0.040
25	2	0.497	0.534	0.662	0.718	0.334	0.404	0.538	0.588	0.264	0.336	0.465	0.506	0.216	0.290	0.411	0.450
	5	0.367	0.436	0.532	0.547	0.220	0.290	0.387	0.415	0.154	0.221	0.310	0.334	0.118	0.179	0.260	0.281
	10	0.313	0.365	0.435	0.445	0.166	0.217	0.286	0.303	0.109	0.154	0.214	0.227	0.079	0.119	0.171	0.180
	20	0.278	0.313	0.358	0.366	0.137	0.167	0.209	0.214	0.084	0.110	0.147	0.148	0.059	0.080	0.112	0.112
	∞	0.250	0.250	0.250	0.250	0.111	0.111	0.111	0.111	0.062	0.062	0.062	0.062	0.040	0.040	0.040	0.040
100	2	0.640	0.578	0.565	0.789	0.492	0.450	0.457	0.683	0.401	0.384	0.406	0.620	0.339	0.336	0.370	0.574
	5	0.471	0.470	0.502	0.661	0.311	0.327	0.375	0.541	0.234	0.253	0.311	0.471	0.187	0.207	0.270	0.422
	10	0.368	0.391	0.441	0.569	0.217	0.241	0.303	0.437	0.153	0.175	0.238	0.364	0.118	0.139	0.200	0.315
	20	0.310	0.327	0.380	0.481	0.165	0.183	0.239	0.338	0.109	0.125	0.179	0.270	0.080	0.094	0.144	0.228
	∞	0.250	0.250	0.250	0.250	0.111	0.111	0.111	0.111	0.062	0.062	0.062	0.062	0.040	0.040	0.040	0.040

Also, from equilibrium, if the total load on the pile group is P_G, then

$$P_G = \sum_{j=1}^{m} P_j \quad \text{.....(8)}$$

Eqs. (7) and (8) may be solved for two limiting conditions:

(*a*) equal load in all piles,

(*b*) equal displacement of all piles, corresponding to a perfectly rigid pile cap.

The displacement of the group so calculated may be expressed either in terms of the settlement ratio R_s of the group, where R_s is the ratio of the settlement of the group to the settlement of a single pile carrying the same *average* load as a pile in the group, or the group reduction factor R_G, where R_G is the ratio of the group settlement to the settlement of a single pile carrying the same *total* load as the group. For a group of m piles, R_s is related to R_G as follows:

$$R_s = m \,.\, R_G \quad \text{.....(9)}$$

It should be noted that for a group in which all piles carry equal load, different values of R_s and R_G may be appropriate for different piles in the group. In practical problems, R_s is likely to be the more useful quantity, but in examining the theoretical behaviour of pile groups under elastic conditions R_G has some advantage as it always lies within the range 1 to $1/m$. Consequently in the solutions described in the following section, displacements are expressed in terms of R_G. It may be helpful to note that R_G in fact represents the settlement of the group if the settlement of the corresponding single pile is unity—thus R_G is a direct measure of the settlement of a group under a given load.

To illustrate the use of the method of superposition for calculating the settlement of a pile group, an example is given in Appendix C. Solutions obtained for square groups of piles are described below.

5.—TYPICAL SOLUTIONS FOR SQUARE PILE GROUPS

Solutions have been obtained for square groups of 4, 9, 16 and 25 piles, denoted subsequently as 2^2, 3^2, 4^2 and 5^2 groups. Both floating and end-bearing piles have been considered and in each case the settlement distribution within a group in which all the piles are equally loaded, and the load distribution and settlement of a group with a rigid cap, have been investigated.

5.1 Floating Pile Groups:

Group reduction factors R_G for typical floating pile groups with rigid caps are given in Table II. For all groups, R_G decreases as the pile spacing increases, and in almost every case, R_G decreases as pile stiffness K decreases, the only exception being groups of slender, very compressible piles at very close spacings.

For a given spacing, R_G decreases as the number of piles in the group increases. If however R_G is plotted against total group breadth, as in Fig. 3, the influence of the number of piles in the group is much smaller, and for larger groups R_G does not vary greatly with the number of piles in the group. For groups containing more than 25 piles it appears that, for a practical range of group breadths, a common limiting curve of R_G versus breadth, almost coincident with the curve for the 5^2 group, is obtained. The dependence of R_G on group breadth rather than on the actual number of piles has also been noted by Poulos (Ref. 9) for incompressible groups.

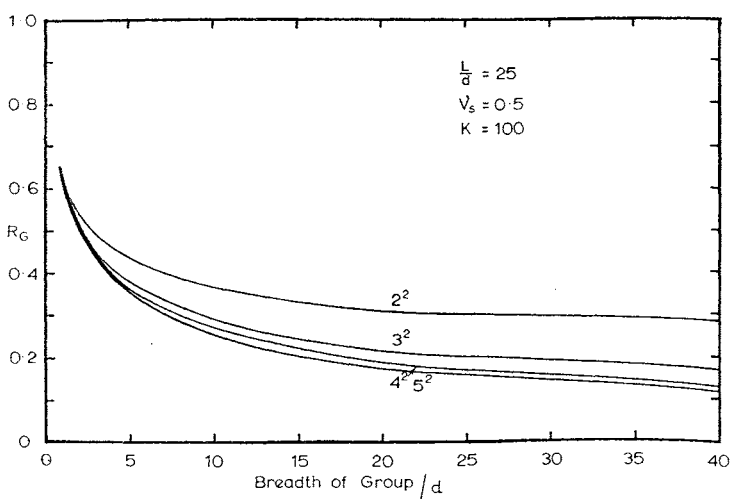

Fig. 3.—R_G versus Group Breadth—Floating Groups.

For a pile group in an ideal two-phase elastic soil mass, it is possible to calculate the ratio of immediate to total final settlement. S_u/S_{TF}, as described by Poulos and Davis (Ref. 10). It is found that for compressible groups the major portion of total final settlement occurs as immediate settlement and that pile compressibility has little influence on the value of S_u/S_{TF}.

Typical load distributions within a floating pile group with a rigid cap are plotted against pile spacing in Fig. 4 for a 3^2 group, for $K = 100$, 1000 and ∞, the pile load being expressed as a fraction of the average pile load in the group. The outer piles take the greatest load while the inner pile takes the least and as with incompressible groups, the non-uniformity of the load distribution becomes more pronounced as L/d increases and the number of piles in the group increases. Table B1 in Appendix B gives load distributions within a floating pile group for a wide range of L/d, s/d, K and group size.

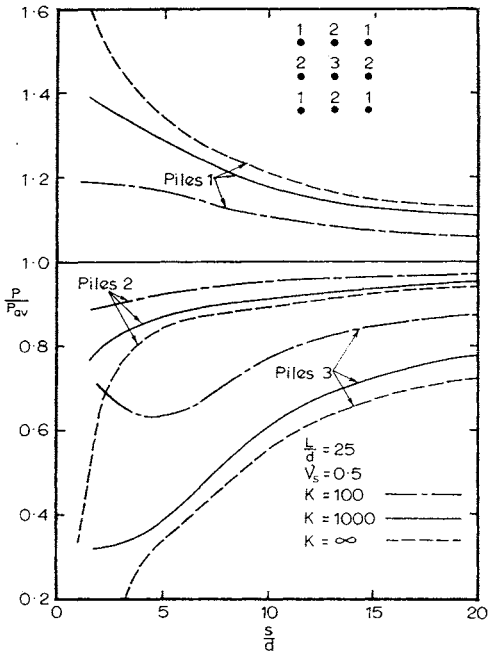

Fig. 4.—Load Distributions in 3^2 Floating Group.

For groups in which all piles are equally loaded, the maximum settlement occurs at the centre pile or piles, and the minimum at the corner piles. It is found that the ratio of the maximum settlement S_{max} of a group to the uniform settlement S_R of the corresponding group with a rigid pile cap is almost independent of pile compressibility, so that values of this ratio tabulated by Poulos (Ref. 9) for incompressible groups may be used for all values of K.

The ratio of the maximum differential settlement S_d between the centre and corner piles of the group, to the settlement S_R of the corresponding group with a rigid cap, is tabulated in Table III, for 3^2 and 5^2 groups with L/d 10, 25 and 100. Although the values in Table III are for a pile stiffness factor K of 1,000, it has been found that pile compressibility has little effect on S_d/S_R, so that the factors in Table III can be used with sufficient accuracy for all values of K.

TABLE III

Differential Settlement of Floating Pile Group

Values of S_d/S_R

L/d	10		25		100	
Group size	3^2	5^2	3^2	5^2	3^2	5^2
s/d						
2	0.155	0.310	0.110	0.208	0.045	0.117
5	0.204	0.340	0.163	0.286	0.108	0.206
10	0.170	0.280	0.170	0.312	0.130	0.226
20	0.111	0.230	0.153	0.277	0.121	0.225

5.2 End-Bearing Groups :

Group reduction factors for end-bearing pile groups with rigid caps are given in Table IV for a wide range of L/d, s/d, group size and K. In general, R_G decreases as pile stiffness increases. The smaller the value of L/d the closer the spacing at which R_G reaches its limiting value of $1/m$ (i.e., no interaction between the piles). As with floating groups, R_G decreases as the number of piles in the group increases, but if R_G is plotted against total group breadth, as in Fig. 5, it will be seen that again there appears to be a limiting curve as the number of piles in the group increases.

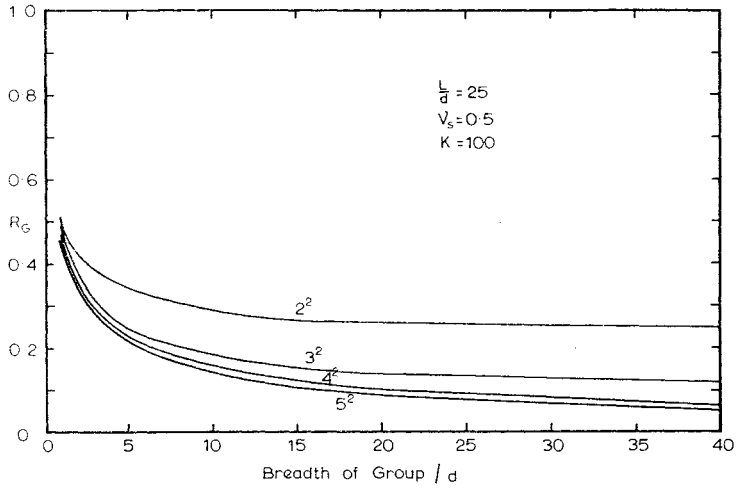

Fig. 5.—R_G versus Group Breadth—End-Bearing Groups.

As similarly found by Poulos and Mattes (Ref. 11) for a single end-bearing pile, the theoretical ratio S_u/S_{TF} of the immediate to total final settlement for groups of end-bearing piles is close to unity; for almost all cases likely to be met in practice, the time-dependent movement is less than 10% of the total final movement.

Typical load distributions within a 3^2 end-bearing group are shown in Fig. 6. As with the floating group, the non-uniformity in the load distribution increases as L/d increases, but in contrast to the corresponding floating groups, the load distribution generally becomes more uniform as pile stiffness increases. A wide range of load distributions is tabulated in Table B2 in Appendix B.

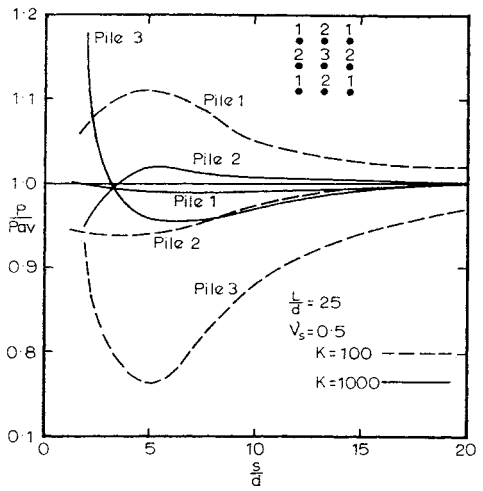

Fig. 6.—Load Distributions in 3^2 End-Bearing Group.

For end-bearing groups in which all piles are equally loaded, the maximum displacement generally occurs at the centre and the minimum at the corner. The ratios S_{max}/S_R and S_d/S_R both decrease as pile stiffness increases, and approach their limiting values of 1 and 0 respectively at relatively close pile spacings. Values of S_d/S_R are given in Table V for relatively compressible piles ($K = 100$).

6.—COMPARISONS BETWEEN THEORETICAL AND OBSERVED GROUP BEHAVIOUR

In order to assess the applicability of the theoretical approach to field cases, it is desirable to compare the theoretical solutions with the published results of observations on model and full-scale pile groups. Such a comparison was made by Poulos (Ref. 9), but no distinction was made between piles having different values of K, all piles being assumed to be incompressible. However, it is possible in some cases to estimate values of K

TABLE IV

End-Bearing Pile Groups, Rigid Cap. Group Reduction Factor, R_G

$\nu_s = 0.5$

Group Size		2^2				3^2				4^2				5^2			
L/d	K / s/d	10	100	1000	∞	10	100	1000	∞	10	100	1000	∞	10	100	1000	∞
10	2	0.379	0.285	0.250	0.250	0.224	0.146	0.111	0.111	0.149	0.093	0.062	0.062	0.108	0.065	0.040	0.040
	5	0.287	0.270	0.252	0.250	0.137	0.124	0.113	0.111	0.081	0.071	0.063	0.062	0.053	0.046	0.041	0.040
	10	0.256	0.252	0.250	0.250	0.115	0.113	0.111	0.111	0.065	0.063	0.062	0.062	0.041	0.041	0.040	0.040
	20	0.250	0.250	0.250	0.250	0.111	0.111	0.111	0.111	0.062	0.062	0.062	0.062	0.040	0.040	0.040	0.040
	∞	0.250	0.250	0.250	0.250	0.111	0.111	0.111	0.111	0.062	0.062	0.062	0.062	0.040	0.040	0.040	0.040
25	2	0.471	0.405	0.263	0.250	0.316	0.286	0.129	0.111	0.231	0.205	0.083	0.062	0.179	0.165	0.060	0.040
	5	0.341	0.341	0.271	0.250	0.186	0.189	0.129	0.111	0.121	0.125	0.077	0.062	0.086	0.089	0.051	0.040
	10	0.284	0.288	0.259	0.250	0.137	0.140	0.118	0.111	0.081	0.083	0.067	0.062	0.053	0.055	0.043	0.040
	20	0.259	0.259	0.251	0.250	0.116	0.117	0.112	0.111	0.066	0.066	0.063	0.062	0.042	0.042	0.040	0.040
	∞	0.250	0.250	0.250	0.250	0.111	0.111	0.111	0.111	0.062	0.062	0.062	0.062	0.040	0.040	0.040	0.040
100	2	0.636	0.565	0.452	0.250	0.489	0.439	0.338	0.111	0.390	0.368	0.288	0.062	0.327	0.317	0.256	0.040
	5	0.463	0.459	0.418	0.250	0.301	0.308	0.280	0.111	0.221	0.234	0.216	0.062	0.173	0.187	0.178	0.040
	10	0.359	0.373	0.365	0.250	0.204	0.221	0.220	0.111	0.138	0.155	0.158	0.062	0.101	0.119	0.124	0.040
	20	0.296	0.310	0.317	0.250	0.149	0.165	0.173	0.111	0.093	0.107	0.115	0.062	0.066	0.078	0.085	0.040
	∞	0.250	0.250	0.250	0.250	0.111	0.111	0.111	0.111	0.062	0.062	0.062	0.062	0.040	0.040	0.040	0.040

TABLE V
Differential Settlement of End-Bearing Pile Group
Values of S_d/S_R
$K = 100$

L/d	10		25		100	
Group size	3^2	5^2	3^2	5^2	3^2	5^2
s/d						
2	0.103	0.197	0.059	0.254	0.096	0.236
5	0.082	0.150	0.181	0.370	0.179	0.336
10	0.001	0.001	0.129	0.240	0.181	0.296
20	0	0	0.041	0.043	0.113	0.236

from the published data, and a summary of these cases is given in Table VI. In all cases, floating pile groups are considered. Comparisons between observed settlement ratios for square pile groups and those calculated theoretically are shown in Fig. 7. In all cases, the load level corresponds to a factor of safety of at least 2 against overall failure. It will be seen that with the exception of the tests by Hanna (Ref. 5) in loose sand, the general agreement is quite satisfactory for both large and small values of K.

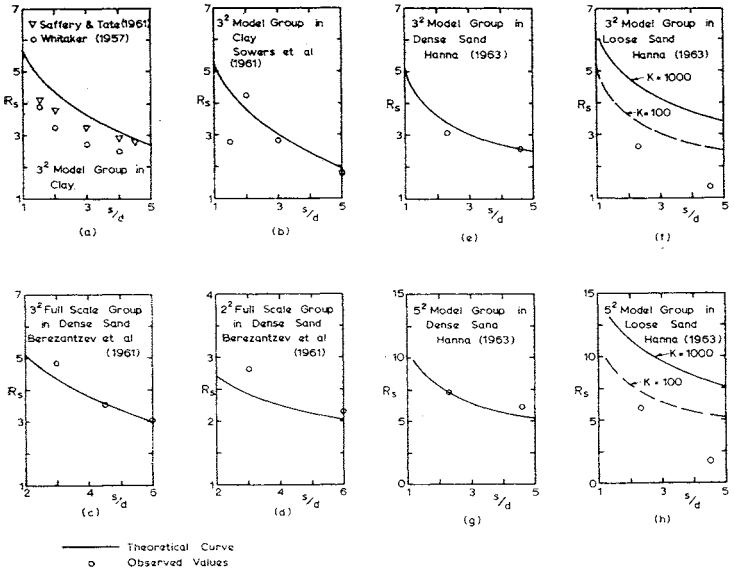

Fig. 7.—Comparison between Theoretical and Observed Settlement Ratios.

The comparisons between theoretical and observed values of R_S for the tests carried out by Hanna (Ref. 5) on wooden piles in initially loose sand (Figs. 7 (*f*) and 7 (*h*)), were made using a value of K estimated from the value of E_s for loose sand. It was found that the observed values were much less than the theoretical and this discrepancy is probably due to a greater degree of densification occurring near the group than near the single piles. However, if the value of K corresponding to dense sand is used for the theoretical values of R_S, the agreement is closer, although R_S is still over-estimated, especially at larger spacings. The less satisfactory agreement for groups in loose sand is not surprising since the local densification around the pile groups leads to inhomogeneity of the sand mass, the extent of this inhomogeneity varying as the pile spacing varies. Because of this inhomogeneity, the sand departs considerably from the ideal homogeneous elastic soil assumed in the analysis.

Comparisons between observed and theoretical load distributions within pile groups have been made by Poulos (Ref. 9). In the cases considered, the piles were effectively incompressible and the agreement between observed and theoretical distributions was found to be close. To the authors' knowledge, no further cases involving relatively low values of K are readily available.

The comparisons shown in Fig. 7, and those obtained previously by Poulos (Ref. 9) suggest that the theoretical approach described in this paper is capable of predicting with reasonable accuracy the settlement ratio and pile load distribution at working loads in practical problems. Some caution however appears desirable in applying the theory to pile groups in initially loose sand.

While no data is available on groups of end-bearing piles, the above comparisons, together with those made by Poulos and Mattes (Ref. 11) for a single end-bearing pile, suggest that a similar measure of agreement between theory and observation may be expected for end-bearing groups. A more reliable assessment of the applicability of the theory must however await results of further field measurements.

7.—APPLICATION OF THEORETICAL SOLUTIONS TO PRACTICAL PROBLEMS

In order to use the preceding theoretical solutions to estimate the immediate and total final settlement of a pile group, it is necessary to determine representative values of the 'elastic' parameters of the soil. The immediate settlement is given by putting E_s equal to the undrained Young's modulus E_u of the soil and using the displacement influence factors and interaction factors for the undrained value of Poisson's ratio ν_u, which is 0.5 for saturated clays. The total final settlement is given by putting E_s equal E'_s, the Young's modulus of the soil skeleton, and using the displacement influence factors and interaction factors for $\nu_s = \nu'_s$, Poisson's ratio of the soil skeleton. Although it is possible to carry out triaxial tests in order to determine representative values of E_u, E'_s and ν'_s (Refs. 3, 4 and 6), the initial and final stress states in the soil near a loaded pile are difficult to estimate, and consequently, the reliability of soil parameters determined in laboratory tests must at present be considered dubious. It would appear that a more satisfactory means of obtaining values of E_u, E'_s and ν'_s is to carry out an actual loading test on a single pile, the results of which may be fitted to the theoretical solutions for the settlement of a single pile to determine the required parameters. These parameters may then be used for calculating the immediate and total final settlement of the pile group.

In order to estimate the settlement of the group on a theoretical basis, it is necessary to use the influence factors for the top displacement of a single compressible pile. These have been presented by Poulos and Mattes (Ref. 11) for end-bearing piles and Mattes and Poulos (Ref. 7) for floating piles.

TABLE VI
Summary of Data on Floating Pile Group Tests

Test	Pile Material	Soil Type	Assumed Parameters for Comparison			Remarks
			L/d	K	Layer Depth/L	
Whitaker (Ref. 14)	Brass	Remoulded London Clay	24	∞	2	Model tests
Saffery and Tate (Ref. 12)	Stainless Steel	Remoulded Clay	20	∞	2	Model tests
Sowers et al (Ref. 13)	Aluminium Tube	Remoulded Bentonite	24	2000	2	Model tests
Berezantzev et al (Ref. 1)	Concrete	Dense Sand	20	1000	∞	Field tests. K estimated from quoted values of E_s.
Hanna (Ref. 5)	Wood	Dense Sand	33	100	2	Model tests. K estimated from Table IX.
Hanna (Ref. 5)	Wood	Loose Sand	33	1000	2	" " " "

For convenience, these influence factors are summarized in Tables VII and VIII for $\nu_s = 0.5$. In both cases, the variation of the influence factors with ν_s is relatively small so that, for practical purposes, the values in Tables II and III may be used for all values of ν_s.

TABLE VII

Displacement Influence Factors for a Single Floating Pile in a Semi-Infinite Mass

$\nu_s = 0.5$

Top Displacement $\rho = I \cdot (P/LE_s)$

Values of I

L/d	10	25	100
K			
10	3.26	6.78	14.45
50	2.05	4.46	12.00
100	1.80	3.58	10.61
500	1.49	2.34	6.60
1000	1.44	2.10	5.18
5000	1.41	1.90	3.26
∞	1.40	1.89	2.70

TABLE VIII

Displacement Influence Factors for a Single End-Bearing Pile Resting on a Rigid Stratum

$\nu_s = 0.5$

Top Displacement $\rho = I \cdot (PL/E_p A_p)$

L/d	10	25	100
K			
10	0.24	0.08	0.01
50	0.57	0.26	0.05
100	0.72	0.38	0.08
500	0.92	0.71	0.26
1000	0.96	0.81	0.38
5000	0.99	0.92	0.72
∞	1.00	1.00	1.00

It is also necessary to estimate a value of the pile stiffness factors K in order to use the theoretical solution. Since the value of E_s of the soil will change from E_u to E'_s as dissipation of excess pore pressures occurs around the pile, the value of K will also change during the consolidation process. However, this change in K is likely to be relatively small and, in view of the uncertainties involved in obtaining values of E_s, may be ignored. As a guide for practical problems, typical values of K for solid steel, concrete and timber piles in various types of soil were suggested by Poulos and Mattes (Ref. 11) and are reproduced in Table IX. It will be seen that, for solid piles, low values of K occur only with concrete or timber piles in stiff clays and dense sands. However, low values of K can also occur with steel pipe piles which typically have an area ratio R_A of 0.1 to 0.2, and for compacted sand piles, for which K may be as low as about 10. For such cases, the compressibility of the pile may significantly influence the behaviour of the pile group, especially if the piles are slender.

It must be borne in mind that the theoretical solutions presented in this paper are strictly only applicable to uniform soil deposits, and that various practical aspects are not taken into account by the present theory, for example, the influence of the method of pile installation, non-homogeneity and anisotropy of the soil, and layering of the soil profile. The application of the theoretical solutions to such field situations therefore requires a certain amount of engineering judgment in order to successfully reduce the actual problem to an idealized one for the purposes of analysis. It should also be reiterated that the piles are assumed free-standing and no account is taken of raft action of the pile cap. However, preliminary analyses have revealed that, at normal pile spacings, the influence of the pile cap resting on the surface on the behaviour of the group at working loads is relatively minor, although at loads approaching the ultimate, the pile cap may largely dictate the behaviour of the group. Another important factor not taken into account in the present analysis is the possibility of increased settlements due to deep-seated compressible layers situated beneath a floating pile group. A method for calculating such settlements will be presented in a subsequent paper.

TABLE IX

Average Values of K for Solid Piles*

(after Poulos and Mattes, Ref. 11)

Soil Type	Pile Material		
	Steel	Concrete	Timber
Soft Clay	60,000	6,000	3,000
Medium Clay	20,000	2,000	1,000
Stiff Clay	3,000	300	150
Loose Sand	15,000	1,500	750
Dense Sand	1,500	150	75

*For piles which are not solid, the above K values should be multiplied by the area ratio R_A.

8.—CONCLUSIONS

The displacement and load distribution within groups of compressible floating end-bearing piles has been analysed by employing the method of superposition as previously applied to incompressible floating pile groups. The influence of the relative compressibility of the piles on the behaviour of groups has been examined in relation to square groups of piles, and it has been found that for floating pile groups, the group reduction factor R_G decreases as the pile stiffness factor K decreases. For a group with a rigid pile cap, the load distribution within the group becomes more uniform as K decreases.

For end-bearing groups, the interaction between the piles in the group increases as the piles become more compressible, and consequently, the group reduction factor R_G increases as K decreases, while the load distribution within a group with a rigid pile cap becomes less uniform.

As with incompressible floating pile groups, it is found that the group settlement is dependent more on the total breadth of the group than on the number of piles in the group, and that the major proportion of the total final settlement occurs immediately for both floating and end-bearing groups.

Comparisons between theoretical values of settlement ratios and values observed in model and field tests on floating pile groups show generally good agreement and suggest that, with the possible exception of pile groups in loose sand, the theory is capable of predicting with reasonable accuracy the settlement ratio and pile load distribution at working loads in practical problems.

ACKNOWLEDGMENTS

The work described in this paper forms part of a general programme of research into the settlement of all types of foundations, being carried out at the University of Sydney under the general direction of Professor E. H. Davis, Professor of Civil Engineering (Soil Mechanics). The work is supported by a research grant from the Australian Research Grants Committee, and by the award of a Commonwealth Research Scholarship to the second author. The computational work was carried out using the facilities of the Basser Computing Department of the School of Physics at Sydney University.

References

1. Berezantzev, G. V. et al—Load Bearing Capacity and Deformation of Piled Foundations. *Proc. Fifth Int. Conf. Soil Mechanics and Foundation Engg., Paris*, 17-22 *July*, 1961, Vol. 2, pp. 11-15.
2. D'Appolonia, E. and Romualdi, J. P.—Load Transfer in End-Bearing Steel H-Piles. *Proc. A.S.C.E., Jour. Soil Mechanics and Foundations Div.*, Vol. 89, No. SM2, March, 1963, pp. 1-25.
3. Davis, E. H. and Poulos, H. G.—Triaxial Testing and Three-Dimensional Settlement Analysis. *Proc. Fourth Aust.-New Zealand Conf. Soil Mechanics and Foundation Engg., Adelaide*, 1963, pp. 233-43.
4. Davis, E. H. and Poulos, H. G.—The Use of Elastic Theory for Settlement Prediction under Three-Dimensional Conditions. *Geotechnique*, Vol. 18, No. 1, 1968, pp. 67-91.
5. Hanna, T. H.—Model Studies of Foundation Groups in Sand. *Geotechnique*, Vol. 13, No. 4, 1963, pp. 334-51.

6. LAMBE, T. W.—Stress Path Method. *Proc. A.S.C.E., Jour. Soil Mechanics and Foundations Div.*, Vol. 93, No. SM6, Nov., 1967, pp. 309-31.
7. MATTES, N. S. and POULOS, H. G.—The Settlement of a Single Compressible Pile. *Proc. A.S.C.E., Jour. Soil Mechanics and Foundations Div.*, Vol. 95, No. SM1, Jan., 1969, pp. 189-207.
8. PICHUMANI, R. and D'APPOLONIA, E.—Theoretical Distribution of Loads among the Piles in a Group. *Proc. Third Pan-American Conf. Soil Mechanics, Caracas, Venezuela*, 1967.
9. POULOS, H. G.—Analysis of the Settlement of Pile Groups. *Geotechnique*, Vol. 18, No. 4, 1968, pp. 449-71.
10. POULOS, H. G. and DAVIS, E. H.—The Settlement Behaviour of Single Axially-Loaded Incompressible Piles and Piers. *Geotechnique*, Vol. 18, No. 3, 1968, pp. 351-71.
11. POULOS, H. G. and MATTES, N. S.—The Behaviour of Axially-Loaded End Bearing Piles. *Geotechnique*, Vol. 19, No. 2, 1969, pp. 285-300.
12. SAFFERY, M. R. and TATE, A. P. K.—Model Tests on Pile Groups in a Clay Soil with Particular Reference to the Behaviour of the Group when it is Loaded Eccentrically. *Proc. Fifth Int. Conf. Soil Mechanics and Foundation Engg., Paris*, 17-22 *July*, 1961, Vol. 2, pp. 129-34.
13. SOWERS, G. F. et al—The Bearing Capacity of Friction Pile Groups in Homogeneous Clay from Model Studies. *Proc. Fifth Int. Conf. Soil Mechanics and Foundation Engg., Paris*, 17-22 *July*, 1961, Vol. 2, pp. 155-9.
14. WHITAKER, T.—Experiments with Model Piles in Groups. *Geotechnique*, Vol. 7, No. 4, 1957, pp. 147-67.

APPENDIX A
Interaction Curves for Floating and End-Bearing Two-Pile Groups

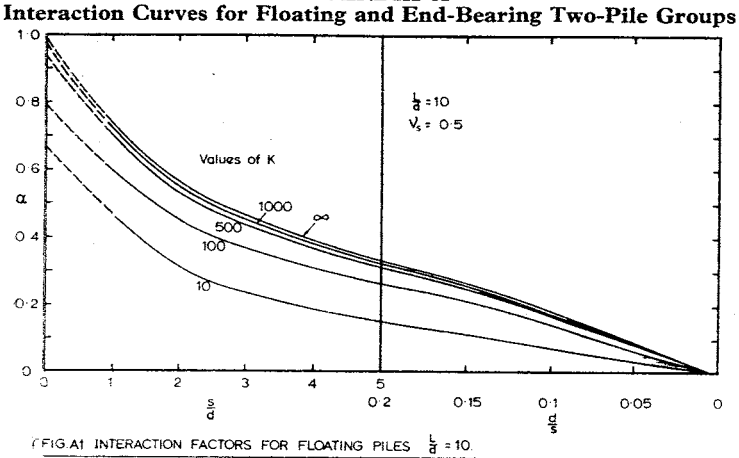

FIG.A1 INTERACTION FACTORS FOR FLOATING PILES $\frac{L}{d}$ = 10

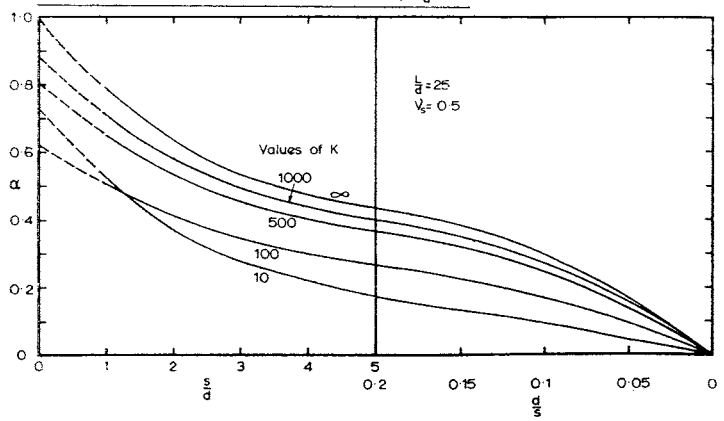

FIG.A2 INTERACTION FACTORS FOR FLOATING PILES $\frac{L}{d}$ = 25

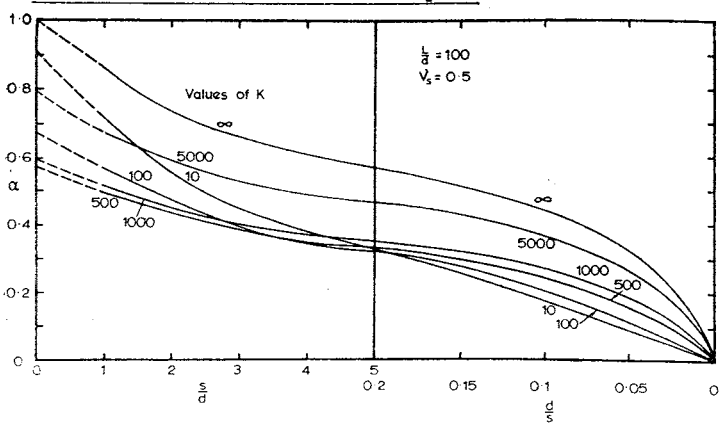

FIG.A3 INTERACTION FACTORS FOR FLOATING PILES $\frac{L}{d}$ = 100

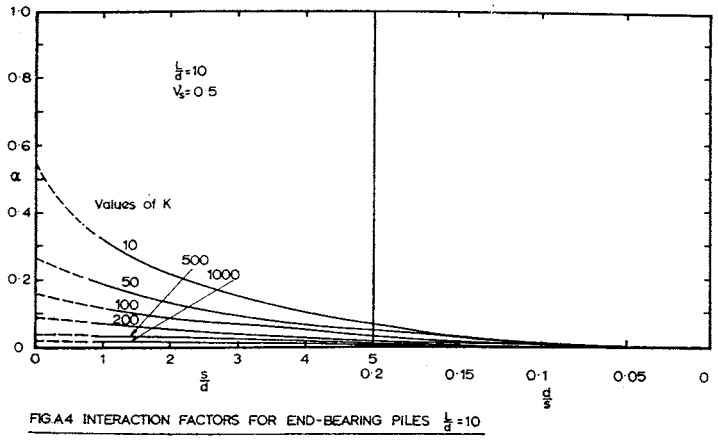

FIG.A4 INTERACTION FACTORS FOR END-BEARING PILES $\frac{L}{d}$ = 10

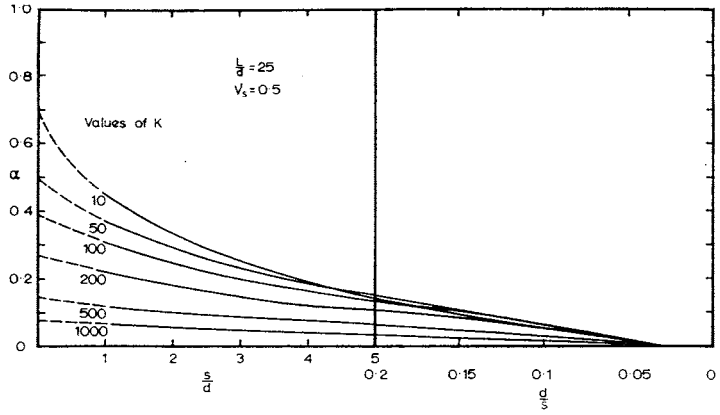

FIG.A5 INTERACTION FACTORS FOR END-BEARING PILES $\frac{L}{d}$ = 25

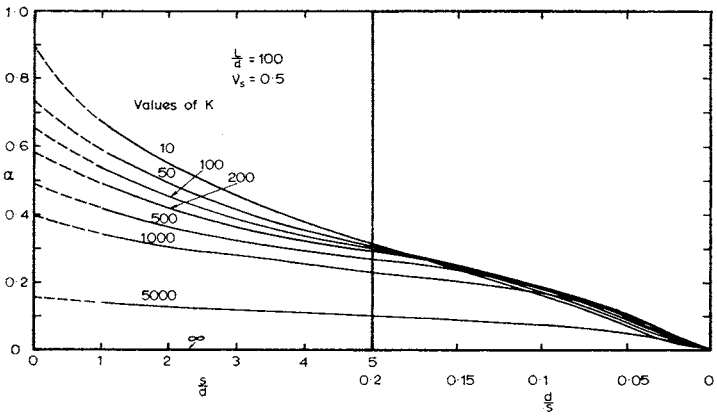

FIG.A6 INTERACTION FACTORS FOR END-BEARING PILES $\frac{L}{d}$ = 100

APPENDIX B
Load Distributions within Floating and End-Bearing Groups with Rigid Pile Caps

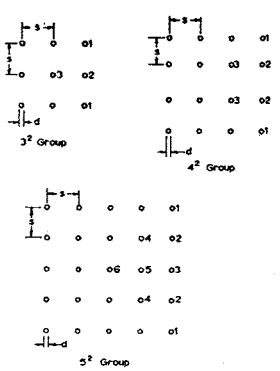

Fig. B1.—Identification of Piles in Square Groups for Tables B1 and B2.

TABLE B1

Load Distributions within Floating Pile Groups

Values of P/P_{av}

			Pile 1			Pile 2			Pile 3		
	L/d	K / s/d	100	1000	∞	100	1000	∞	100	1000	∞
3^2 Group	10	2	1.28	1.47	1.56	0.84	0.75	0.72	0.52	0.16	−0.15
		5	1.20	1.25	1.26	0.91	0.88	0.88	0.57	0.47	0.45
		10	1.10	1.13	1.14	0.95	0.94	0.94	0.78	0.73	0.70
		20	1.04	1.05	1.06	0.98	0.97	0.97	0.91	0.88	0.88
	25	2	1.18	1.38	1.50	0.89	0.79	0.65	0.71	0.32	−0.35
		5	1.17	1.29	1.32	0.92	0.87	0.84	0.63	0.38	0.34
		10	1.11	1.18	1.21	0.95	0.91	0.89	0.77	0.61	0.55
		20	1.06	1.11	1.12	0.97	0.95	0.94	0.87	0.77	0.73
	100	2	1.24	1.11	1.70	0.86	0.93	0.66	0.58	0.84	−0.45
		5	1.22	1.17	1.37	0.90	0.92	0.81	0.53	0.61	0.24
		10	1.14	1.15	1.28	0.94	0.93	0.86	0.70	0.68	0.42
		20	1.07	1.10	1.21	0.97	0.95	0.90	0.86	0.79	0.55
4^2 Group	10	2	1.68	2.00	2.14	0.97	0.95	0.95	0.38	0.09	−0.04
		5	1.42	1.51	1.52	1.01	1.00	1.00	0.56	0.48	0.47
		10	1.21	1.25	1.28	1.01	1.00	1.00	0.77	0.73	0.70
		20	1.10	1.13	1.12	1.00	1.00	1.00	0.89	0.86	0.86
	25	2	1.50	1.87	2.25	0.97	0.95	0.89	0.54	0.23	−0.05
		5	1.40	1.62	1.70	1.01	1.01	0.99	0.59	0.36	0.30
		10	1.25	1.41	1.48	1.00	1.01	1.00	0.74	0.57	0.50
		20	1.14	1.23	1.26	1.00	1.00	1.00	0.85	0.76	0.72
	100	2	1.56	.135	2.30	0.96	0.97	1.01	0.52	0.70	−0.15
		5	1.50	1.45	1.84	1.02	1.01	0.98	0.47	0.52	0.18
		10	1.29	1.35	1.65	1.00	1.00	1.00	0.70	0.63	0.34
		20	1.15	1.24	1.42	1.00	1.01	1.00	0.83	0.75	0.56

			Pile 1			Pile 2			Pile 3			Pile 4			Pile 5			Pile 6		
	L/d	K / s/d	100	1000	∞	100	1000	∞	100	1000	∞	100	1000	∞	100	1000	∞	100	1000	∞
5^2 Group	10	2	2.12	2.48	2.65	1.18	1.19	1.12	1.05	1.07	1.20	0.42	0.21	− 0.15	0.26	0.10	0.16	0.12	0.01	0.45
		5	1.64	1.75	1.79	1.13	1.14	1.15	1.07	1.09	1.10	0.60	0.53	0.49	0.55	0.49	0.46	0.49	0.45	0.42
		10	1.31	1.39	1.41	1.07	1.09	1.09	1.03	1.04	1.05	0.81	0.75	0.74	0.76	0.71	0.69	0.73	0.68	0.64
		20	1.18	1.22	1.19	1.05	1.06	1.05	1.01	1.02	1.02	0.90	0.87	0.89	0.86	0.83	0.85	0.82	0.79	0.82
	25	2	1.90	2.46	2.90	1.17	1.19	1.13	1.01	1.09	1.20	0.58	0.20	− 0.20	0.38	0.12	0.09	0.24	0.04	0.25
		5	1.62	1.98	2.11	1.14	1.18	1.19	1.05	1.09	1.07	0.63	0.40	0.35	0.54	0.34	0.27	0.46	0.29	0.22
		10	1.39	1.63	1.73	1.10	1.14	1.16	1.04	1.05	1.07	0.77	0.64	0.56	0.70	0.55	0.47	0.64	0.45	0.37
		20	1.22	1.37	1.40	1.06	1.09	1.09	1.02	1.04	1.05	0.87	0.77	0.74	0.82	0.72	0.71	0.78	0.68	0.67
	100	2	2.06	1.75	3.00	1.15	1.14	1.10	1.08	1.00	1.20	0.41	0.65	− 0.30	0.33	0.48	0.05	0.25	0.33	0.40
		5	1.77	1.78	2.34	1.18	1.18	1.22	1.07	1.06	1.09	0.54	0.55	0.21	0.48	0.42	0.14	0.33	0.30	0.07
		10	1.45	1.58	2.05	1.10	1.13	1.21	1.05	1.04	1.08	0.72	0.66	0.38	0.68	0.58	0.26	0.63	0.49	0.17
		20	1.25	1.41	1.78	1.17	1.10	1.13	1.02	1.02	1.02	0.85	0.77	0.55	0.80	0.70	0.50	0.75	0.62	0.52

TABLE B2
Load Distributions within End-Bearing Pile Groups

			Pile 1		Pile 2		Pile 3	
	L/d	K / s/d	100	1000	100	1000	100	1000
3^2 Group	10	2	0.98	0.92	0.99	1.01	1.11	1.20
		5	1.02	1.00	0.99	1.00	0.94	1.00
		10	1.00	1.00	1.00	1.00	1.00	1.00
		20	1.00	1.00	1.00	1.00	1.00	1.00
	25	2	1.07	0.95	0.94	1.00	0.93	1.17
		5	1.11	1.02	0.94	0.99	0.76	0.96
		10	1.05	1.01	0.98	0.99	0.88	0.97
		20	1.02	1.00	1.00	1.00	0.97	1.00
	100	2	1.22	1.02	0.87	0.97	0.65	1.04
		5	1.21	1.13	0.90	0.94	0.53	0.73
		10	1.13	1.10	0.94	0.95	0.71	0.78
		20	1.06	1.06	0.97	0.97	0.88	0.87
4^2 Group	10	2	1.04	0.88	0.98	0.98	1.00	1.17
		5	1.05	1.00	1.00	1.00	0.94	1.00
		10	1.00	1.00	1.00	1.00	0.99	1.00
		20	1.00	1.00	1.00	1.00	1.00	1.00
	25	2	1.26	0.95	0.98	0.98	0.77	1.10
		5	1.23	1.05	1.01	1.00	0.75	0.94
		10	1.10	1.02	1.00	1.00	0.88	0.98
		20	1.02	1.00	1.00	1.00	0.98	1.00
	100	2	1.61	1.19	0.97	0.98	0.44	0.86
		5	1.48	1.33	1.00	1.00	0.51	0.65
		10	1.27	1.23	1.00	1.00	0.72	0.75
		20	1.14	1.13	1.00	1.00	0.85	0.84

			Pile 1		Pile 2		Pile 3		Pile 4		Pile 5		Pile 6	
	L/d	K / s/d	100	1000	100	1000	100	1000	100	1000	100	1000	100	1000
5^2 Group	10	2	1.11	0.86	1.02	0.94	0.95	0.95	0.99	1.13	0.90	1.14	0.81	1.18
		5	1.06	1.01	1.02	1.00	1.01	1.00	0.96	1.00	0.95	1.00	0.94	1.00
		10	1.00	1.00	1.00	1.00	1.00	1.00	1.00	1.00	1.00	1.00	1.00	1.00
		20	1.00	1.00	1.00	1.00	1.00	1.00	1.00	1.00	1.00	1.00	1.00	1.00
	25	2	1.55	0.99	1.12	0.99	0.99	0.96	0.77	1.07	0.59	1.03	0.44	0.99
		5	1.37	1.09	1.09	1.03	1.04	1.00	0.77	0.95	0.72	0.92	0.67	0.87
		10	1.15	1.03	1.04	1.01	1.02	1.01	0.90	0.98	0.88	0.97	0.86	0.97
		20	1.02	1.00	1.00	1.00	1.00	1.00	0.98	1.00	0.98	1.00	0.98	1.00
	100	2	2.08	1.48	1.20	1.11	1.01	0.96	0.48	0.83	0.25	0.63	0.36	0.44
		5	1.75	1.55	1.16	1.13	1.08	1.04	0.53	0.68	0.46	0.58	0.39	0 47
		10	1.42	1.39	1.08	1.09	1.04	1.04	0.73	0.77	0.70	0.71	0.67	0.65
		20	1.21	1.22	1.05	1.05	1.01	1.01	0.88	0.87	0.83	0.82	0.79	0.78

APPENDIX C

Illustrative Example:

A free-standing group of six 12 in. dia. concrete piles is driven into a deep layer of medium clay, and is to be subjected to a load of 300 tons (see Fig. C1). A test on a single pile gives a final settlement of 0.60 in. under a load of 50 tons. It is required to determine the final settlement of the 6-pile group.

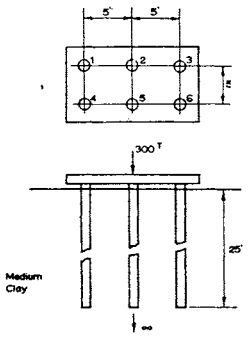

Fig. C1.

From Table IX, the value of K is about 2,000. Piles 1, 3, 4 and 6 behave identically and will be called piles A while piles 2 and 5 will be called piles B. The loads on Piles A and B are P_A and P_B respectively. From Fig. A2 for $L/d = 25$, the interaction factors may be interpolated for $K = 2{,}000$. The factors are tabulated in Table C1.

The settlement of pile 1 (and all piles A) is given by Eq. (7), as

$$\rho_A = \rho_1\{P_A(0.27 + 0.42 + 0.25) + P_B(0.42 + 0.35) + P_A\}$$

i.e.,

$$\rho_A/\rho_1 = 1.94\,P_A + 0.77\,P_B \quad \text{.....(C1)}$$

where ρ_1 is the settlement of a single pile under unit load. Similarly for pile 2 (and all piles B),

$$\rho_B = \rho_1\{P_A(0.42 + 0.42 + 0.35 + 0.35) + P_B(0.42) + P_B\}$$

i.e.,

$$\rho_B/\rho_1 = 1.54\,P_A + 1.42\,P_B \quad \text{.....(C2)}$$

TABLE C1

	Pile 1 (Type A)		Pile 2 (Type B)	
Pile j	s/d	α_{1j}	s/d	α_{2j}
1	0	—	5	0.42
2	5	0.42	0	—
3	10	0.27	5	0.42
4	5	0.42	7.07	0.35
5	7.07	0.35	5	0.42
6	11.2	0.25	7.07	0.35

Also, from equilibrium,

$$4P_A + 2P_B = 300 \quad \text{.....(C3)}$$

For a rigid cap, $\rho_A = \rho_B$.

Solution of Eqs. (C1), (C2) and (C3) for this case yields the following solutions:

$$P_A = 57.4 \text{ tons}$$
$$P_B = 35.2 \text{ tons}$$
$$\rho_A/\rho_1 = \rho_B/\rho_1 = 138.4$$

From the pile load test,

$$\rho_1 = 0.60/50 = 0.012 \text{ in./ton.}$$
$$\therefore \quad \rho_A = \rho_B = 1.66 \text{ in.}$$

(The settlement ratio $R_S = \dfrac{1.66}{0.60} = 2.77$.)

If the pile cap is sufficiently flexible and the load is uniformly distributed so that all piles are equally loaded, then

$$P_A = P_B = 50 \text{ tons}$$
$$\rho_A = 50 \times 2.71 \times \rho_1 = 1.62 \text{ in.}$$
$$\rho_B = 50 \times 2.96 \times \rho_1 = 1.77 \text{ in.}$$

Displacements in a Soil Mass Due to Pile Groups

BY H. G. POULOS, B.E., PH.D., M.I.E.AUST. and N. S. MATTES, B.E., STUD.I.E.AUST.*

LIST OF SYMBOLS

A_p Cross-sectional area of pile.
D Depth of finite layer.
E_p Young's modulus of pile material.
E_s Modulus of elasticity of soil.
E_{sj} Modulus of elasticity of soil layer j.
E'_s Modulus of elasticity of soil skeleton.
E_u Undrained modulus of elasticity of soil.
H Depth of point below soil surface.
$_pI$ Influence factor for vertical displacement due to a vertical point load.
I_{ib} Influence factor for displacement at i due to the base stress p_b.
I_{ij} Influence factor for displacement at i due to uniform shear stress at j.
$I_{i,j}$ Influence factor for displacement beneath the centre of the pile group for the level of the top of layer j due to pile i.
I_j Displacement influence factor on the pile axis at the level of the top of layer j.
I_{xj} Displacement influence factor I for $H/L = 0$ corresponding to the distance between the centre of pile j and the point x.
I'_{xj} Value of I for $H = D$ corresponding to the distance between the centre of pile j and the point x.
I_ρ Influence factor for displacement due to a single pile.
I Influence factor for displacement of a pile in a layer of depth D.
K Pile stiffness factor, $= (E_p/E_s) \cdot R_A$.
L Length of pile.
L_e Length of equivalent pier.
P Total load on pile.
P_{av} Average pile load.
P_i, P_j Load in pile i and pile j respectively.
R_s Settlement ratio.
Z, Z_1, R, R_1, c Variables in Mindlin's equation (Fig. 1 (*b*)).
d Diameter of pile shaft.
d_b Diameter of pile base.
d_e Diameter of equivalent pier.
i, j Integers.
m Total number of different layers.
n Number of pile elements.
p Uniformly distributed shear stress.
p_b Uniform vertical stress on base.
p_j Uniform shear stress on element j.
r Radial distance.
δ Height of pile element $= L/n$.
ρ Displacement.
ρ_{GD} Displacement of the pile group in a layer of depth D and modulus of elasticity E_1 which is underlain by a rigid base.
ρ_i Displacement at i due to all elements of the pile.
ρ_x Displacement at point x.
ν_s Poisson's ratio of soil.

1.—INTRODUCTION

The settlement behaviour of single piles and pile groups has recently been examined theoretically in a series of papers (Refs. 5, 9, 10 and 11). In these papers, solutions have been obtained for the settlement at the head of a pile or pile group situated in an ideal elastic homogeneous soil mass, and it has been found that such solutions for an ideal soil reproduce observed behaviour of piles in real soils with encouraging accuracy. In many cases in practice however, the soil profile is layered with compressible layers present below the piles, and hence the solutions previously obtained for the displacement of piles in a uniform soil may not be directly applicable. An outstanding example of such a case has been reported by Golder and Osler (Ref. 4) in which a pile foundation supporting a furnace was founded in compact sand which was underlain at a considerable depth by a deep deposit of compressible clay. It was found that the settlement of the piles in the sand was responsible for only about 10% of the final settlement, the remaining 90% being attributable to the underlying clay deposit. In view of the not-infrequent occurrence of such situations, it is desirable to develop a method by which the settlement of compressible soil layers underlying the piles may be determined. In some cases, it may also be of interest to estimate the settlement of the ground surface at some distance away from the piles, for example, in determining the additional settlement of an existing building due to a new structure.

In this paper, the above two problems are considered in detail. Numerical solutions are obtained firstly for the vertical displacement within a soil mass due to a single loaded pile, and using these solutions, methods are described for calculating the surface displacement profile around a pile group and the settlement of soil layers beneath a pile or pile group.

In obtaining the solutions for the displacements due to a single pile, it is assumed that no local yield occurs between the pile and the soil and that conditions within the soil remain purely elastic. Also, in considering the settlement of pile groups, the groups are assumed to be free-standing with no contact between the pile cap and the soil. Analysis has shown that, even if the pile cap is, in fact, in contact with the soil, it has little influence on the settlement of the group, provided the pile spacing is relatively close and elastic conditions prevail within the soil.

2.—ANALYSIS

A pile of length L, shaft diameter d, base diameter d_b, area A_p and Young's modulus E_p, is situated in an ideal elastic homogeneous isotropic soil mass having parameters E_s and ν_s. At any point i within the soil mass, the vertical displacement due to the stress p_j on a cylindrical element j may be obtained by double integration of the Mindlin equation for the vertical displacement due to a vertical point load within a semi-infinite elastic mass. Referring to Fig. 1 (*a*), the displacement influence factor for the point i due to loading on element j is

$$I_{ij} = 2\int_{(N-1)\delta}^{N\delta}\int_0^\pi {}_pI\,\frac{d}{2}\,d\theta\,dz \qquad \text{.....(1)}$$

where $\delta = L/n$,

$_pI$ = Influence factor for vertical displacement due to a vertical point load.

From Mindlin's equation,

$$_pI = \frac{(1+\nu_s)}{8\pi(1-\nu_s)E_s}\left[\frac{z_1^2}{R_1^3} + \frac{(3-4\nu_s)}{R_1} + \frac{5-12\nu_s+8\nu_s^2}{R} + \frac{(3-4\nu)z^2 - 2cz + 2c^2}{R^3} + \frac{6cz^2(z-c)}{R^5}\right] \qquad \text{.....(2)}$$

where z_1, z, R_1, R and c are geometrical parameters defined in Fig. 1 (*b*).

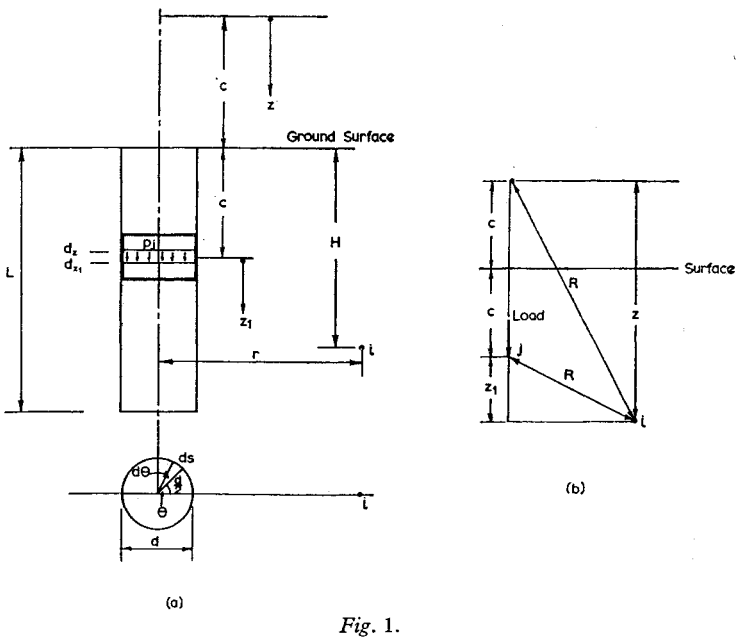

Fig. 1.

As described by Poulos and Davis (Ref. 10), the integration with respect to z is done analytically, while the integration with respect to θ is done numerically.

*Paper No. 2969, submitted by the authors on 28th August, 1970.
The authors are, respectively, Senior Lecturer and Research Student, School of Civil Engineering, The University of Sydney.

Similarly, the influence factor for vertical displacement at i due to the uniform base stress p_b is given by

$$I_{ib} = \int_0^{2\pi} \int_0^{d_b/2} {}_pI \, r \, dr \, d\theta \qquad \text{.....(3)}$$

where ${}_pI$ is given by Eq. (2).

The integration is done analytically with respect to r and numerically with respect to θ.

The displacement at point i due to all elements of the pile is then given by

$$\rho_i = \sum_{j=1}^{n} I_{ij} \, p_j + I_{ib} \, p_b \qquad \text{.....(4)}$$

Values of p_j and p_b have been obtained for various values of L/d by Poulos and Davis (Ref. 10) for incompressible piles, and Mattes and Poulos (Ref. 5) for compressible piles. In the latter paper, the relative compressibility of the pile is defined by the pile stiffness factor $K = (E_p/E_s) \cdot R_A$, where $R_A = A_p/(\pi d^2/4)$. The larger K, the less compressible is the pile. These values have been used with the values of I_{ij} and I_{ib} calculated from Eqs. (1) and (3) to obtain displacement distributions for a wide range of cases. In evaluating I_{ij} and I_{ib}, intervals of $\pi/20$ have been used for the numerical integrations. In all cases computed, d_b has been taken equal to d.

3.—DISPLACEMENT DISTRIBUTIONS DUE TO A SINGLE LOADED PILE

Influence factors I_ρ for the displacement due to a single loaded pile have been obtained for values of L/d ranging from 1 to 100 and are shown in Figs. 2 to 7 for various dimensionless depths H/L and radii r/L, and for $\nu_s = 0.5$. The actual displacement ρ is given by

$$\rho = \frac{P}{L \, E_s} \cdot I_\rho \qquad \text{.....(5)}$$

In Figs. 2 to 6, $K = 1000$, while in Fig. 7, values of I_ρ are given for $K = 20\,000$, for $L/d = 100$. K has a considerable influence on the displacements near the pile for $L/d > 10$, I_ρ increasing as K decreases, but only a small influence for $L/d < 10$ or at points remote from the pile. The influence of ν_s on I_ρ is relatively small, especially for $L/d > 10$, so that for practical purposes, the values of I_ρ for $\nu_s = 0.5$ may be used for all values of ν_s.

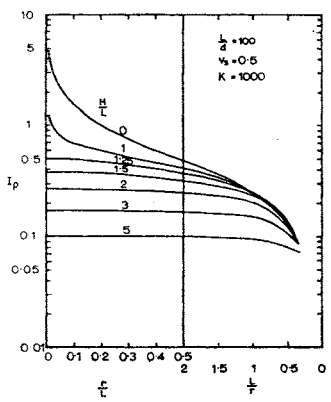

Fig. 2.—Displacement Influence Factors.

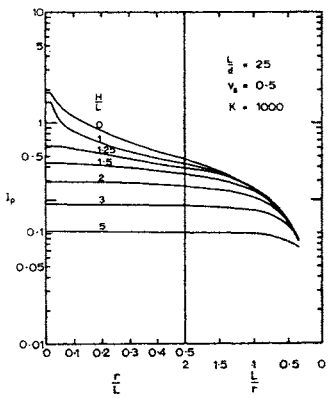

Fig. 3.—Displacement Influence Factors.

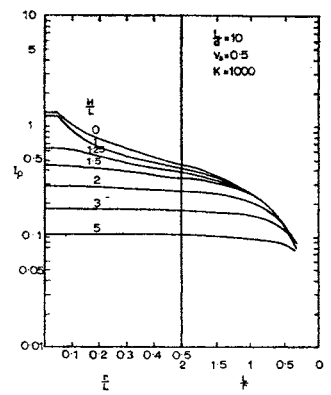

Fig. 4.—Displacement Influence Factors.

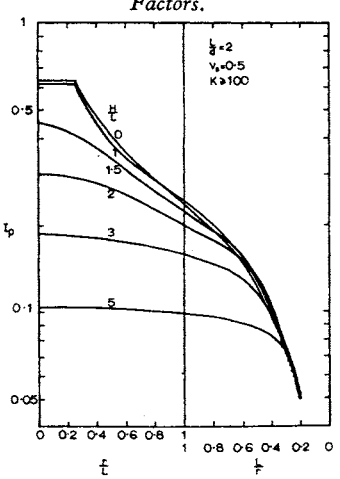

Fig. 5.—Displacement Influence Factors.

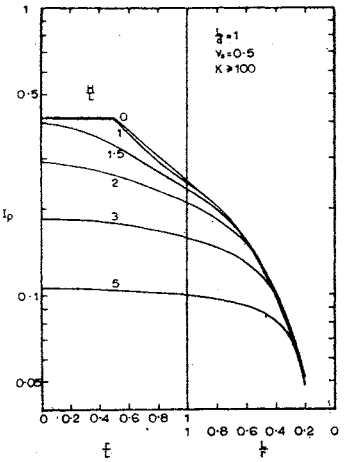

Fig. 6.—Displacement Influence Factors.

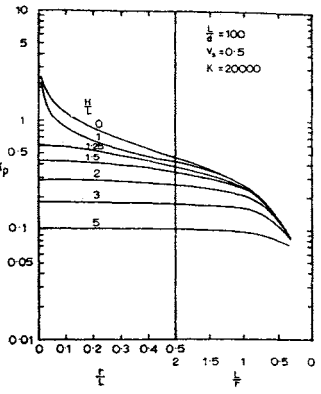

Fig. 7.—Displacement Influence Factors.

For points remote from the axis, it is found that the pile may be replaced by a point load of magnitude equal to the load on the pile, and acting at a depth of $2/3L$ below the surface. The Mindlin equation for vertical displacement due to a point load may then be used, viz.,

$$\rho = P \cdot {}_pI \qquad \text{.....(6)}$$

where P is the total load on the pile, and ${}_pI$ is defined in Eq. (2).

On the soil surface ($H = 0$), this equation reduces to the following simple form:

$$\rho = \frac{P(1 + \nu_s)}{2\pi \, E_s} \left[\frac{c^2}{R^3} + \frac{2(1 - \nu_s)}{R} \right] \qquad \text{.....(7)}$$

where $R = (c^2 + r^2)^{\frac{1}{2}}$.

It is found that for $r/L \geqslant 0.4$, the surface displacement calculated from Eq. (7) gives a value which agrees to within $\pm$ 3% of the more correct value calculated from Eq. (4), provided that $L/d \geqslant 10$. Even for shallow piers (e.g., $L/d = 1$), the use of Eq. (7) for surface displacements gives results almost identical with the more correct analysis for $r/L \geqslant 0.75$.

4.—DETERMINATION OF SURFACE DISPLACEMENT PROFILE DUE TO A PILE GROUP

The displacement distributions for a single pile in Figs. 2 to 7 may be used to determine the surface displacement profiles due to a loaded pile group by superposition of the displacements due to each individual pile in the group at the point in question. Thus, for a group of n piles situated in a deep homogeneous soil layer, the displacement ρ_x at a point X on the soil surface is

$$\rho_x = \frac{1}{L \, E_s} \sum_{j=1}^{n} P_j \, I_{xj} \qquad \text{.....(8)}$$

where P_j is the load on pile j,

I_{xj} is the displacement influence factor I_ρ, for $H/L = 0$, corresponding to the distance between the centre of pile j and the point X.

It should be noted that in this method, no account can be taken of the reinforcing effect of any piles which may be present between the point X and the pile j. The presence of such piles will tend to decrease the influence of pile j on the displacement at X and hence the displacement will be overestimated by using Eq. (8). Some indication of the extent to which the displacement may be overestimated may be inferred from Fig. 8 (see later) which suggests that the overestimate will be relatively small.

If the pile group is situated on a finite layer of depth D, which is underlain by a rigid base, the Steinbrenner approximation (Ref. 13) may be used to estimate the displacements. In this case,

$$\rho_x = \frac{1}{L \, E_s} \sum_{j=1}^{n} P_j \, (I_{xj} - I'_{xj}) \qquad \text{.....(9)}$$

where I'_{xj} is the value of I_ρ for $H = D$ and for the value of r equal to the distance between the centre of pile j and the point X.

The work of Davis and Taylor (Ref. 2) and Poulos (Ref. 8) in connection with surface footings suggests that the above approximation will be reasonably accurate in the vicinity of the pile but may be inaccurate remote from the pile (e.g., for $r/D > 1$) or for very shallow layers.

If the pile group has a rigid cap, the distribution of loads P_j within the group will generally be non-uniform. This load distribution may be calculated by the method described by Poulos (Ref. 9) and Poulos and Mattes (Ref. 12). For square groups of incompressible piles, values of P_j are tabulated by Poulos (Ref. 9) for 3^2, 4^2 and 5^2 groups for $L/d = 25$, while some load distributions for groups of compressible floating piles are presented by Poulos and Mattes (Ref. 12).

In cases in which the load distribution within a group is not available or where a rough estimate only of the surface displacement is required, it is more convenient to assume a uniform distribution of pile loads (i.e., $P_j = P/n$) or else, if the group is large, to consider it as an equivalent single pier. In the latter case, the diameter of the pier should be taken such that the cross-sectional area of the equivalent pier equals the gross plan area of the group while the equivalent length of the pier may generally be taken in the range $0.6L$ to $0.9L$ (Ref. 9).

For a square group of 9 piles with a centre-to-centre spacing of 5 dia., Fig. 8 shows a typical comparison between the surface displacement profile for the group with a rigid cap, calculated from Eq. (9), that calculated by assuming the pile loads in the group are equal (i.e., that the pile cap is perfectly flexible) and that calculated by assuming the group to have a rigid cap and to be a single equivalent cylindrical pier of equivalent length $L_e = 0.8L$. It will be seen that there is close correspondence between all three displacement profiles away from the immediate vicinity of the group. Underneath the pile group, the displacement distribution for the case of equal loads in all piles is not uniform and hence there is some difference between this case and the other two curves for a rigid pile cap. However, the differences are localised and for $x/L \geqslant 0.3$, the surface displacement profile for equal pile loads is virtually identical with that for the case of a rigid pile cap. Remote from the group, there is, however, a small discrepancy between the profile for the equivalent single pier and the profiles calculated for the actual group, the displacements in the latter case being greater than those for the equivalent pier. This discrepancy may possibly reflect the small order of overestimation of displacement involved in neglecting the reinforcing effect of intervening piles when using Eq. (9).

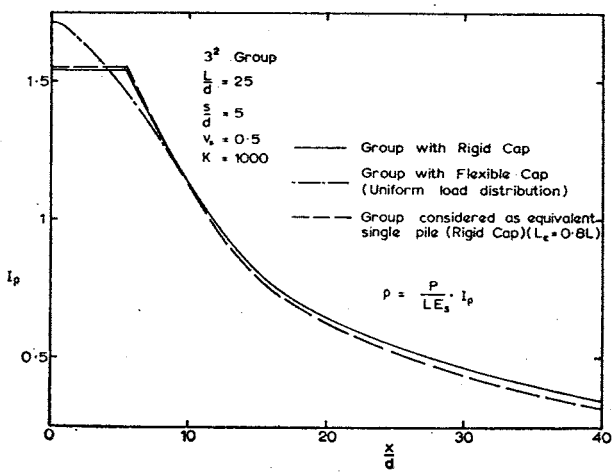

Fig. 8.—Comparison between Correct and Approximate Surface Displacement Profiles.

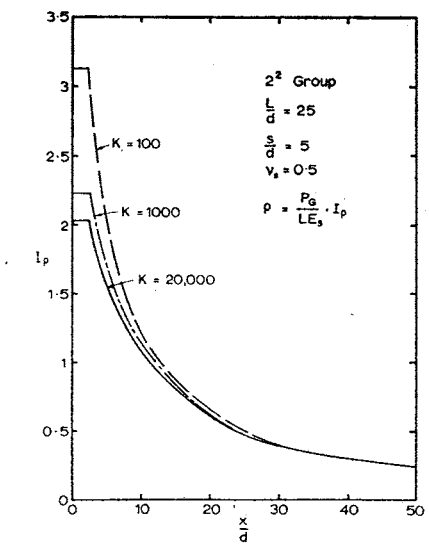

Fig. 9.—Influence of K on Surface Displacement Profiles.

Typical surface displacement profiles are shown in Fig. 9 for a square four-pile group (2^2 group) in a semi-infinite mass. The increased displacements with decreasing values of K are clearly shown. However, for $x/L > 1$, the surface displacements are almost independent of K.

The influence of the layer depth on the surface displacement profile is shown in Fig. 10 for a 2^2 group. As the layer depth decreases, the surface displacements are "damped" and, for relatively shallow layers (e.g., $D/L = 1.5$), may be negligible at distances of one pile length or more from the centre of the group.

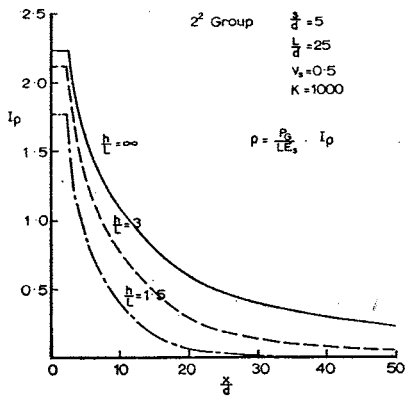

Fig. 10.—Influence of Layer Depth on Surface Displacement Profiles.

5.—DETERMINATION OF SETTLEMENT OF PILES AND PILE GROUPS UNDERLAIN BY LAYERED STRATA

The method outlined in the previous section for calculating surface displacement may be extended to the case where a pile or pile group is founded in a homogeneous layer which is underlain by further layers of different soils. In this case, the settlement may be calculated approximately by adding to the settlement of the pile or pile group in the founding layer, the contributions of the underlying layers.

Considering first the case of a single pile founded in a uniform layer of depth D, a convenient method of calculating the settlement of the pile is as follows:

$$\rho = \frac{P I_1}{L E_{s1}} + \frac{P}{L}\left\{\sum_{j=2}^{m-1} \frac{(I_j - I_{j+1})}{E_{sj}} + \frac{I_m}{E_{sm}}\right\} \qquad \text{.....(10)}$$

where I_1 = displacement influence factor for a pile in a layer of depth D (obtained from Poulos and Davis (Ref. 10) for incompressible piles, Mattes and Poulos (Ref. 5) for compressible piles or Poulos and Mattes (Ref. 11) for end-bearing piles),

I_j = displacement influence factor on the pile axis at the level of the top of layer j (obtained from Figs. 2 to 7),

E_{sj} = Young's modulus of layer j,

m = total number of different layers (including the founding layer).

The above method of calculation is similar to that suggested by Nair (Ref. 7) for piles and that used by Egorov et al (Ref. 3) for surface foundations and, in effect, makes use of the Steinbrenner approximation for the calculation of the displacements of the underlying layers.

Before proceeding, it is useful to consider briefly the limitations of Eq. (10) to calculate settlements. The major limitation is that no account is taken of the influence of changes in stress distribution below the pile which may occur because of the layering of the soil profile. In particular, if a stiffer layer overlies a softer layer, some concentration of stress into the stiffer layer will occur. Although the influence of such stress concentration on pile behaviour cannot readily be determined at the present time, some idea of the errors involved in using Eq. (10) may be obtained by considering the case of a circular surface footing on a two-layer elastic system underlain by a rough rigid base. It is found that the displacements calculated from Eq. (10) are generally greater than the more correct values, (obtained either from Burmister (Ref. 1) or from Odemark's method, quoted by Ueshita and Meyerhof (Ref. 14)). The errors are greatest when a stiff layer of considerable thickness overlies a thick softer layer, but unless the ratio of the Young's moduli of the upper and lower layers is greater than about 10, the resulting overestimate is not serious. Furthermore, if softer layers overlie stiffer layers, Eq. (10) gives a displacement which agrees closely with the correct value.

A further limitation of Eq. (10) is that it inherently assumes that the shear stress distribution along the pile is that for a pile in a semi-infinite homogeneous soil mass and is unaffected by any heterogeneity of the soil below the pile. For cases involving different soil layers at some depth below the pile tip, the above assumption should be satisfactory as it has been found by Poulos and Davis (Ref. 10) that the shear stress distribution remains substantially unchanged if a rigid base exists below the tip of the pile. However, the approximation may be in error if the pile bears directly on to a stratum of considerably greater stiffness than the upper layer. The distribution of shear stress along the pile in this case may be considerably different from that for a pile in a semi-infinite mass, especially if the pile is relatively incompressible (Poulos and Mattes, Ref. 11). In such a case, the displacement factor for the pile in the upper layer of depth H should be calculated from the solutions for an end-bearing pile presented by Poulos and Mattes (Ref. 11). The displacement factors for the underlying layers are calculated as before.

It therefore appears that Eq. (10) will give a reasonable estimate of the settlement of the pile unless a very stiff layer of considerable thickness beneath the pile overlies a very soft layer. The error involved in using Eq. (10) will generally lead to an overestimate of the settlement.

The calculation of the settlement of a single pile from Eq. (10) may be extended to the case of a pile group. For a group of n piles situated in a homogeneous layer of depth D, underlain by a series of other strata, the displacement at the centre of the pile group can be calculated by summation of the settlement of the underlying layers due to all piles in the group. Thus

$$\rho = \rho_{GD} + \sum_{i=1}^{n} \frac{P_i}{L} \sum_{j=2}^{m-1} \left\{ \frac{(I_{i,j} - I_{i,j+1})}{E_{sj}} + \frac{I_{i,m}}{E_{sm}} \right\} \quad \text{.....(11)}$$

where ρ_{GD} = displacement of the pile group in a layer of depth D and Young's modulus E_1 which is underlain by a rigid base,

P_i = load in pile i,

$I_{i,j}$ = displacement influence factor beneath the centre of the pile group for the level of the top of layer j due to pile i (obtained from Figs. 2 to 7).

The value of ρ_{GD} may be calculated as

$$\rho_{GD} = R_s \cdot \rho_1 \quad \text{.....(12)}$$

where R_s = the settlement ratio of group settlement to the settlement of a single pile under the same average load as a pile in the group,

ρ_1 = settlement of single pile at the average pile load.

For a floating pile group, ρ_1 may either be calculated from the influence factors presented by Poulos and Davis (Ref. 10) or Mattes and Poulos (Ref. 5), or from a field load test on a single pile. R_s may be calculated by the method described by Poulos (Ref. 9). For a group which rests on a firmer stratum below which a softer layer exists, ρ_1 may be calculated from the influence factors presented by Poulos and Mattes (Ref.11), or again from a field load test, while R_s may be calculated, as if the group was end-bearing, by the method described by Poulos and Mattes (Ref. 12).

For a pile group with a rigid cap, the values of P_i in the group will not be uniform, as previously mentioned. The load distributions obtained by Poulos (Ref. 9) and Poulos and Mattes (Ref. 12) for a pile group in a homogeneous mass may be used to obtain values of P_i although some slight inaccuracy may result because of the influence of the underlying compressible layers in modifying the load distribution. However, as shown in the previous section, little error will ensue if the load distribution within the group is assumed uniform. Alternatively, and again more expediently, the pile group may be replaced by an equivalent single pier as previously outlined. A further advantage of this latter method is that, for the relatively small value of L/d which the equivalent pier will have, the values of I_ρ will be almost independent of K and thus it will generally not be necessary to consider different values of K for different layers.

An example is given below of the calculation of the settlement of a floating pile group using both the correct load distribution and a uniform load distribution in the group and also replacing the group by an equivalent single pier. An example is also given of the settlement calculation for a group which rests on a firmer stratum below which a softer layer exists.

6.—ILLUSTRATIVE EXAMPLES

6.1 Floating Pile Group:

The example considered is shown in Fig. 11. A 3^2 group of concrete piles with a rigid cap is founded in a soil layer which is underlain by a further three layers and it is desired to calculate the settlement of the pile group. The values of Young's modulus E_s of the soil layers are given in Fig. 11 and are taken to be average values of the Young's modulus of the soil skeleton so that the settlements calculated will be total final settlements.

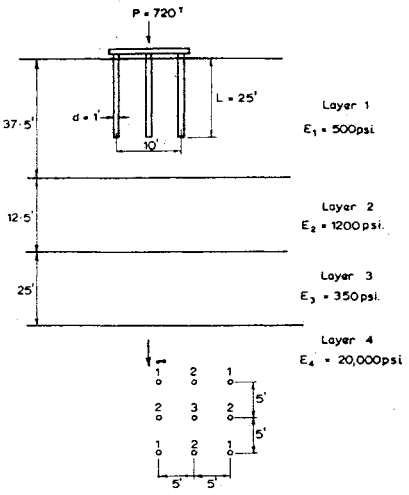

Fig. 11.—Illustrative Example No. 1.

The settlement of the pile group in layer 1 may be calculated from Eq. (12). For the piles in layer 1, assuming E of the concrete to be 3×10^6 lb./sq. in., $K = (3\times10^6)/(5\times10^2) = 6{,}000$. For this value of K, the piles may be considered incompressible (Mattes and Poulos, Ref. 5). From the influence factors given by Poulos and Davis (Ref. 10), for $L/d=25$ and $H/L = 1.5$, $I_1 = 1.38$. For the pile spacing of $s = 5d$, the value of R_s is estimated from the results of Poulos (Ref. 9) to be 2.3. Hence the settlement of the pile group in layer 1 $= (P_G/n) \cdot (R_s/LE_{s1}) \cdot I_1 = 3.78$ in., where P_G is the total load on the pile group.

In order to calculate the additional settlements due to the underlying layers, three alternative methods will be used. Firstly, the correct non-uniform load distribution in the group will be considered; secondly, it will be assumed that the load distribution in the group is uniform; thirdly, the group will be replaced by an equivalent single pier.

(i) *Considering Non-Uniform Pile Loads*

From the tabulated results presented by Poulos (Ref. 9), the load distribution in the group may be obtained. The average pile load $P_{av} = 720/9 = 80$ tons, and using the key to the piles shown in Fig. 11, the pile loads are as follows:

$$P_1 = 1.32\,P_{av} = 106 \text{ tons}$$
$$P_2 = 0.84\,P_{av} = 67 \text{ tons}$$
$$P_3 = 0.34\,P_{av} = 28 \text{ tons.}$$

Since the settlement beneath the centre of the group is required, only three piles of the group need be considered because of symmetry. Because of the relatively large values of H/L involved in this problem, the displacement influence factors are unaffected by the value of K. The calculations are shown in Table I. The total additional setltement due to the underlying layers is found to be 2.25 in. The overall settlement of the group is therefore 3.78 + 2.25 = 6.03 in.

(ii) *Considering Uniform Pile Load Distribution*

In this case, the load P_i on each pile is 80 tons. From Table I, the values of $(I_j - I_{j+1})/E_{sj}$ may be extracted for each pile and each layer. The resulting calculations are shown in Table II. In this case, the settlement of the group is 3.78 + 2.29 = 6.07 in. It will be seen that the calculated settlement is almost identical with that calculated from Table I using the correct non-uniform pile load distribution.

(iii) *Considering the Group as an Equivalent Single Pier*

The gross plan area of the group = 11 × 11 = 121 sq. ft. Therefore the equivalent diameter of a single pier $d_e = 12.4$ ft. From Poulos (Ref. 9), the equivalent length L_e of the pier may be taken as $0.8L = 20$ ft.

$$\therefore \quad L_e/d_e = 20/12.4 = 1.6.$$

Eq. (10) may now be used to determine the settlement of the underlying layers. Since values of I_ρ are only given for $L/d = 1$ and $L/d = 2$, the values of I_ρ for the required value of $L_e/d_e = 1.6$ will be interpolated from the values for $L/d = 1$ and 2. The calculations are shown in Table III. Because the settlements are calculated beneath the centre of the group, only values of I_ρ for $r/L = 0$ are required. The settlement of the group in this case is 3.78 + 2.52 = 6.30 in.

The calculated additional settlement due to the underlying layers from Table III is about 10% greater than the values calculated by the two previous methods. Nevertheless, the agreement is sufficiently good to suggest that, for a group containing a large number of piles, the replacement of the group by an equivalent single pier provides a convenient and reasonably accurate method of calculating the settlement of the group.

TABLE I

Pile No. i	Pile Load P_i (tons)	$\frac{r_i}{L}$	Layer 2					Layer 3					Layer 4		
			$\frac{H_2}{L}$	I_2	$\frac{H_3}{L}$	I_3	$\frac{P_i(I_2-I_3)}{E_{s2}}$ (in.²)	$\frac{H_3}{L}$	I_3	$\frac{H_4}{L}$	I_4	$\frac{P_i(I_3-I_4)}{E_{s3}}$ (in.²)	$\frac{H_4}{L}$	I_4	$\frac{P_i(I_4)}{E_{s4}}$ (in.²)
1	106	0.28	1.5	0.400	2	0.285	24.6	2	0.285	3	0.175	74.5	3	0.175	2.1
2	67	0.20	1.5	0.410	2	0.285	15.7	2	0.285	3	0.180	45.0	3	0.180	1.4
3	28	0	1.5	0.435	2	0.295	7.3	2	0.295	3	0.185	19.7	3	0.185	0.6

Settlement of each layer = 4 × (settlement due to pile 1 + settlement due to pile 2 + settlement due to pile 3).

For layer 2, Settlement $= \frac{1}{25 \times 12}[4 \times (24.6 \times 15.7) \times 7.3] = 0.56$ in.

For layer 3, Settlement $= \frac{1}{25 \times 12}[4 \times (74.5 + 45.0) + 19.7] = 1.64$ in.

For layer 4, Settlement $= \frac{1}{25 \times 12}[4 \times (2.1 + 1.4) + 0.6] = 0.05$ in.

Total settlement of layers 2 to 4 = 2.25 in.

TABLE II

Pile No. i	Values of $\frac{P_i(I_j - I_{j+1})}{E_{sj}}$		
	Layer 2	Layer 3	Layer 4
1	18.8	56.2	1.6
2	18.8	54.7	1.7
3	20.8	56.3	1.7

For layer 2, settlement $= \frac{1}{25 \times 12}[4 \times (18.8 + 18.8) + 20.8] = 0.57$ in.

For layer 3, settlement $= \frac{1}{25 \times 12}[4 \times (56.2 + 54.7) + 56.3] = 1.67$ in.

For layer 4, settlement $= \frac{1}{25 \times 12}[4 \times (1.6 + 1.7) + 1.7] = 0.05$ in.

Total settlement of layers 2 to 4 = 2.29 in.

The above example emphasizes that compressible layers well beneath the pile group may contribute significantly to the settlement of the group. In this case, the additional settlement due to the underlying layers comprises about 37% of the overall settlement. The example also highlights the possible consequence of incomplete site investigation.

6.2 End-Bearing Pile Group:

The problem is shown in Fig. 12. A 3^2 group of concrete piles is founded through alluvial clay on to a medium dense sand, which is underlain by a soft clay layer which rests on shale. Average values of both undrained Young's modulus E_u and Young's modulus of the soil skeleton E'_s are given and both the immediate and total final settlements are calculated. Because the displacement influence factors I_ρ are not seriously influenced by Poisson's ratio ν_s (see Section 3), it has been assumed that, under both undrained and drained conditions, I_ρ values are those for $\nu_s = 0.5$.

The group is considered first as end-bearing. The value of K of the piles is about 6,000, so that from the results of Poulos and Mattes (Ref. 11), such piles are virtually incompressible, and hence the settlement of a single pile is merely the elastic settlement of the pile itself. Furthermore, from the results of Poulos and Mattes (Ref. 12), no interaction occurs between adjacent piles, i.e., $R_s = 1$, and all piles are equally loaded**.

**Because the supporting sand layer is not perfectly rigid, some interaction may in fact occur, but it is unlikely to be significant.

TABLE III

L/D	Layer 2					Layer 3					Layer 4		
	$\frac{H_2}{L_e}$	I_2	$\frac{H_3}{L_e}$	I_3	$\frac{(I_2 - I_3)}{E_{s2}}$ (sq.in./ton)	$\frac{H_3}{L_e}$	I_3	$\frac{H_4}{L_e}$	I_4	$\frac{(I_2 - I_3)}{E_{s3}}$ (sq.in./ton)	$\frac{H_4}{L_e}$	I_4	$\frac{I_4}{E_{s4}}$ (sq.in./ton)
1	1.88	0.186	2.5	0.136		2.5	0.136	3.75	0.082		3.75	0.082	
2	1.88	0.468	2.5	0.300		2.5	0.300	3.75	0.180		3.75	0.180	
1.6 (by linear interpolation)	1.88	0.355	2.5	0.235	0.223	2.5	0.235	3.75	0.141	0.601	3.75	0.141	0.016

For layer 2, settlement $= \frac{P_{\frac{1}{2}}}{L_e} \cdot \frac{(I_2 - I_3)}{E_{s2}} = \frac{720}{20 \times 12} \times 0.223 = 0.67$ in.

For layer 3, settlement $= \frac{720}{20 \times 12} \times 0.601 = 1.80$ in.

For layer 4, settlement $= \frac{720}{20 \times 12} \times 0.016 = 0.05$ in.

Total settlement due to layers 2 to 4 = 2.52 in.

Hence, the settlement of the piles, when considered as bearing on a rigid stratum, is

$$S_1 = \frac{P\,L}{A_p\,E_p}$$

where P is the average pile load,
A_p is the area of the pile,
E_p is Young's modulus of the pile.

In this case, it is found that, for $E_p = 3 \times 10^6$ lb./sq. in.,

$$S_1 = 0.16 \text{ in.}$$

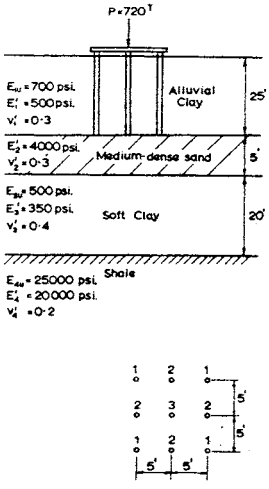

Fig. 12.—Illustrative Example No. 2.

The calculation of the additional settlements due to the underlying layers is shown in Table IV. The settlement of the sand layer is assumed to occur immediately. The immediate settlement of the group is the sum of the elastic pile settlement and the immediate settlement of the underlying layers, i.e., 0.16 + 3.21 = 3.37 in. The total final settlement is 0.16 + 4.46 = 4.62 in. Thus, because of the underlying soft clay layer, a considerable amount of consolidation settlement (1.25 in.) occurs in this case, whereas if the pile were founded on a truly rigid stratum, only an immediate settlement of 0.16 in. would occur.

7.—COMPARISON WITH FIELD CASE

As an indication of the applicability of the method described to field situations, an attempt was made to compare the measured settlements of the furnace foundation described by Golder and Osler (Ref. 4) with the calculated values. The foundation supported a total load of 2,400 tons and consisted of 32 Franki piles of 22-ft. length arranged in a generally rectangular pattern consisting of 3 interior rows of 8 piles each, the rows spaced at 10.5 ft. and the piles at 6 ft., and at each end, 4 piles spaced at 7-ft. centres. The soil profile could generally be characterised as about 95 ft. of sand interspersed with layers of silty clay and sandy clay, and underlain by a very deep deposit of a firm grey silty clay (Leda clay).

A single pile test was carried out and revealed that, under the average working load, the single pile settlement was about 0.04 in. An analysis carried out, as described by Poulos (Ref. 9), gave a value of settlement ratio R_s of the pile group in the sand of 8.5. Thus, the settlement of the piles in the sand (ρ_{GD}) is 8.5 × 0.04 = 0.34 in.

Considering now the settlement due to the Leda clay, only oedometer results are given for this clay and it is therefore necessary to use these results to estimate Young's modulus E'_s of the clay. The data given is compression index $C_c = 0.33$, and void ratio = 1.25. From these results, a value of the coefficient of volume decrease m_v may be derived for a typical depth of say 50 ft. below the sand-clay interface. This gives $m_v = 6.3 \times 10^{-6}$ ft.²/lb. Using now the theory for an ideal elastic soil,

$$E'_s = \frac{(1 + \nu'_s)(1 - 2\nu'_s)}{(1 - \nu'_s)\,.\,m_v}$$

Assuming a typical value of ν'_s for the firm clay of 0.2, it is found that E'_s = 1,000 lb./sq. in.

Considering now the calculation of the settlement due to the clay, and assuming the clay to be semi-infinite, it is found that the settlement is 3.3 in. Thus, the total settlement of the group is 3.3 + 0.34 = 3.7 in.

The actual foundation was in fact demolished before the final settlement had been attained, at which time, the measured settlement had reached about 1.8 in. Measured values of the coefficient of consolidation c_v vary too widely to be able to accurately estimate the degree of settlement at the time of demolition. However, if an average value of c_v of 1×10^{-2} in.²/min. is assumed, the dimensionless time factor $T_v = (c_v\,t)/a^2$ (assuming the foundation to be replaced by an equivalent circular foundation of radius a) after 11 years is 0.91. From the three-dimensional rate of settlement analysis of Mandel (Ref. 6) for a circular foundation on a sand layer overlying a deep clay layer, it is found that the appropriate degree of settlement is about 0.38. Thus, the estimated final settlement (taking account of an initial sand settlement of 0.5 in.) = (1.3/0.38) + 0.5 = 3.9 in., which is in general agreement with the calculated value. In addition, the initial settlement of the group, of about 0.5 in., due largely to the sand, is consistent with the calculated value of ρ_{GD} of 0.34 in.

Although the settlements calculated by the method in this paper are very similar to those produced by Golder and Osler using one-dimensional theory, the present method would appear somewhat more logical as it does not require any arbitrary selection of rigid boundaries beneath the clay or reductions for foundation rigidity as is the case with the one-dimensional predictions.

8.—CONCLUSIONS

Distributions of vertical displacement within a semi-infinite mass due to a loaded pile have been obtained for various length-to-diameter ratios of the pile. It has been found that, even at points relatively close to the pile, the displacements due to a pile agree closely with those due to an equivalent single point load acting at a depth of two-thirds of the pile length. A method of calculating the surface displacement profile around a pile group and the settlement of a pile group underlain by layered strata, using the single pile displacement distributions, has been suggested. It has been found that, for a pile group having a rigid pile cap, the displacements may be calculated with sufficient accuracy by assuming all piles

TABLE IV

Pile No. i	Pile Load P_i (tons)	r_i/L	Layer 2					Layer 3						Layer 4			
			H_2/L	I_2	H_3/L	I_3	$P_i(I_2-I_3)/E_{s2}$ (in.²)	H_3/L	I_3	H_4/L	I_4	$P_i(I_3-I_4)/E_{3u}$	$P_i(I_3-I_4)/E_3'$	H_4/L	I_4	$P_i\,.\,I_4/E_{4u}$ (in.²)	$P_i\,.\,I_4/E_4'$ (in.²)
1	80	0.28	1	0.58	1.2	0.51	3.1	1.2	0.51	2	0.285	80.7	115.2	2	0.285	2.1	2.6
2	80	0.20	1	0.68	1.2	0.56	5.4	1.2	0.56	2	0.285	98.5	140.8	2	0.285	2.1	2.6
3	80	0	1	1.63	1.2	0.72	40.8	1.2	0.72	2	0.295	152.3	217.5	2	0.295	2.1	2.6

Settlement of each layer = 4 × (settlement due to pile 1 + settlement due to pile 2) + settlement due to pile 3.

Immediate settlement of layers 2, 3 and 4 $= \frac{1}{25 \times 12}[4 \times (3.1 + 5.4) + 40.8 + 4(80.7 + 98.5) + 152.3 + 4(2.1 + 2.1) + 2.1] = 3.21$ in.

Total final settlement of layers 2 to 4 $= \frac{1}{25 \times 12}[4 \times (3.1 + 5.4) + 40.8 + 4(115.2 + 140.8) + 217.5 + 4(2.6 + 2.6) + 2.6] = 4.46$ in.

∴ Immediate settlement = 0.16 + 3.21" = 3.37 in.
Total final settlement = 0.16 + 4.46" = 4.62 in.

are equally-loaded and ignoring the correct non-uniform load distribution within the group. The replacement of the pile group by an equivalent single pier has been shown to lead to an estimate of the displacement which is quite adequate for practical purposes. Such a procedure appears to be most convenient when considering displacements due to a group containing a large number of piles.

ACKNOWLEDGMENTS

The work described in this paper forms part of a general programme of research into the settlement of all types of foundations, under the general direction of Professor E. H. Davis, whose comments are gratefully acknowledged. The work was carried out in the School of Civil Engineering at The University of Sydney, the Head of which is Professor J. W. Roderick, and was supported by a grant from the Australian Research Grants Committee. The computational work was carried out using the facilities of the Basser Computing Department of the School of Physics at the University of Sydney.

References

1. BURMISTER, D. M.—The Theory of Stresses and Displacements in Layered Systems and Applications to the Design of Airport Runways. *Proc. Highway Research Board*, Vol. 23, 1943, pp. 126-48.
2. DAVIS, E. H. and TAYLOR, H.—The Movement of Bridge Approaches and Abutments on Soft Foundation Soils. *Proc. First Conf. Aust. Road Research Board, Canberra*, 1962, Vol. 1, Part 2, pp. 740-64.
3. EGOROV, K. E., KUZMIN, P. G. and POPOV, B. P.—The Observed Settlements of Buildings as Compared with Preliminary Calculation. *Proc. Fourth Int. Conf. Soil Mechanics and Foundation Engg., London*, 12-24 *August*, 1957. London, Butterworth, 1957, Vol. 1, pp. 291-6.
4. GOLDER, H. Q. and OSLER, J. C.—Settlement of a Furnace Foundation, Sorel, Quebec. *Canadian Geotech. Jour.*, Vol. 5, No. 1, Feb., 1968, pp. 46-56.
5. MATTES, N. S. and POULOS, H. G.—The Settlement of a Single Compressible Pile. *Proc. A.S.C.E., Jour. Soil Mechanics and Foundations Div.*, Vol. 95, No. SM1, Jan., 1969, pp. 189-207.
6. MANDEL, J.—Tassements produits par la consolidation d'une couche d'argile de grande épaisseur. *Proc. Fifth Int. Conf. Soil Mechanics and Foundation Engg., Paris*, 17-22 *July*, 1961, Vol. 1, pp. 733-6.
7. NAIR, K.—Load Settlement and Load Transfer Characteristics of a Friction Pile Subject to a Vertical Load. *Proc. Third Pan-American Conf. Soil Mechanics, Caracas, Venezuela*, 1967, p. 565.
8. POULOS, H. G.—Stresses and Displacements in an Elastic Layer Underlain by a Rough Rigid Base. *Geotechnique*, Vol. 17, No. 4, 1967, pp. 378-410.
9. POULOS, H. G.—Analysis of the Settlement of Pile Groups. *Geotechnique*, Vol. 18, No. 4, 1968, pp. 449-71.
10. POULOS, H. G. and DAVIS, E. H.—The Settlement Behaviour of Single Axially-Loaded Incompressible Piles and Piers. *Geotechnique*, Vol. 18, No. 3, 1968, pp. 351-71.
11. POULOS, H. G. and MATTES, N. S.—The Behaviour of Axially Loaded End-Bearing Piles. *Geotechnique*, Vol. 19, No. 2, 1969, pp. 285-300.
12. POULOS, H. G. and MATTES, N. S.—Settlement and Load Distribution Analysis of Pile Groups. *Aust. Geomechanics Jour.*, Vol. G1, No. 1, 1971, pp. 18-28.
13. STEINBRENNER, W.—Tafeln zur Setzungberechnung. *Die Strasse*, Vol. 1, 1934, p. 121.
14. UESHITA, K. and MEYERHOF, G. G.—Deflection of Multilayer Soil Systems. *Proc. A.S.C.E., Jour. Soil Mechanics and Foundations Div.*, Vol. 93, No. SM5, Sept., 1967, pp. 257-82.

A Study of the Settlement Characteristics of the Soil Deposits at Kingsford-Smith Airport, Sydney

By I. K. Lee, B.C.E., M.Eng.Sc., Ph.D., M.I.E.Aust., E. H. Davis, B.Sc., F.I.E.Aust., B. Rodway, B.E., M.Eng.Sc., M.I.E.Aust. and R. Mallam, B.E., M.Eng.Sc., M.I.E.Aust.*

Summary.—The paper describes the geotechnical studies carried out to establish the origin and rate of settlement of the soil deposits at Kingsford-Smith Airport, Mascot, Sydney.

Settlements were predominantly due to compression of a highly compressible ($I_c \simeq 1$) silt-clay of low permeability. This soil occurred in layers up to 25 ft. thick.

A comparison of the theoretical settlement (based on the actual loading history) with measured settlements at times when the consolidation was only partially completed, showed excellent agreement provided the coefficient of consolidation was recorded on samples with a drainage path in excess of the drainage path of conventional samples. The typical comparative values were 15×10^{-3} sq. ft./day and 5×10^{-3} sq. ft./day, respectively.

It was considered that the post-construction settlements could be confidently predicted.

1.—INTRODUCTION

As part of the design studies of the pavements and structures in the vicinity of the New International Terminal, Kingsford-Smith Airport, Sydney, a geotechnical investigation was made of the soils in the north-western area of the airport. The primary purpose of these studies was to predict the total settlement and the rate of settlement of the soils in the period following construction of the pavements.

The north-western section of the airport was originally a shallow swamp. There was no development in this area until the late 1940's so that prior to initial filling operations, which commenced in 1961, the land level was a few feet below sea level with a few grassed areas just above the water level. The Cooks River partially enclosed the site of the International Terminal, and there is evidence to suggest that it had meandered over the surrounding areas in Recent times.

In 1947, work commenced on new runways and filling of sections of the Cooks River was commenced. The diversion channel for the river was under construction. Fill for the operations was sand obtained by dredging of Botany Bay. The Cooks River east of the terminal had been filled by 1954 and some limited filling adjacent to the banks of the river had also been completed.

In 1961, filling of the terminal area was commenced and continued until 1964. Flyash from Bunnerong Power Station was used to fill part of the river south-east of the terminal and in the proposed car parking area. The flyash was removed from the latter area in 1966 and the whole site filled and surcharged with sand late in 1966.

Fig. 1 shows the location of the terminal relative to the runways and existing development. Fig. 2 was taken in 1948 when filling of Cooks River had commenced, and Fig. 3 shows the progress in 1953. The diversion canal was completed (marked as (1) in the photograph), filling of the river adjacent to the north-south runway was well advanced (2), construction of the East-West runway and taxiways was completed (3) and filling of the river was partially completed in the area of the East-West runway (4). Fig. 4 was taken in 1963 when portion of the river had been filled with flyash (1), and filling of the proposed car park had commenced (2).

Investigations by the Commonwealth Department of Works had established that relatively large settlements due to filling and pavement loadings were likely, and the decision was made to surcharge the area to reduce the settlement in the post-construction period.

The fill and surcharge, which was pumped from Botany Bay had an in-situ dry density of 97-100 lb./cu. ft. The maximum dry density is 115 lb./cu. ft. (Kolbuszewski, Ref. 12). There was no mechanical compaction of the fill.

The subsequent investigations discussed in this paper were aimed at establishing the magnitude of the settlements from the time filling operations commenced in 1961 to 20-25 years after construction of the pavements were completed.

From aerial photographs and levelling data it was possible to reconstruct the loading history at selected points in the terminal area. The likely accuracy of the calculated levels of the surface was considered to be $\pm$ 6 in.

*Paper No. 2876, submitted by the authors on 29th October, 1969.

The authors are, respectively, Professor Lee, School of Civil Engineering, The University of New South Wales; Professor Davis, Professor of Civil Engineering (Soil Mechanics), The University of Sydney; Messrs. Rodway and Mallam, Engineers with the Commonwealth Department of Works.

Five sites were analysed in detail. At each site the soil was continuously sampled over the full depth of the deposits thus providing a complete undisturbed profile of the soils. Piezometers were installed with the object of recording the magnitude of the excess pore water pressures at the time of the investigation (1967) and to provide data for calculating the field coefficient of consolidation. Settlements at each selected site had been recorded since filling and surcharging so that a comparison of predicted and measured settlements was possible.

2.—FIELD INVESTIGATIONS

Preliminary investigations had shown that the soil profile was extremely variable, and this fact established the need for continuous sampling over the full depth of the soil deposit. This was achieved by pushing 3-in. internal dia. by 24-in. long thin-walled sampling tubes into the soil a distance of 18 in., withdrawing the tube, pushing the casing to the level reached by the end of the sampling tube, and repeating the procedure. The usual technique was to use 8-in. dia. casing driven into the less permeable layers to a depth sufficient to seal off the hole from the more permeable layers. Six-in. dia. casing was then used to complete the hole. At all stages the water level in the bore hole was maintained a few feet above the observed water table to eliminate the possibility of severe hydraulic gradients in the soil immediately beneath the level of the casing tip. Diamond drilling was used to drill into the shale and sandstone which forms the bedrock in the area.

Sample recovery was generally extremely good, and there were no visual signs or laboratory evidence of significant sample disturbance.

At the time of the field investigations, a theoretical analysis of the rate of settlement, predicted relatively large excess pore-water pressures in the less permeable (organic silt-clay) deposits. In order to register these pressures a series of piezometers were installed. A total of 19 piezometers were located in the vicinity of the terminal. After installation of the tips. the bore holes were sealed by AM9 chemical grout and bentonite.

The effectiveness of the sealing along the borehole of some of the piezometers became suspect when the readings were not consistent during installation. The reliability of the chemical grout appeared to be doubtful as the setting time varied considerably and, on some occasions, no set took place.

In an investigation to establish whether a group of piezometers installed in one borehole were functioning properly, a field test was carried out by placing 5 ft. of surcharge over a circular area 200 ft. in diameter with the piezometers centrally placed relative to the surcharge area. At this particular site there was an organic silt-clay layer 22 ft. thick. Seven piezometers had been installed in this layer. The theoretical increase in pore-water pressure in the layer due to the extra surcharge was 10 ft. of water, whereas measured values were within the range of 4 to 10.5 ft. of water.

On the basis of this test, and an overall analysis of the piezometers, it became evident that the recorded pore-water pressures were less than the actual values due to ineffective sealing along the borehole. This was unfortunate as one of the purposes of the installation was to provide a further check on the predicted rate of settlement by calculating the field value of the coefficient of consolidation from the finite difference form of the one-dimensional consolidation equation and measured pore-water pressures over a period of 6 to 12 months.

However, there were two major conclusions which were drawn from the piezometer data:—

(*a*) There were large excess pore-water pressures in the organic silt-clay deposits in the northern area of the terminal site.

(*b*) The sand layers which occurred between the relatively impermeable clay deposits were of sufficient extent and adequate permeability to be regarded as drainage layers.

The water level observed in open boreholes in the terminal area was RL 7.0 ft., whereas the water level in the bedrock was at sea level. A perched water table was initially developed during the hydraulic filling, and it was evident that some excess water pressure still remained at the time of the investigation due to the slow rate of flow through the underlying silt and clay layers.

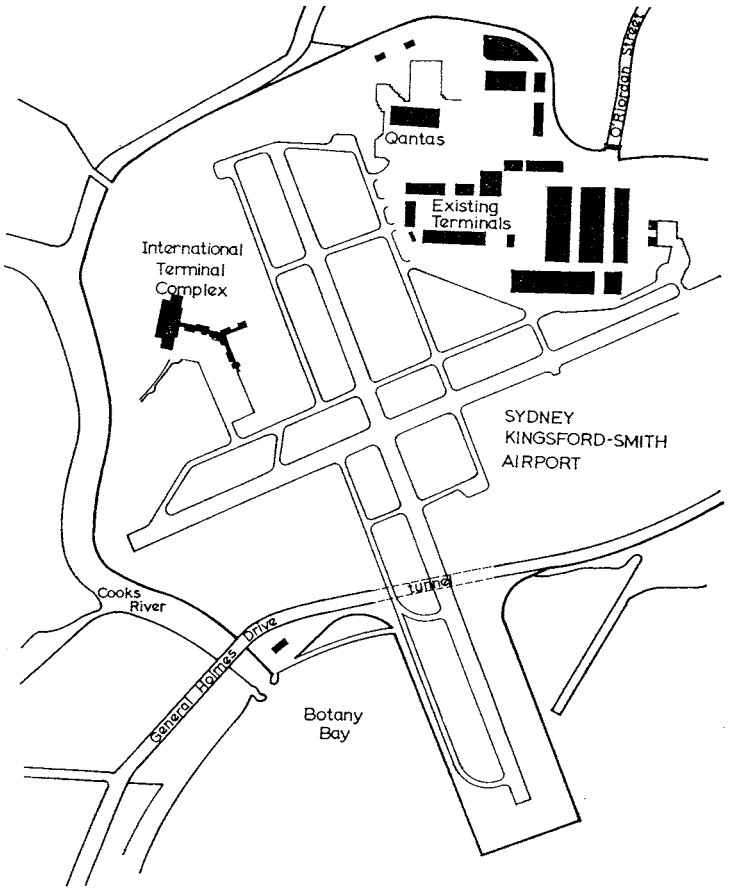

Fig. 1.—*Location of International Terminal Area.*

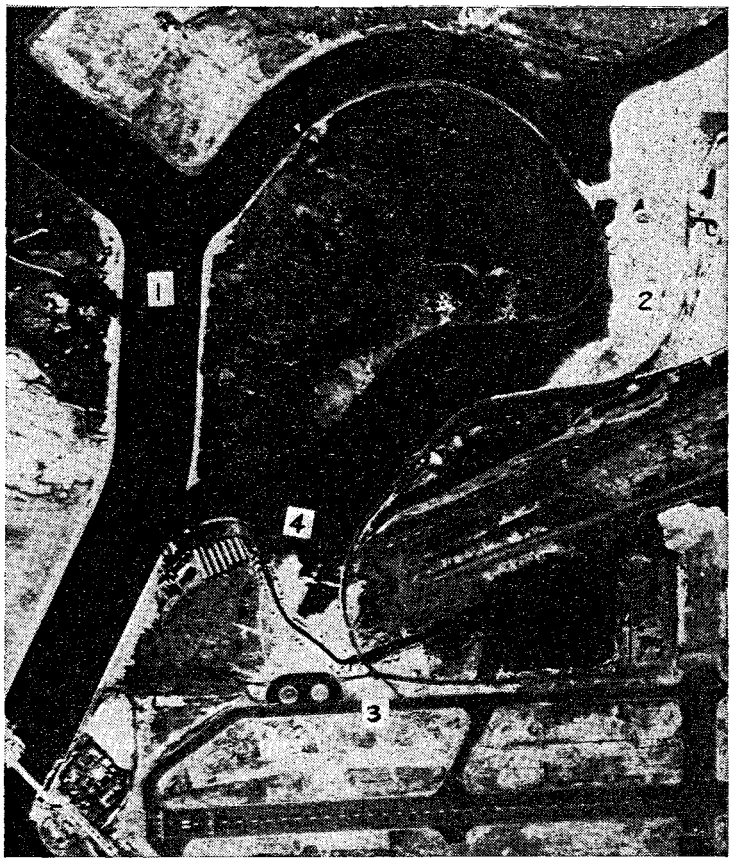

Fig. 3.—*Cooks River on 23rd June,* 1953.

1. Diversion Channel of Cooks River completed.
2. Filling of old river adjacent to North-South runway well under way.
3. Construction of East-West runway and taxiways completed.
4. Filling of old river almost complete in area of East-West runway.

Fig. 2.—*Cooks River on 8th March,* 1948.

1. Work has commenced on the filling in of Cooks River.
2. Filling has also commenced on the filling in of the ponding area.
3. More sand fill is being placed adjacent to the old runway.

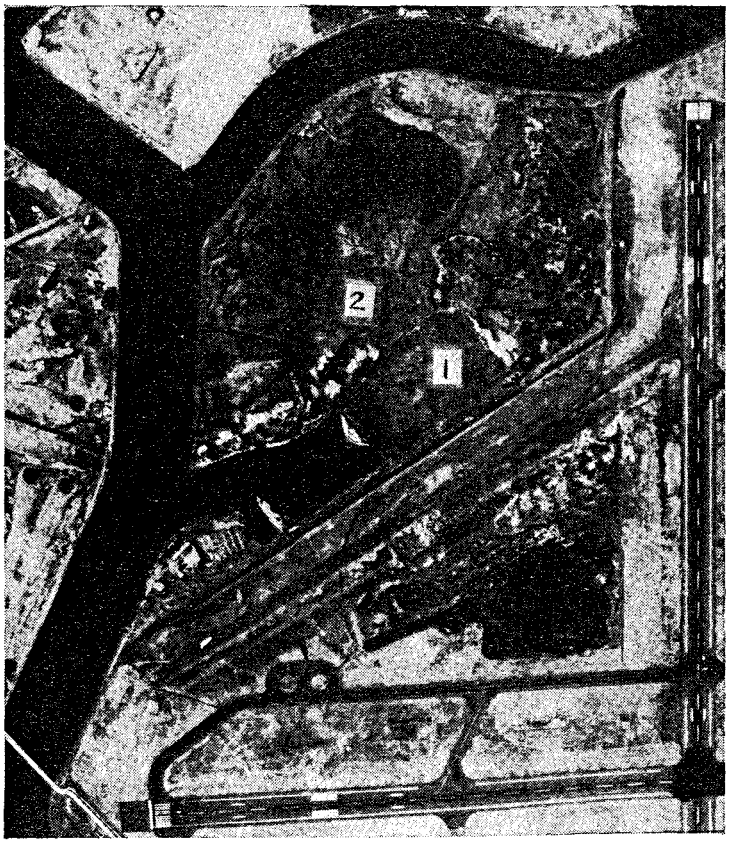

Fig. 4.—*Cooks River on 10th November,* 1963.

1. Portion of old river filled with flyash.
2. Flyash spreading out over car parking area for new terminal.

3.—GEOTECHNICAL PROPERTIES OF SOIL DEPOSITS

The soil profile in the airport area is quite typical of many of the deposits in bay areas near Sydney. It is also very similar to other deposits in coastal regions (Roberts and Darragh, Ref. 8). There is generally a layer or lens of a highly compressible organic silt-clay of a total thickness varying up to 25 ft. Beneath this layer there are commonly variable sand or sandy clay layers of limited thickness overlying a relatively stiff inorganic clay. The bedrock in the area is the Sydney sandstone. The total depth of soils is generally of the order of 80 to 120 ft. Fig. 5 shows contours of the rock surface. It will be noted that the course of Cooks River was not controlled by the profile of the bedrock surface.

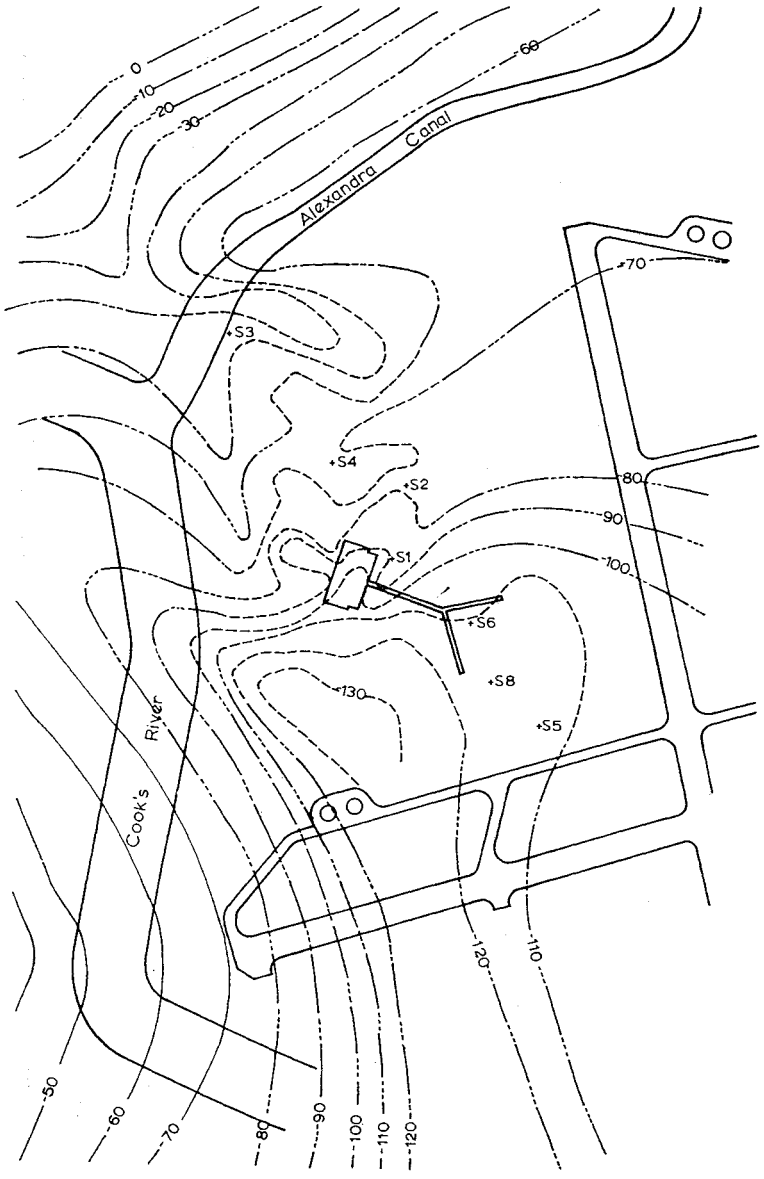

Fig. 5.—Contours of Bedrock—International Terminal Area.

The origin of the stiff inorganic clay is unknown although there is the probability that it is the result of the degradation of shale. The shale occurs in isolated areas immediately overlying the bedrock. There are fine well defined bedding planes in some sections of the clay but these are not consistent throughout the deposit. The clay is generally light grey in colour in the fresh state.

In some areas there are two distinct layers of the inorganic clay with a sand layer between the clay layers. Such a sand layer was found to vary in thickness from a few inches to 13 ft. and piezometric measurements established that it was of sufficient lateral extent to be regarded as a drainage layer. The in-situ bulk density was 130 lb./cu. ft. with S.P.T. values of 10 to 30.

The upper inorganic clay layer, when it was present, had engineering properties essentially identical with the lower inorganic clay layer. Typical properties are given in Table I.

From the point of view of long term settlement, the highly compressible, relatively impermeable organic silt-clays were of greatest significance. This clay is a normally consolidated deposit up to 25 ft. thick occurring in lenses of large lateral extent. There is some evidence to show that some of the deposition occurred during the meandering of Cooks River. Some deep local lenses appear to be the result of mud slides into holes made by dredging of Cooks River.

TABLE I

Geotechnical Properties of Inorganic Clay

Property	Value
Water Content	20%
Bulk Density	130 lb./cu. ft.
Liquid Limit	45-60%
Plasticity Index	25-35%
Undrained Shear Strength	> 1500 lb./sq. ft.
Compression Index (compression)	0.080
Compression Index (rebound)	0.015
Vertical Coefficient of Consolidation (oedometer)	50×10^{-3} sq. ft./day

There are numerous fibrous plant roots throughout the deposit at spacings varying from 0.1 in. to several inches. Shells, typically $\frac{1}{2}$ to $1\frac{1}{2}$ inches in size, are frequent in layers but are not uniformly dispersed over the whole deposit. Samples for oedometer testing using the conventional 3-in. and 1.35 in. dia. rings were necessarily taken from zones free of large shells and roots and are thus more representative of the more impermeable layers, and as shown in this paper do not give a good measure of the field value of the coefficient of consolidation of the whole deposit. Such samples are referred to as " clear " samples.

The deposit is anisotropic with respect to permeability. Values of vertical permeability were found to be as low as 10^{-6} ft./min. The horizontal permeability appears to be an order higher than this although still very low by comparison with many clay soils. The ratio of horizontal to vertical coefficient of consolidation C_h/C_v recorded in a K_0 test (Ref. 5) was twelve to one. Similarly, comparative oedometer tests on samples normally prepared, and prepared by cutting a sample so that the load was applied in the direction of the layers instead of normal to the layer direction (termed a pseudo-radial consolidation test), showed an anisotropy with respect to values of compression index and coefficient of consolidation. It should be recognized, however, that the pseudo-radial consolidation test does not give the value of C_h directly but gives a coefficient of consolidation associated with compression in the direction of layers say, C_{hv}. To establish the value of C_h from such tests it would be necessary to correct for the anisotropy of the coefficient of volume decrease. Thus if m_{vv} is the coefficient of volume decrease with the consolidation pressure applied in a direction at right angles to the bedding planes, and m_{hv} is the coefficient of volume decrease with the consolidation pressure applied in the direction of the bedding planes, then

$$C_h = C_{hv} \cdot (m_{hv}/m_{vv}).$$

In the present investigation C_h was measured in the K_0 test, but the radial oedometer (Ref. 10) would be also eminently suitable. The latter has the advantage that large diameter samples can be tested.

The anisotropy is reflected on a macro-scale by layering and laminations. The degree and type of layering is extremely variable and often cannot be observed unless the soil samples are broken open and observed continually as the soil dries out (Ref. 9).

The organic silt-clay is readily distinguishable from the other soils in the area provided undisturbed samples are examined. The characteristic features are the dark colour, occasional presence of shells and fibrous roots, the slight organic odour, obviously low strength, and virtual loss of strength on remoulding. More specifically, typical properties in the terminal area are listed in Table II.

The oedometer results for the organic silt-clay were found to be consistent from borehole to borehole provided the soil was systematically identified. It was found that there were regions north of the terminal area where the compression index of the organic silty clay varied between 1 and 2 with a typical value of 1.5. Values of c_v were similar to those listed in Table II, although there was a greater scatter in measured values.

Fig. 6 shows contours of equal thickness of the organic silt-clay in the vicinity of the terminal.

Acceleration of the rate of settlement of this type of soil can be effected by electro-osmosis (Ref. 2) provided the voltage gradient required to produce a practical discharge does not involve excessive current. A saline environment of the type at Mascot increases the conductivity of the soil-water combination compared with a fresh water environment and the process finally proved to be rather uneconomical for this reason.

TABLE II
Geotechnical Properties of Organic Silt-Clay

Property	Value
Organic Content	12%
Water Content	70-90%
Bulk Density	100-105 lb./cu. ft.
Liquid Limit	80-100%
Plastic Index	40-60%
Linear Shrinkage	20%
Clay Fraction	10-30%
Activity	2-6
Undrained Shear Strength	500-1,000 lb./sq. ft.
Compression Index (compression)	0.8-1.0
Compression Index (rebound)	0.2
Vertical Coefficient Consolidation (oedometer)	4-5 × 10^{-3} sq. ft./day
Vertical Coefficient Consolidation (K_0 test)	15 × 10^{-3} sq. ft./day

Values of the coefficient of osmotic permeability k_e were found from laboratory tests to be 1.4 × 10^{-5} sq. cm./sec. volt using the soil water from the site. For voltage gradients up to 0.6 volts/cm. there was an essentially linear relationship between discharge and voltage gradient, but the value of k_e was slightly dependent on voltage gradient in excess of this range and

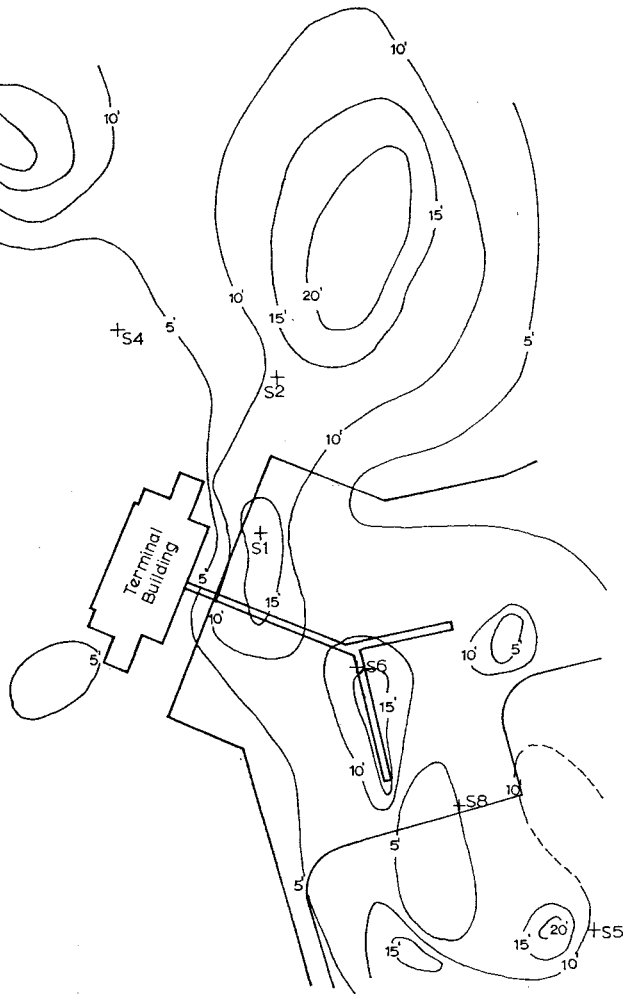

Fig. 6.—Contours of Equal Thickness of Silt-Clay.

was therefore not a unique constant as originally suggested by Casagrande (Ref. 3). The specific soil resistance was 80 to 140 ohm-cm. which can be compared with 4,000-5,000 ohm-cm. in a distilled water environment.

One particular aspect of laboratory investigations into the electro-osmotic properties worthy of further consideration involves a scale effect. In the usual test the assumption is made that the voltage gradient is uniform over the length of the sample, whereas measurements have indicated that there is a sharp gradient in the region of the anode. This is illustrated in Fig. 7 which shows the voltage distribution along the length of a sample immediately the electro-osmotic process was commenced. It is evident that the average gradient differs quite significantly from the local gradient so that the size of the sample will influence the recorded value of k_e and the discharge-time relationships.

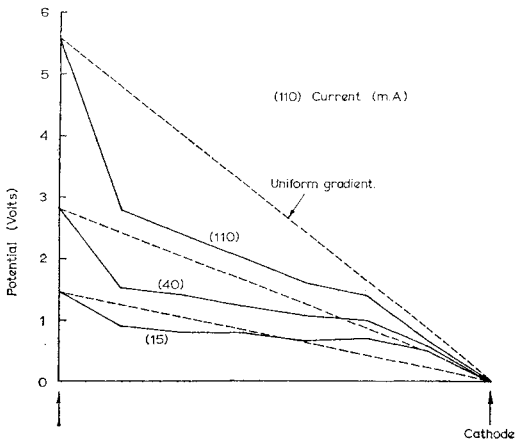

Fig. 7.—Potential Distribution over Length of Sample Undergoing Electro-Osmotic Drainage.

It has been observed that there is a severe drying out of the soil in the immediate vicinity of the anode. This would appear to be due to the relatively large potential gradient in this region. The non-uniform potential gradient may also prove to be the reason for the difference between the conclusion made by Casagrande regarding the constancy of k_e, and the observations made in the present investigations and by Bjerrum (Ref. 2) that k_e was dependent on the voltage gradient.

4.—SETTLEMENTS IN THE INTERNATIONAL TERMINAL AREA

4.1 Nature of the Settlements:

From a knowledge of the loading history, the soil profile and the consolidation properties of the individual soil layers it was possible to predict by a finite-difference approach the settlement contributed by each soil layer from the time initial filling commenced in 1961.

The calculations were based on the assumption that the soils were completely consolidated under the overburden existing prior to initial filling. This appeared to be a reasonable assumption in view of the history of the area. The assumption of a one-dimensional strain state was considered to be justified in view of the fact that the lateral extent of the filling was large compared with the total depth of the consolidating layers. This is, however, a poor approximation in the areas where there was a change in surcharge level and the general conclusions do not apply to such areas.

It was not necessary to take non-linear effects into account (Ref. 6) as the typical loading increment ratio did not lead to predicted values which differed from the traditional Terzaghi analysis by more than 5%. Similarly, the anisotropic nature of the deposit was of little importance in the one-dimensional calculations, and only became significant in the prediction of settlement due to isolated loadings such as that due to aircraft parking.

Detailed settlement calculations were made for five sites taking into account the loading history of each site and the properties of the individual layers.

It was evident that the smaller value of c_v for the organic silt-clay obtained by testing samples in the oedometer free of roots and shells represented the settlement properties of the least permeable layers within the organic silt-clay deposit. The fact that the longer samples in the K_0 test (3 in. compared with oedometer thickness of ½-¾ in.) showed a c_v value three times the oedometer value (see Table II) suggested that the inclusions had a significant effect on the rate of settlement, and that the c_v value measured using the longer sample, with inclusions, was more representative of the field value. A comparison of measured and predicted settlement rates showed that this was the case and the results of the comparison can now be discussed in more detail.

Fig. 8 shows the profile and loading history of one of the typical sites (designated S1) where the organic silt-clay was 23 ft. 6 in. thick. After filling and surcharging the organic silt-clay was overlain by 33 ft. 6 in. of sand. The inorganic clay occurred as a thin deposit 5 ft. below the organic silt-clay and as a 17 ft. thick deposit at a lower level. There was a thin layer of weathered shale overlying the sandstone.

For the purposes of calculation it was assumed that surcharge was removed and pavements constructed in mid-1968. These calculations showed that the total settlement at any time can be considered to be composed of the very long term settlements due to consolidation of the organic silt-clay, the relatively rapid settlement of the deep inorganic clay layers and the very rapid settlement of sand, sandy clay, and thin clay layers.

Depth Below Ground Level (May 1967)	Reduced Level (Standard Datum)	Layer Thickness	Diagram of Log	Description
33'-6"	-16·5	33'-6"		Sand
53'-0"	-36·0	19'-6"		Uniform dark grey organic silt-clay
57'-0"	-40·0	4'-0"		Uniform stiff organic black silt with sand intermixed
62'-0"	-45·0	5'-0"		Sand
65'-6"	-48·5	3'-6"		Stiff grey-brown clay (Inorganic)
88'-6"	-71·5	23'-0"		Sand
105'-6"	-88·5	17'-0"		Stiff grey clay (Inorganic)
109'-0"	-92·0	3'-6"		Weathered shale & clay
				Sandstone

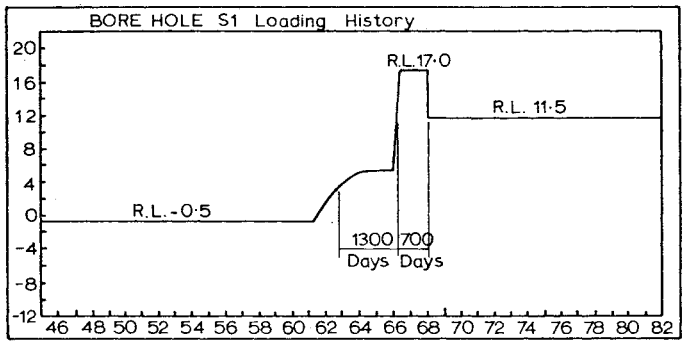

Fig. 8.—Profile of Site S1—Loading History.

By mid-1968 the settlement of the organic silt-clay was, theoretically, 35% complete. The calculated consolidation settlement during the surcharge period was 1.03 ft., 0.84 ft. being due to compression of the organic silt-clay layer and 0.19 ft. due to compression of the other layers. Furthermore, the surcharging had resulted in very rapid consolidation of the latter layers thus eliminating post-construction settlements due to compression of such layers.

The nature of the settlements in areas where there was a thin deposit of the organic silt-clay may be contrasted with an area typified by S1. At a site designated as S8 the organic silt-clay was only 4 ft. 6 in. thick whereas the stiff inorganic clay was a continuous deposit 41 ft. 6 in. thick. Only 47% of the total final settlement of the inorganic clay was completed in the surcharge period. However, the magnitude of the total final settlement is an order less than that in the areas typified by S1.

A comparison of predicted and measured settlements from the commencement of filling to the dates listed is shown in Table III for the five sites.

TABLE III

Comparison of Predicted and Measured Settlements (ft.)

Area	May, 1967		Aug., 1967		May, 1968		Total Final Settlement if Surcharge Remained
	Pred.	Meas.	Pred.	Meas.	Pred.	Meas.	
S1	0.57	0.70	0.65	0.80	0.80	—	1.7
S2	0.75	0.60	0.82	—	1.03	—	2.0
S4	0.20	0.30	0.25	—	0.29	—	0.5
S6	1.12	0.80	1.27	1.10	1.46	—	1.8
S8	0.72	0.55	0.76	0.60	0.84	—	0.9

The predicted values were based on the c_v values obtained in the K_0 test and showed that these values were more representative than the smaller values of the conventional oedometer tests. Fig. 9 shows the measured settlement contours with the calculated values superimposed.

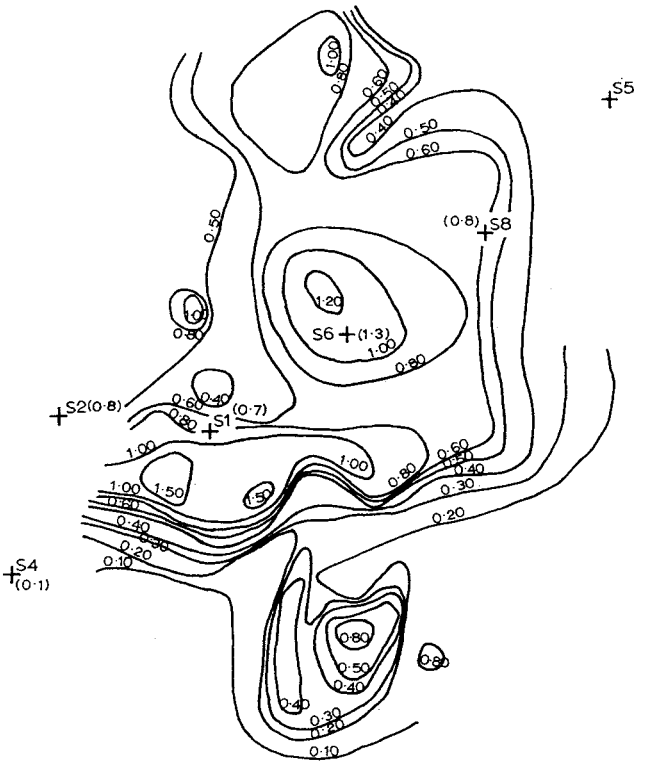

Fig. 9.—Settlement Contours (August, 1967).

Up to the proposed time of surcharge removal (May, 1968) the consolidation was only partially completed, so that a comparison of predicted and measured settlements is a severe test on both the total settlement and rate calculations. For the purpose of establishing the degree of consolidation, the total final settlement is quoted in Table III as if the surcharge was maintained for infinite time. The theoretical degree of consolidation at May, 1967, varied between 34% (S1) and 80% (S8).

The agreement between predicted and measured values was considered to be consistent evidence of the validity of the settlement analysis, and justified the extension of the analysis to the prediction of settlements in the post-construction period, that is, in the period subsequent to surcharge removal and construction of the pavement.

4.2 Post-Construction Settlements:

The general effect of surcharging where there was a substantial deposit of the organic silt-clay, was to eliminate post-construction settlements due to compression of layers other than the organic silt-clay layer.

If pavement construction had proceeded immediately after filling, the typical long-term settlement in an area where the organic silt-clay layer was 10 to 15 ft. thick was calculated to be of the order of 18 in. This value can be compared with the post-construction settlements quoted in Tables IV and V which apply to construction of the pavement preceded by two years of filling and surcharging.

TABLE IV

Calculated Post-Construction Settlements (ft.)
(10 ft. of Organic Silt-Clay)

Time after Pavement Construction	Filled Only (5 ft. Fill)	Filled Plus 6 ft. Surcharge	Filled Plus 10 ft. Surcharge*
2 years	0.12	0.01	−0.02
5 years	0.17	0.01	−0.03
10 years	0.18	0.01	−0.05
Total Final Settlement	0.18	0.01	−0.03

*Negative sign means a heave.

Filling alone to the final construction level leads to the post-construction settlements being restricted to compression of the organic silt-clay. The long-term post-construction settlement contributed by 10 to 15 ft. of organic silt-clay was of the order of 3 to 7 in. Surcharging to a height

TABLE V
Calculated Post-Construction Settlements (ft.)
(20 ft. of Organic Silt-Clay)

Time after Pavement Construction	Filled Only (5 ft. Fill)	Filled Plus 6 ft. Surcharge	Filled Plus 10 ft. Surcharge
2 years	0.21	0.15	0.16
5 years	0.42	0.32	0.25
10 years	0.61	0.44	0.34
Total Final Settlement	0.82	0.56	0.44

of 6 ft. above final construction level decreased the long-term post-construction settlement to the range 1 to 6 in., that is, the general effect of the surcharge was a further settlement reduction of 2 in.

The calculations predict that if the pavement had been constructed immediately after filling (no surcharge) the predicted consolidation settlement would have been 12 in., ten years later. In contrast the calculations predict 3 to 5 in. if pavement construction was delayed 2 years and 1 to 4 in. if, in addition, the area was surcharged for these two years.

The calculations also established that there was no significant reduction in post-construction settlements by maintaining the fill and surcharge for a period in excess of 18 months to 2 years, so that it was not necessary to delay construction of pavements in areas filled in 1966.

A further important conclusion is that the reduction in post-construction settlement by increasing the height of surcharge from 6 to say, 10 ft., is relatively small. For example, referring to Table V the decrease in settlement for 10 years following construction is seen to be 0.10 ft.

In areas where post-construction settlements are primarily due to compression of the deep seated clay layers surcharging has little practical effect due to the reduced order of magnitude of these settlements compared with areas of thick layers of the organic silty clay.

From the preceding discussion it is evident that large long term settlements in previously surcharged areas will be primarily due to compression of the organic silt-clay layer. Thus the future settlements of pavement areas can generally be satisfactorily predicted by a consideration of the organic silt-clay layers alone, and making a small allowance for compression of other layers where the thickness of the organic silt-clay is less than, say, 10 ft. From the layer thickness, either from Fig. 6 or in-situ drilling, and using a coefficient of consolidation of 15×10^{-3} sq. ft./day and a compression index of 1.0, the post-construction settlements can be predicted with sufficient accuracy for most purposes. This does, however, necessitate a consideration of the loading history from commencement of filling (1966) and usually the use of a finite-difference technique to provide a sufficiently flexible analysis for any particular loading history. Such an analysis led to the post-construction settlements quoted in Tables IV and V. This approach will be termed the " simplified analysis ".

Fig. 10 shows the predicted settlements obtained by a detailed finite-difference analysis of the deposits which took into account the loading history prior to 1966, and the contributions to settlement by each layer. Two theoretical settlement time curves are shown. The dotted lines correspond to a c_v of 15×10^{-3} sq. ft./day and the full lines correspond to the c_v value obtained with the small " clear " samples (5×10^{-3} sq. ft./day).

A comparison shows the influence of the accuracy of the coefficient of consolidation on the predicted results. It will be noted in Fig. 10 (*a*) that the total final post-construction settlement for the more realistic field value (15×10^{-3} sq. ft./day) is relatively reduced because of the greater settlement during the surcharge period.

The post-construction settlements of Fig. 10 are similar to the values obtained by considering the silt-clay alone (Tables IV and V). For example, for Site S1 the calculated post-construction settlement after 5 years is 0.43 (Fig. 10 (*a*)) compared with 0.42 by the approximate method (Table V). At other sites the agreement was within 0.10 ft.

In one area it was necessary to consider the simultaneous consolidation of two contiguous layers of significantly different consolidation properties. This problem was solved by a finite difference approach and is detailed elsewhere (Ref. 4). It was found possible to present the settlement-time behaviour of such a two-layer system in a form which can be used directly in analysis, but for more than two layers a finite difference solution may have to be carried out for each individual case.

4.3 Settlements Due to Surface Loadings:

Two further loading cases were considered in detail. As a possible foundation system for the passenger concourse a raft foundation 40 ft. wide superimposing a gross pressure of 0.5 tons/sq. ft. was considered. For the purpose of illustrating the relative magnitude of the extra settle-

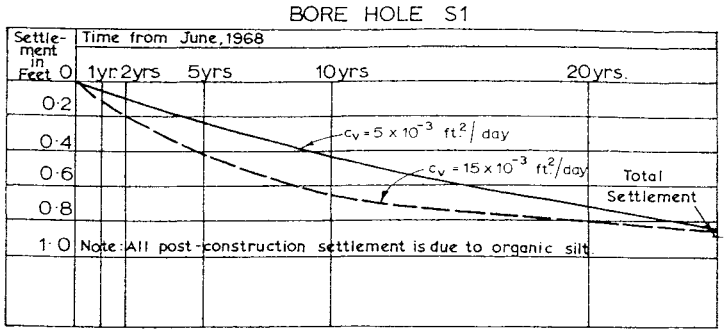

(a) BORE HOLE S2

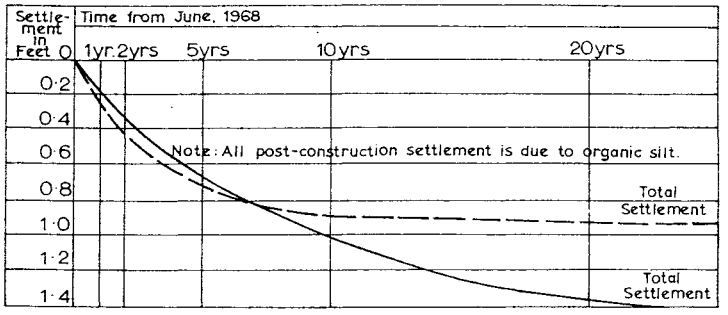

(b) BORE HOLE S8

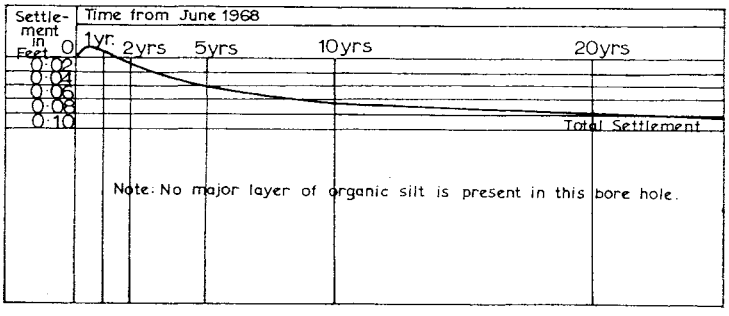

(c)

Fig. 10.—*Predicted Post-Construction Settlement-Time Relationships of Pavement Area.*

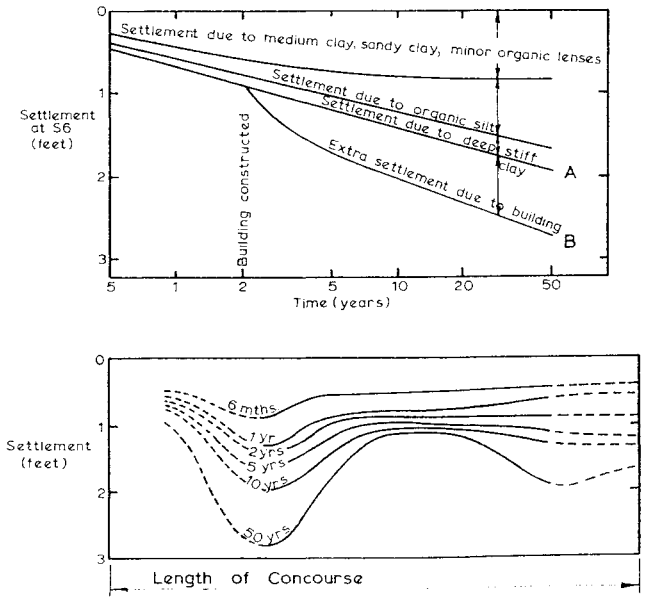

Fig. 11.—*Predicted Post-Construction Settlement-Time Relationships of Concourse.*

ment due to filling and surcharging, two major settlement-time curves are plotted in Fig. 11. Curve A is the consolidation settlement without concourse loading and Curve B includes the extra settlement which would occur if the concourse was placed on a raft foundation. The extra settlement five years after construction was found to be of the order of 7 in. increasing to approximately 11 in. ten years after construction. Of greater importance is that the settlements would not be uniform and the concourse structure would be subjected to rather severe differential settlements unless provision was made to compensate for the local settlements by jacking of the structure as the foundation settled.

The second type of surface loading considered was that due to parked aircraft. Taking into account the likely percentage of the total time aircraft were parked in the area adjacent to the terminal, the total final settlement was found to be 0.32 ft. for the Boeing 747 aircraft. Some creep settlement was predicted so that the total settlement after ten years could increase to 0.45 ft., being composed of 0.25 ft. of creep settlement. However, at the present time, the creep behaviour is not completely understood and the figure of 0.25 ft. can only be regarded as a first estimate of the creep settlement.

A further aspect of settlement considered in relation to the aircraft was the possibility of further compaction of the cohesionless fill by dynamic engine forces transmitted to the ground. Further compaction of such soils is primarily controlled by the maximum acceleration of the imposed vibrations (Refs. 1 and 7). From a study of the maximum acceleration of the out-of-balance forces and the likely damping due to wings and under carriage movement it appeared that the existing density was sufficiently high to obviate further settlement, and special deep seated compaction was considered unnecessary.

5.—CONCLUSIONS

The comparison of predicted and measured settlements clearly established that the long-term settlements are primarily due to compression of the organic silt-clay which occurs in deposits of varying lateral extent and of thickness up to 25 ft. Where the organic silt-clay deposits are relatively thin (less than 5 ft.) compression of the underlying stiffer inorganic clays will be the primary source of long term settlements although the total final settlement is likely to be an order less than in areas where the organic silt-clay is 20-25 ft. thick.

Filling and surcharging for a two-year period virtually eliminates post-construction settlements due to compression of layers other than the organic silt-clay. In areas where the organic silt-clay is 20 ft. thick, filling immediately followed by construction would have lead to a predicted post-construction total final settlement of the order of 18 in. compared with 10 in. for a 5 ft. fill maintained for 2 years prior to construction and 7 in. for fill plus 6 ft. of surcharge maintained for 2 years prior to construction.

The time rate of settlement was most closely predicted by use of the coefficient of consolidation obtained in a K_0 test. This was due to the fact that the longer samples used in the K_0 test were more representative of the average field element than the thinner " clear " samples used in the oedometer tests. The use of larger than normal samples has also been advocated by Rowe (Ref. 11) where there is a scale effect.

Although the organic silt-clay could be consolidated in limited regions by electro-osmosis, the conductivity of the soil-water system is too high to make the process an economically feasible procedure.

ACKNOWLEDGMENTS

The work described in this paper was carried out by personnel from the Commonwealth Department of Works and the School of Civil Engineering, University of Sydney, under the direction of the senior authors.

The senior authors would like to acknowledge the outstanding co-operation and encouragement of the Commonwealth Department of Works. The authors acknowledge the benefit of discussion and the valuable assistance given by Dr. H. G. Poulos, Senior Lecturer, Civil Engineering, University of Sydney. The paper is published by permission of the Director of Works.

References

1. BARKAN, D. D.—*Dynamics of Bases and Foundations.* New York, McGraw-Hill, 1962.
2. BJERRUM, L., MOUM, J. and EIDE, O.—Application of Electro-osmosis on a Foundation Problem in a Norwegian Quick Clay. *Geotechnique*, Vol. 17, No. 3, 1967, pp. 214-35.
3. CASAGRANDE, L.—Electro-osmotic Stabilization of Soils. *Boston Soc. Civil Engrs., Contributions to Soil Mechanics*, Vol. 2, 1941-53, p. 285.
4. DAVIS, E. H. and LEE, I. K.—One-Dimensional Consolidation of Layered Soils. *Proc. Seventh Int. Conf. Soil Mechanics and Foundation Engg., Mexico City*, 1969, Vol. 2, p. 65.
5. DAVIS, E. H. and POULOS, H. G.—Triaxial Testing and Three-Dimensional Settlement Analysis. *Proc. Fourth Aust.-New Zealand Conf. Soil Mechanics and Foundation Engg., Adelaide*, 1963, pp. 233-43.
6. DAVIS, E. H. and RAYMOND, G. P.—A Non-Linear Theory of Consolidation. *Geotechnique*, Vol. 15, No. 2, 1965, pp. 161-73.
7. LAMBE, T. W. and WHITMAN, R. V.—*Soil Mechanics.* New York, Wiley, 1969.
8. ROBERTS, D. V. and DARRAGH, R. D.—Areal Fill Settlements and Building Foundation Behaviour at San Francisco Airport. *ASTM Special Tech. Publication No.* 322, 1962, pp. 211-30.
9. ROWE, P. W.—Measurement of the Coefficient of Consolidation of a Lacustrine Clay. *Geotechnique*, Vol. 9, No. 3, 1959, pp. 107-17.
10. ROWE, P. W. and SHIELDS, D. H.—Radial Drainage Oedometer for Laminated Clays. *Proc. A.S.C.E., Jour. Soil Mechanics and Foundations Div.*, Vol. 91, No. SM1, Jan., 1965, pp. 15-23.
11. ROWE, P. W.—The Calculation of the Consolidation Rates of Laminated Varved, or Layered Clays, with Particular Reference to Sand Drains. *Geotechnique*, Vol. 14, No. 4, 1964, pp. 321-40.
12. KOLBUSZEWSKI, J.—An Experimental Study of the Maximum and Minimum Porosities of Sands. *Proc. Second Int. Conf. Soil Mechanics and Foundation Engg.*, 1948, Vol. 1, pp. 158-62.